

ABSTRACT

Title of Document:

MECHANICAL AND ELECTRICAL
PROPERTIES OF METAL-CARBON
CONNECTIONS FOR BATTERY
APPLICATIONS.

Christopher John Bilger, Master of Science, 2014

Directed By:

Dr. Hugh Bruck, Professor and Director of
Graduate Studies
Department of Mechanical Engineering

Material selection and processing techniques were investigated to form carbon-metal bonds. Mechanical and electrical characterization was performed to more fully comprehend the bonding mechanisms and properties. Utilizing carbon fibers as a primary conduction medium, the specimens from the processes investigated were utilized with lithium-ion cells to further characterize the electrical performance. Electroplating nickel onto the ends of the carbon fibers provides a relatively simple processing technique which improves fiber adhesion to nickel tabs by over 4.7 times when compared to conductive silver epoxy and over 5 times greater than a 1 inch immersion of carbon fiber into a SAC305 solder ingot. Additionally, a reduction of electrical resistance by 0.7 times over the solder ingot is achieved with the electroplating technique. The results of the electroplating are achieved by using about 25% less available contact area than the solder ingot and are scalable for usage in electrical circuits.

MECHANICAL AND ELECTRICAL PROPERTIES OF METAL-CARBON
CONNECTIONS FOR BATTERY APPLICATIONS

By

Christopher John Bilger.

Thesis submitted to the Faculty of the Graduate School of the
University of Maryland, College Park, in partial fulfillment
of the requirements for the degree of
Master of Science
2014

Advisory Committee:
Professor Hugh A. Bruck. Chair
Professor Abhijit Dasgupta
Professor F. Patrick McCluskey

© Copyright by
Christopher John Bilger
2014

Acknowledgements

First and foremost, I would like to thank and praise God for the opportunities that He has provided me.

I would like to express my sincere gratitude to Professor Hugh Bruck for serving as my primary advisor through the past year and a half. His determination and drive to push me out of my comfort zone have led to the greatest advances in this research. The guidance that I received has allowed me to make it to this point of my educational and academic career. It has been a privilege to work with him.

I would also like to thank Professor Abhijit Dasgupta for serving as my co-advisor, with whom I started my research career as an undergraduate. The opportunity to be enrolled in the BS/MS program has been greatly fulfilling. His input and knowledge have helped me to advance my understanding of the technical aspects that surround electronic components.

I would also like to thank those who have helped me in the lab, spending hours creating and preparing specimens. Specific thanks go to Hannah Cetuk, Micah Segal, Darius Quach, and Vincent Cheng for helping me prepare specimens for experiments when I needed them most.

The lab group in the Advanced Manufacturing Laboratory has kept me sane and provided daily comic relief, company, and encouragement to keep moving on.

The Department of Mechanical Engineering at the University of Maryland has provided me with a great environment to both further my education and fulfill my research. The professors that I had for both undergraduate and graduate courses have helped me form a greater

understanding and appreciation for all of the complexities that fill our world.

Thanks to Dr. Bradley Boyerinas, who provided me facility and E-Beam PVD equipment access and assistance at the National Institute of Standards and Technology. Additionally, thanks to the CALCE lab managers who have helped me troubleshoot numerous issues and train me on the equipment.

Finally, I would like to express my unending gratitude to my friends and family for their continued encouragement and support. Special thanks go to my family, especially my parents, who have ceaselessly encouraged me throughout my education to excel and perform with the highest of standards. After spending many hours in the lab, the emotional support that all of you provide have helped me keep my head up and moving forward.

Table of Contents

Acknowledgements.....	ii
Table of Contents.....	iv
List of Figures.....	vii
Chapter 1: INTRODUCTION.....	1
1.1 Research motivation.....	1
1.2 Research objectives.....	1
1.3 Thesis overview.....	2
Chapter 2: LITERATURE SURVEY.....	4
2.1 Processing.....	4
2.2 Structure.....	6
2.3 Properties.....	8
Chapter 3: EXPERIMENTAL METHODS AND PROCESSING TECHNIQUES.....	11
3.1 Materials.....	11
3.1.1 Carbon fibers.....	11
3.1.2 Solders.....	11
3.2 Carbon fiber preparation.....	12
3.2.1 Pyrolization.....	12
3.2.2 Braided carbon fiber.....	14
3.2.3 Activated rosin solder flux.....	14
3.3 Solder deposition.....	16
3.3.1 Solder casting.....	16

3.3.2 Direct soldering.....	20
3.4 Intermediate carbon fiber processing	21
3.4.1 Physical vapor deposition	22
3.4.2 Silver epoxy	24
3.4.3 Electroplating.....	25
3.5 Mechanical characterization.....	28
3.5.1 Pull-out testing.....	28
3.5.2 Shear bonding testing.....	29
3.5.3 Microscopy	31
3.6 Electrical measurements.....	33
3.6.1 Two-point resistance measurement.....	33
3.6.2 Four-point resistance measurement	34
Chapter 4: INITIAL EXPERIMENTS.....	42
4.1 Uncoated pultruded carbon fiber	42
4.1.1 Mechanical characterization	42
4.1.2 Electrical characterization.....	45
4.2 Kester 1544 flux coated carbon fiber	49
4.2.1 Mechanical characterization	49
4.2.2 Electrical characterization.....	55
4.3 Physical vapor deposition.....	70
4.3.1 Mechanical characterization	70
4.4 Nickel tab	76
4.4.1 Mechanical characterization	76

4.4.2 Electrical characterization.....	78
Chapter 5: EXPERIMENTS USING SILVER EPOXY.....	84
5.1 Mechanical characterization.....	84
5.1.1 Braided carbon fiber specimens.....	86
5.2 Electrical characterization	87
5.2.1 Pultruded carbon fiber.....	87
5.2.2 Braided carbon fiber	89
Chapter 6: EXPERIMENTS USING ELECTROPLATING.....	90
6.1 Mechanical characterization.....	90
6.1.1 Shear load testing.....	90
6.1.2 Microscopy	93
6.2 Electrical characterization	97
6.2.1 Battery performance.....	100
Chapter 7: CONTRIBUTIONS AND SUGGESTIONS FOR FUTURE WORK.....	106
7.1 Contributions	106
7.2 Suggestions for future work	110
Appendix.....	112
MATLAB: Resistance processing and plotting.....	112
MATLAB: Load processing and plotting comparison.....	114
MATLAB: LabView load formatting	115
MATLAB: Excel load formatting	116
MATLAB: Load plotting	117
Bibliography	118

List of Figures

Figure 1 - S-Bond published images indicating the metallic properties of the proprietary bonding technique	5
Figure 2 - Correlations between carbon specimens and electrical capacities	9
Figure 3 - Pyrolysis of epoxy encasement for a pultruded carbon fiber rod.....	13
Figure 4 - Process of treating the pyrolyzed carbon fibers with Kester 1544 activated rosin liquid flux.....	15
Figure 5 - Open mold versus sand casting solder deposition.....	16
Figure 6 - Melting the bulk solder in a crucible with a propane blow torch.....	17
Figure 7 - Heating of borax flux during solder melt	18
Figure 8 - Prepared pyrolyzed solder ingot specimens.....	19
Figure 9 - Nickel plated carbon fiber sleeve and nickel tab placement for soldering	20
Figure 10 - DC magnetron sputtering physical vapor deposition of carbon fiber	23
Figure 11 - Prepared 1.5 inch braided carbon fiber sleeve	25
Figure 12 - Watts nickel plating setup for braided carbon fiber	27
Figure 13 - Solder joint load apparatus with force transducer.....	30
Figure 14 - IMADA force measurement setup for shear joint testing	31
Figure 15 - Electrical schematic of DAQ 4-point resistance measurement of specimen	35
Figure 16 - Voltage and current versus time used for resistance measurement.....	36
Figure 17 - Revised electrical schematic of 4-point resistance measurement setup to reduce noise and increase repeatability.....	36
Figure 18 - Voltage versus current of specimen 3e for resistance measurement.....	37
Figure 19 - Physical setup for revised 4-point resistance measurement	38
Figure 20 - Voltage and current versus time from improved resistance measurement setup	39
Figure 21 - Visual comparison of alligator clip versus crimp terminal electrical connections	39

Figure 22 - Process of connecting ring-tongue crimp connection to pyrolyzed portion of specimen	40
Figure 23 - 4-point resistance measurement of nickel 200 tab using Agilent Milliohmmeter	41
Figure 24 - 4-point resistance measurement of nickel 200 tab using Agilent Milliohmmeter	41
Figure 25 - Force versus distance for pull-out testing of uncoated pyrolyzed pultruded carbon fibers.....	42
Figure 26 - PVD nickel plated carbon fiber soldered to nickel tab	43
Figure 27 - Optical and ESEM microscopy images of carbon fibers with EDXS analysis	44
Figure 28 - Cross section of SAC305 solder ingot with non-flux-treated pyrolyzed carbon fibers	45
Figure 29 - Resistance measurements of pultruded carbon fibers with varying measurement positions.....	46
Figure 30 - Resistance versus length of pyrolyzed and non-pyrolyzed carbon fiber specimens	48
Figure 31 - Electrical circuits using both pyrolyzed and non-pyrolyzed pultruded carbon fiber rods	49
Figure 32 - Force versus displacement of flux treated and non-flux treated carbon fiber specimens	50
Figure 33 - Force versus displacement of flux treated hollow-core carbon fiber specimens	51
Figure 34 - Force versus displacement of flux treated hollow and solid-core carbon fiber specimens	52
Figure 35 – ESEM image of fracture of carbon fiber after loading.....	53
Figure 36 – ESEM image of evidence of solder wetting on carbon fiber.....	54
Figure 37 - Carbon fiber soldered onto a lithium-ion battery for electrical testing.....	54
Figure 38 - Voltage versus current of specimen from 4-point resistance measurement.....	56
Figure 39 - Voltage and current versus time plot of specimen from 4-point resistance measurement	56
Figure 40 - Voltage versus current of specimen 3e during 4-point resistance measurement	57

Figure 41 - Resistance versus current of specimen 3e with step change locations indicated	58
Figure 42 - Resistance versus voltage of specimen 3e with step change locations indicated	58
Figure 43 - Resistance versus time of specimen 3e during 4-point resistance measurement	59
Figure 44 - Voltage and current versus time plot of specimen 3e from revised 4-point resistance measurement	60
Figure 45 - Voltage versus current of specimen 3e with step change locations indicated	60
Figure 46 - Resistance versus time of specimen 3e with step change locations indicated	61
Figure 47 - Voltage and current versus time profile used for evaluating crimped carbon fiber resistances.....	62
Figure 48 - Visual display of crimp tab connection on pyrolyzed section of carbon fiber specimen for electrical characterization.....	62
Figure 49 – Three trials of voltage versus current plot of electrical characteristics for non-crimped specimen 1	63
Figure 50 - Three trials of voltage versus current plot of electrical characteristics of crimped specimen 1	64
Figure 51 - Three trials of voltage versus current plot of electrical characteristics for non-crimped specimen 2	65
Figure 52 - Three trials of voltage versus current plot of electrical characteristics of crimped specimen 2	65
Figure 53 - Carbon fiber in SAC305 ingot connected in series with light bulb and power supply	67
Figure 54 - Bulb temperature versus time comparison of nickel wire and crimped carbon fiber used in electrical circuit.....	68
Figure 55 - Crimped carbon fiber terminal connections to lithium-ion battery, lighting a bulb	69
Figure 56 – Bulb brightness comparison between carbon fiber and nickel tab connections	70
Figure 57 - Picture of PVD nickel coated carbon fibers	71
Figure 58 - Pictures indicating the quality of the PVD nickel coated CF solder joints to nickel tabs	72

Figure 59 - Pictures indicating the steps of soldering the carbon fibers to a nickel tab for adhesion testing.....	73
Figure 60 - Individual carbon fibers remaining attached to nickel tab after adhesion failure	74
Figure 61 - Force versus displacement of PVD nickel coated carbon fibers.....	75
Figure 62 - Force versus displacement of nickel tab in SAC305 solder ingot	77
Figure 63 - Failed nickel tab specimen embedded in SAC305 solder ingot.....	78
Figure 64 - Nickel tab before and after embedding in SAC305 solder ingot	79
Figure 65 – Voltage versus current profile of the nickel tab in series with 11 Ω resistor	79
Figure 66 - Voltage versus current profile of 11 Ω resistor.....	80
Figure 67 - 400047 Nickel 200 (0.1 mm x 3.14 mm) tab specimen resistance versus length	81
Figure 68 - 400353 Nickel 200 (0.05 mm x 1.53 mm) tab specimen resistance versus length.....	81
Figure 69 - Agilent Milliohmeter setup for nickel tab resistivity measurements	82
Figure 70 - 400047 Nickel 200 (0.1 mm x 3.14 mm) tab specimen resistance versus length	83
Figure 71 - Demonstration of silver epoxy shear loading failure	84
Figure 72 - Force versus displacement of pyrolyzed pultruded carbon fiber attached to nickel tabs with silver epoxy.....	85
Figure 73 – Prepared specimens for braided carbon fiber connected to nickel tabs via silver epoxy.....	86
Figure 74 - Force versus displacement of braided carbon fiber specimens with silver epoxy bonding	87
Figure 75 - Voltage versus current of silver epoxy bonded specimens	88
Figure 76 - Voltage versus current of braided carbon fiber specimens with silver epoxy bonding	89
Figure 77 - Force measurement setup before (left) and after (right) failure.....	91
Figure 78 - Force vs. displacement of braided carbon fiber sleeve soldered to nickel tabs	92

Figure 79 - Comparison of slope and maximum load from mechanical tests of braided CF with electroplated Ni soldered to Ni tabs using SAC305 with flux.....	93
Figure 80 - ESEM images of plated carbon fiber with EDS elemental composition composite image	94
Figure 81 - Plated carbon fiber encased in SAC305 matrix with spectral analysis of the bulk solder.....	95
Figure 82 - ESEM images of nickel tab – SAC305 interface with EDS elemental composition composite image.....	96
Figure 83 - ESEM image of globule formations on the end of nickel plated carbon fiber specimens	97
Figure 84 - Voltage vs. current of unsoldered plated braided carbon fiber sleeves.....	98
Figure 85 - Voltage vs. current comparison of plated and unplated braided carbon fiber sleeves	99
Figure 86 - Voltage vs. current of soldered plated braided carbon fiber sleeves to nickel tabs	100
Figure 87 – Light bulb voltage versus time of discharge circuits comparing connector types	101
Figure 88 - Thermal image of the discharge circuits indicating the locations of the hot spots on the connectors	103
Figure 89 - Battery voltage versus current of charging circuits comparing connector types	104
Figure 90 - Thermal images comparing the temperatures of the connectors in cell discharge circuits	105

Chapter 1: INTRODUCTION

1.1 Research motivation

Electrical circuits are full of metallic components, including the wires that connect various devices together. There exist niche applications where the metallic content of a circuit should be minimized and non-metallic and low density conductors must be used. Carbon presents adequate conductive properties, but many electrical connection methods have gone uninvestigated due to the reduced need in industry.

Utilizing carbon as a conductor can provide a low-power circuit additional mechanical flexibility, while maintaining adequate electrical conduction. With the world improving on the forms of carbon as a conductor, such as carbon nanotubes and graphene, functional joining methods must be investigated to interconnect these carbon components into the electrical circuits.

1.2 Research objectives

The primary objective of this study is to investigate and characterize the mechanical and electrical properties for carbon connections to battery tabs. The complexity of this problem delves further beyond the characterization, but also requires engineering and material analyses to determine optimal connections. A primary goal of this study is to identify potential materials and processes which can be utilized to enhance the bonding mechanisms, creating stronger adhesion and minimizing interfacial resistance.

Identification of processing techniques is not only essential to improve the interfacial characteristics of the carbon to tab connection, but also to create repeatable results. Having

desirable characteristics without a process that can reliably produce said characteristics greatly reduces the probability of successful implementation.

Identifying a repeatable process in conjunction with desirable mechanical and electrical characteristics lends the potential to introduce carbon into circuits as a conductive medium. While carbon has an inherent resistance higher than that of most metallic connections, the flexibility that it provides can provide a niche for circuits that require such flexibility and are able to sacrifice the resistance for that enhanced movement.

1.3 Thesis overview

This thesis investigates the material processing techniques for joining carbon material in the form of carbon fibers to conductive compounds including solders and conductive epoxies.

Chapter 2 investigates the past research that has been carried out in the field of connecting carbon material to metal compounds. This chapter explores the processing techniques used, the structures formed to create the carbon-metal adhesion, and the properties that these bonds exhibit. While many of the documents search to provide mechanical enhancements only, the processes can be investigated to improve on electrical characteristics as well.

Chapter 3 discusses the experimentation processes and material selection for the research. These processes include the bonding procedures for the investigated methods, in addition to the methodologies and procedures utilized to conduct electrical and mechanical performance testing. Maintaining consistency with these procedures is the key to providing comparable results for characterization testing.

Chapter 4 identifies the results of the testing for the procedures and tactics used during the early stages of the research investigation. These results help to provide a baseline of performance that future processes can reference. Including solder infiltration, liquid rosin flux additives, and physical vapor deposition coatings, this chapter identifies the variations and characteristics achieved using these different processing methods and techniques.

Chapter 5 introduces a cold application approach to conductive joining of carbon fibers to nickel tabs, commonly used in batteries. The silver epoxy results are investigated both with pultruded carbon fiber and the braided carbon fiber. Electrical and mechanical characterization is evaluated and discussed.

Chapter 6 includes the mechanical and electrical characterization study of electroplated nickel coatings on braided carbon fibers. This chapter discusses the performance of both the electrical and mechanical aspects of the joints formed by using various tests. To further substantiate and understand the results of the testing, microstructural analysis has been undertaken to identify mechanisms present which enhance the interface and joints as a whole.

Finally, Chapter 7 summarizes the findings of this research investigation and discusses suggestions for further study and examination. Providing an overview of the findings and future tasks helps to frame the contributions of the research and shed light upon how the processes and findings can be implemented into various applications.

Chapter 2: LITERATURE SURVEY

2.1 Processing

Identifying different connection processes for various experiments, the primary methods of connection are welds, electrically conductive adhesives, and soldering. “Joining of metal films to carbon-carbon composite material by metal plasma immersion ion implantation,” by Anders et. Al, soldering graphite and other carbon materials had not been previously explored, so the team approached the situation by precoating the carbon or graphite surface with a metallic or intermetallic layer so that the material can be braised with a conventional filler material. One example suggests, chemical vapor deposition (CVD) can be used to precoat the carbon (carbon-carbon) with molybdenum or tungsten; this is often accompanied by carbide formation which strengthens the bond between the carbon and the metal layer.¹ The document continues to explore copper coated carbon-carbon. Copper coated carbon can lend to enhanced conductivity and serve as a metallic medium to bond to for soldering applications. Copper may also have higher corrosion potential, so the environment of which the carbon would be subjected to must be evaluated.

In addition to traditional lab manufactured interfaces, there is a commercial organization that provides services to join metals to pyrolytic carbon, graphite, and carbides. The company claims the rights to the proprietary process used. Research into the patents filed by the company shows that utilizing an active solder can bond graphite without chemical fluxes or pre-metallization. Many of the processing steps have been obscured and not thoroughly described, demonstrating that the process may be kept proprietary. The organization’s website indicates that a “special high temperature / vacuum metallization with a specially formulated S-Bond paste

/ suspension” is used, which contains Titanium which reacts with the carbon base. This company claims to: “join carbon based materials to most metals, ceramics and composites.”² The S-Bond paste indicates and evidences the potential for successful metallic interconnection with carbon. While the processing may be proprietary, the alloy forms intermediate phases which can assist with adhesion. The conductivity of the material is not known and the company reserves the rights to the processing, which may require high temperature or unsafe environments for lithium-ion cells.

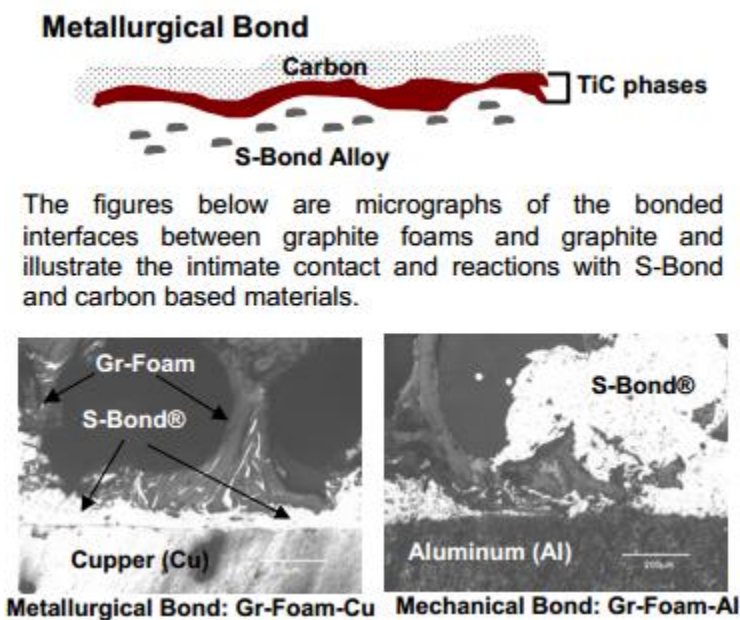


Figure 1 - S-Bond published images indicating the metallic properties of the proprietary bonding technique

In a paper titled “Interface Interaction in Aluminum--Carbon System” by M.H. Shorshorov et al., a composite was created with carbon tape and molten aluminum. The experiments demonstrated that increasing the contact time of the fiber with the melt, temperature and infiltration pressure increased growth of the carbide phase and bond strength along the fiber/matrix interface.³ Depending on the carbide phase produced, the resistivity of the bond can vary. Ideally, a high conductivity carbide phase could be formed to produce a strongly adhesive

and conductive interconnect. While aluminum may not be the metal of choice, starting with the processing methodology, while using another metal, can provide a firm foundation to identify potential processing steps to form higher strength bonds.

2.2 Structure

A paper titled “Interface characteristics and mechanical properties of short carbon fibers/Al composites with different coatings” by Yiping Tang et al. discusses the interface between Short Carbon Fibers (SCFs) and aluminum melt. The document does not address the usage on longer carbon fibers, such as those used in pultruded rods. The paper discusses and reached the conclusion that an “Al₂O₃ coating protected the SCFs and prevented the harmful reaction of Al and SCFs. The interface of Al/Al₂O₃/SCF without any other phase was clean and well bonded, and the Al₂O₃-coated SCFs/Al composite had the highest mechanical properties.” Unfortunately aluminum oxide is a highly resistive material. In addition, “the results showed that, compared to non-coating, Ni or Cu coating improved the wettability of SCFs and Al melt. However, the harmful phases Al₃Ni or CuAl₂ generated in interface zone and Al matrix result in the lower mechanical properties.”⁴ The processing and structure of the interface may be useful to look into to see if the mechanical properties are still within tolerance for electrical interconnect purposes and if the interface is electrically conductive.

The previously mentioned paper, “Interface Interaction in Aluminum--Carbon System” by M.H. Shorshorov et al., also discusses the aluminum carbide (Al₄C₃) interphase that forms at the fiber/matrix interface during infiltration of the molten aluminum into the carbon tape. The effect on strength of the composite was investigated. Fracture under tensile load varied from ductile with fiber pull-out from the matrix to brittle. Maximum tensile strength was obtained on

specimens having intermediate-type fractures. The ratio of the length of fiber pull-out to the diameter was approximately 100:1. The quantity of carbide phases was 13.8 mg Al₄C₃ per gram of carbon fiber. The average carbide phase size was 0.1 μm and the average distance between particles was approximately 1.0 μm.⁵ The formation of the carbide phase demonstrates increased mechanical adhesion of the metal to the carbon fiber. By seeking similarly structured interphases, high adhesive strengths can be realized between metals and carbon fibers.

The paper, “Influence of Fiber Surface Structure on Interface Reaction Between Carbon Fiber and Aluminum” by Kuang-chih Chang et al., discusses different structures of carbon fiber and the interfaces between the fibers and aluminum. The team prepared the composite structures by hot-pressing. Utilizing unprocessed vapor grown carbon fibers and graphitized carbon fiber surfaces, graphitic lamella lattices formed. This layer was formed on the interface between the carbon fiber/aluminum composite and the graphitized carbon fiber/aluminum composite. Additionally, when the composites were hot-treated, aluminum carbide crystallization formed on the irregular layers.⁶ The formation of these structures, as mentioned previously, do not allow free movement between the layers in the composites, lending way to enhanced mechanical adhesion properties. While the interfacial products are of potential interest for future investigation, the conductivities of the products must first be investigated to determine if such a structure or process would be a viable solution to bonding carbon to metal for use in electrical circuits.

Focusing on aluminum composites, Silvain et al. investigated aluminum/carbon composites with the presence of a nickel interlayer deposited on the carbon fibers being studied. The presence of this nickel eliminates the diffusion of the carbon into the aluminum, which in

turn greatly removes the possibility for the formation of a carbide layer. In this situation, the nickel is used as a sacrificial layer to not react with the aluminum to cause brittle interphase structures. Alternatively, the nickel can be used as an additional conductive medium to prevent carbides from forming and create strong metallic bonding between the nickel and solder. The nickel coating was performed electrochemically and deposited on the carbon fibers.⁷

Zhongsheng Hua et al. discuss in their paper, “Preparation and Characterization of Nickel-Coated Carbon Fibers by Electroplating” a technique to produce uniform, smooth, and bright nickel depositions on carbon fibers. By utilizing a nitric acid treatment on the carbon fibers, the surface is roughened for enhanced adherence to the carbon fibers. They indicate that there are metal-carbon-oxygen bonds present at the interface between the nickel coatings and the carbon fibers. Additionally, the nickel provides excellent oxidation resistance at high temperatures. Although the carbon fibers will most likely not be subjected to high temperatures for traditional electrical circuits, lower temperature oxidation resistance is crucial in electronics. The team also indicated that wettability of aluminum on the carbon fiber has greatly improved, due to the nickel coating.⁸

2.3 Properties

The correlation between the microstructural parameters and electrochemical properties of conventional and novel types of carbon materials for Li-ion batteries is discussed in the paper titled, “Recent development of carbon materials for Li ion batteries” by M. Eno et al. from Shinshu University. The carbon materials investigated include, graphitizable carbons such as milled mesophase pitch-based carbon fibers, polyparaphenylene-based carbon heat-treated at low temperatures and boron-doped graphitized materials. Displayed in Figure 2, the team

investigated the charge and discharge capacities of several carbon specimens. The studies and results may lend closer relation the usage of carbon as an electrode in electrochemical cells, but the identification of such plausible materials can help to determine ideal carbon materials to investigate. If a carbon material is used as an electrode in an electrochemical cell, then the step of connecting the metallic tab to carbon is removed. Instead, carbon-to-carbon bonding should be investigated.

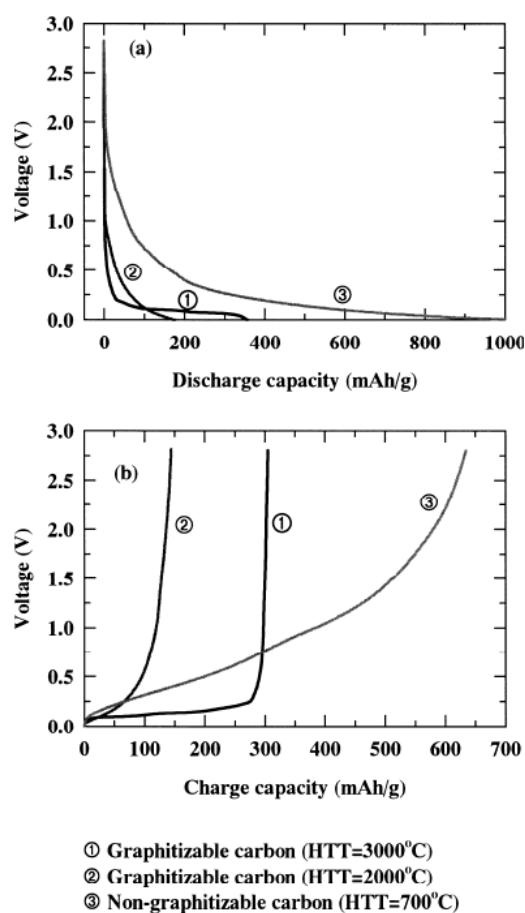


Fig. 6. Plots of voltage vs. reversible capacity for (a) the second discharge and (b) charge cycle of representative carbon and graphite samples, ① graphitizable carbon heat-treated at 3000°C, ② graphitizable carbon heat-treated at 2000°C, ③ non-graphitizable carbon heated at 700°C.

Figure 2 - Correlations between carbon specimens and electrical capacities

“Trends of Metal-Carbon Bond Strengths in Transition Metal Complexes” by E.M. Siegbahn, investigates two different types of trends of metal-carbon (M-C) bond strengths for the sequence of second row transition metal atoms. In the first trend, the bond strength dependence on the hybridization on carbon has been studied. It is found that sp hybridized carbon atoms form much stronger M-C bonds than sp² hybridized carbon atoms. The bonds formed by sp³ hybridized carbon atoms are still weaker. The M-C bond strengths decrease markedly to the right in the periodic table. Siegbahn indicates that these trends of M-C bond strengths can best be explained by observing the ionic contributions in the M-C bonding and repulsive effects, depending on the number and type of ligands on the bonding carbon atom.⁹ This study focuses on the bonding for pure metals and does not investigate other compounds or alloyed metal interactions. However it does indicate which metals will create stronger bonds with the carbon structures. This is useful in determining candidate metals to use for intermediate additives to create strong and conductive structures.

Furthermore, the paper “Resistivity of carbon material-metal alloy welded joint interface” discusses the resistivity of the interface between titanium, aluminum, copper, and platinum alloys with porous carbon material.¹⁰ The information from Lakomskii et al. can identify and help categorize the candidate compounds for metallic selection for carbon bonding. The resistivities must be compared with the mechanical potential for bonding with the carbon structures. Prioritization can be accomplished by weighing the values of both of these characteristics and comparing them with the desired outcome and environmental usage of the bonds.

Chapter 3: EXPERIMENTAL METHODS AND PROCESSING TECHNIQUES

3.1 Materials

3.1.1 Carbon fibers

3.1.1.1 Pultruded carbon fiber

The pultruded carbon fibers chosen for investigation are 1 mm diameter Graphlite fibers obtained from The Composites Store with a modulus of 134 GPa, a density of approximately 1.7 g/cc (67 vol. % microfiber), and a tensile strength of 3.1 GPa. The diameter of the microfibers was found to be approximately 8 micron, and they are pultruded in a Bisphenol F epoxy with a glass transition temperature of 100 °C.¹¹

3.1.1.2 Braided carbon fiber

The previously chosen pultruded carbon fibers were replaced by carbon fiber braided sleeve for investigation. These carbon fiber braided sleeves are more flexible than the pultruded carbon fiber because they do not have an epoxy encasement. The braided sleeves are the 0.1 inch diameter carbon fiber braided sleeves with 1K tow count obtained from The Composites Store. The carbon sleeve is braided with +/- 45° fiber orientations. The braided sleeve contains 10 1K tow bundles, yielding a sleeve weight of 66g/100m.¹²

3.1.2 Solders

The solders that were identified as possible candidates for metallic interconnection with the carbon fibers included SAC305 and SAF-A-LLOY.

3.1.2.1 SAF-A-LLOY

SAF-A-LLOY, a solder made by Kester with a T_m of 219-235 °C, was used during exploratory testing. The SAF-A-LLOY has a composition displayed in Table 1.¹³

Table 1 - SAF-A-LLOY elemental composition

Chemical Name	CAS#	Ingredient Percent
Zinc	7440-66-6	0 - 10 by weight
Antimony	7440-36-0	0 - 10 by weight
Copper	7440-50-8	0 - 10 by weight
Bismuth	7440-69-9	0 - 70 by weight
Silver	7440-22-4	0 - 10 by weight
Tin	7440-31-5	0 - 100 by weight

Following early testing, the SAF-A-LLOY was replaced in testing with SAC305.

3.1.2.2 SAC305

SAC305 is a lead-free solder that has been widely used in the electronics industry following the Restriction of Hazardous Substances (RoHS) directive. This solder is comprised of 96.5% tin (Sn), 3.0% silver (Ag), and 0.5% copper (Cu). This composition leads to the name SAC305.

The SAC305 has wider studied characteristics in the electronics industry and has higher availability from various retailers and comes in a variety of forms.

3.2 Carbon fiber preparation

3.2.1 Pyrolization

The pultruded carbon fibers chosen for further investigation were 1 mm diameter Graphlite fibers obtained from The Composites Store with a modulus of 134 GPa, a density of

approximately 1.7 g/cc (67 vol. % microfiber), and a tensile strength of 3.1 GPa. The diameter of the microfibers was found to be approximately 8 micron, and they are pultruded in a Bisphenol F epoxy with a glass transition temperature of 100 °C.

Due to the encasement, the epoxy prevents the carbon fibers from freely moving and adds much rigidity. When investigating carbon bonding and the electrical characteristics of the fibers, the epoxy must be successfully removed to expose the bare carbon fibers. To do this, the epoxy encasement is “pyrolized.” Pyrolysis is the process of thermochemically decomposing a material. Applying sufficient heat to the pultruded carbon fiber causes the epoxy to decompose, but keeps the carbon fibers intact.

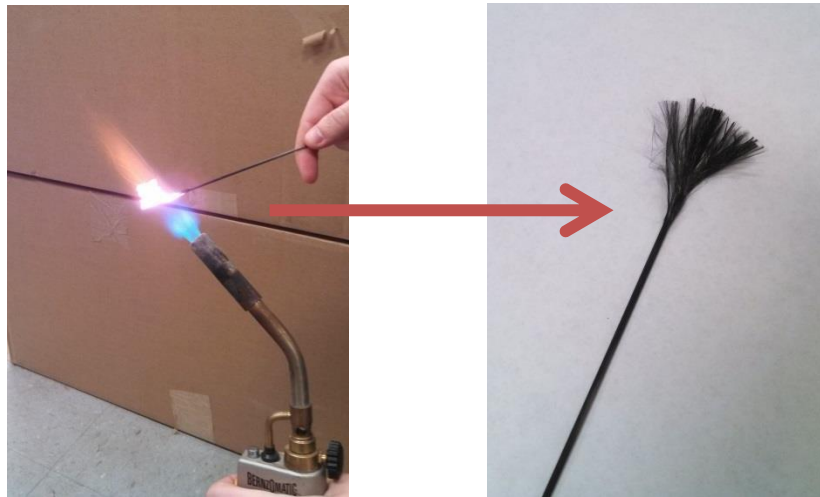


Figure 3 - Pyrolysis of epoxy encasement for a pultruded carbon fiber rod

As demonstrated in Figure 3, the pultruded carbon fiber rod is exposed to a flame to burn off the epoxy encasement around the carbon fibers. In order to get a more precise length of pyrolyzed fibers, metal pliers can be used to clamp the rod to the desired length. A propane blow torch is used to burn off the epoxy. Propane torches, reaching temperatures of upwards of 2000 °C with ambient air providing the oxygen is sufficient enough to degrade the thermoset epoxy.

The blow torch is used to heat the carbon fiber rod for approximately 20-30 seconds, while rotating the rod to ensure complete pyrolysis of the desired area.

3.2.2 Braided carbon fiber

Choosing the braided carbon fiber sleeve in lieu of the pultruded carbon fiber removes the processing steps that were necessary to produce a usable product from the pultruded fibers. Additionally, the braided carbon fibers are able to freely flex and be manipulated out of packaging because they are not encased in epoxy to form a composite material.

The lack of the epoxy encasement allows the reduction of fiber damage due to processing. Previously, the pultruded carbon fibers needed to have segments of epoxy removed by heat induced degradation by means of pyrolyzation. This process burned away the epoxy, but often left residues and particles stuck and attached to the pyrolyzed segments. In order to remove a lot of the debris, and to free all of the fibers, mechanical pressure and agitation was needed to create free fibers. This process, accompanied with the pyrolyzation often damaged some of the carbon fibers, causing them to detach from the remainder of the pultruded rod. This may lead to less consistency and repeatability due to a varying number of fibers per specimen.

3.2.3 Activated rosin solder flux

Kester 1544 activated rosin liquid flux is applied to the pyrolyzed end of the carbon fiber rod or the bare carbon fibers in the braided strand. Activated rosin solder flux is a compound which contains an acid, which is most commonly hydrochloric acid, to dissolve and remove any oxidation layers on the surface of the metal to be soldered. The rosin is a viscous liquid, which also reacts to remove the metal oxides and protect the surface from further oxidation. The application was done by dipping the free end of the carbon fiber into the liquid flux, then

removing the excess flux with a paper towel. The dipped end was flayed out, to provide more contact area between the carbon fibers and solder. A demonstration of the process can be seen in Figure 4.

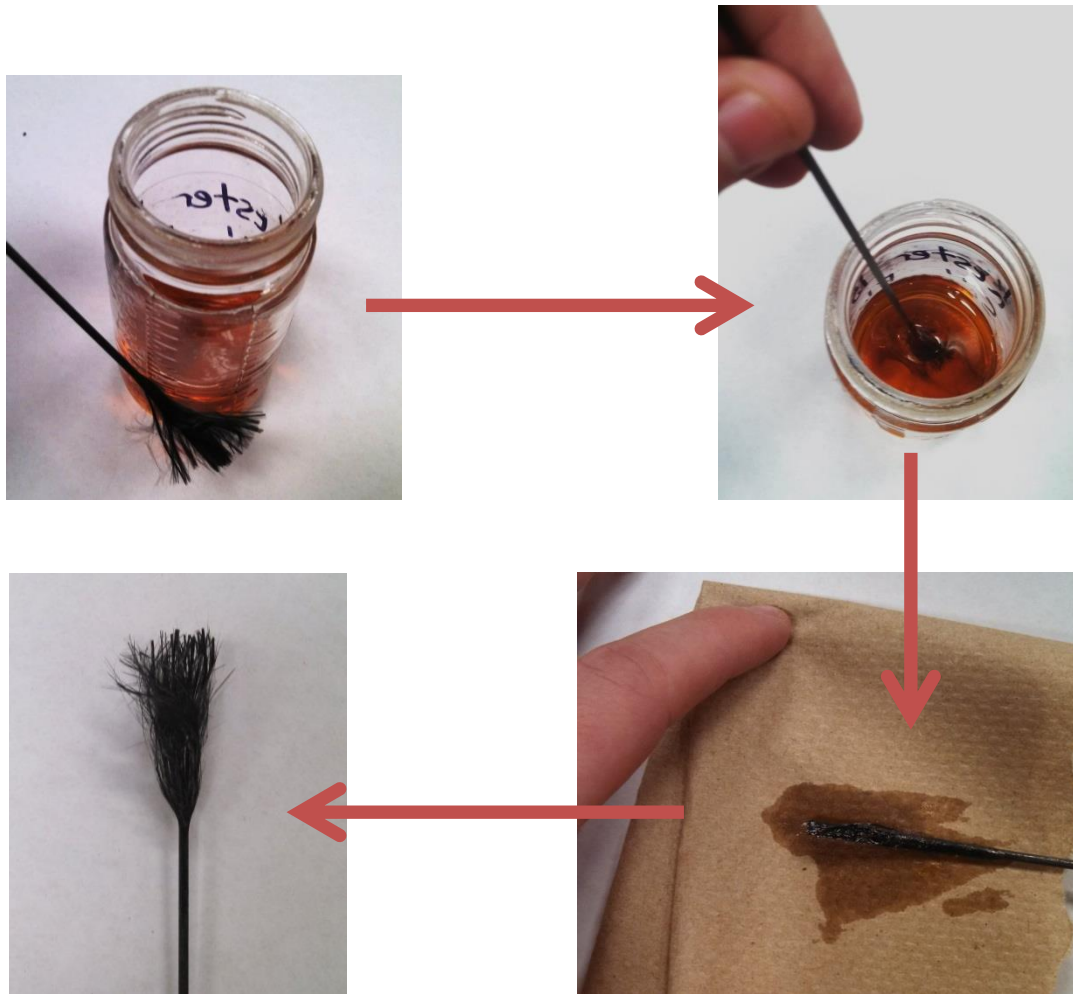


Figure 4 - Process of treating the pyrolyzed carbon fibers with Kester 1544 activated rosin liquid flux

When the braided carbon fibers were attached to the nickel tabs, the Kester 1544 was applied to the carbon fibers using a dropper. Since the carbon fiber for the braided strands needs less flux, due to the reduced connection size and solder usage, a dropper is used to precisely apply the flux. Further details of this process are discussed in the “3.3.2.1 Electroplated carbon fibers” section on page 20.

3.3 Solder deposition

3.3.1 Solder casting

For the melt process, both an open mold and a sand casting approach were developed as seen in Figure 5. These two approaches were used to fabricate specimens for further characterization. The sand casting approach was chosen for future investigation based on the flexibility of creating test specimens with different geometries that were appropriate for the desired electrical and mechanical testing.

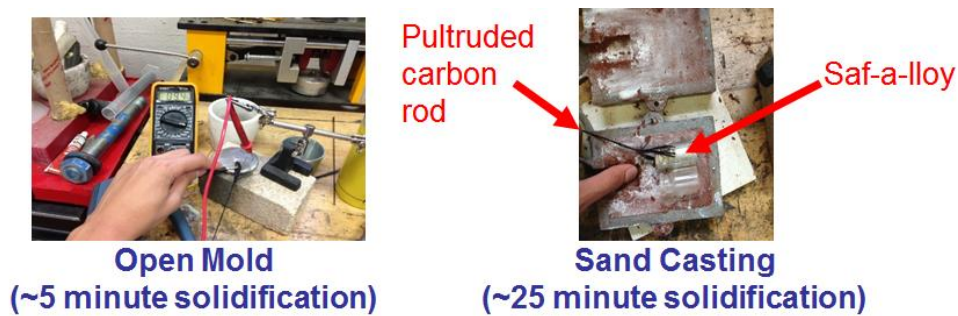


Figure 5 - Open mold versus sand casting solder deposition

3.3.1.1 Open mold casting

The open mold casting method was used during the early stages of research experimentation to provide a method to easily characterize the mechanical and electrical characteristics of the carbon fiber to metal connection. In this process, the bulk solder was put into a crucible, and then melted with a propane blow torch, as demonstrated in Figure 6. While the solder was in its liquid phase, the pyrolyzed end of the carbon fiber was embedded into the solder by submerging the free end. From this point, the carbon fiber rod was held in place using alligator clips and a stand, and the solder was allowed to solidify. The solidification process

takes approximately thirty seconds until the surface starts to become rigid, and then the whole solder is allowed to solidify for approximately five minutes.



Figure 6 - Melting the bulk solder in a crucible with a propane blow torch

This process does not allow solder geometries other than the shape of the bottom of the crucible. Additionally, much more solder must be used to create a depth deep enough to encase the carbon fiber. Therefore, much solder is wasted, which is very costly. This setup also does not allow more precise control over where the fibers are situated in the melt. Since the fibers are added post-melting, they must be quickly moved into a desirable location and can disrupt the solidification, yielding an inconsistent structure in the solder.

3.3.1.2 Sand mold casting

To create a sand molded specimen, an appropriate mold of the specimen geometry is made using casting sand. This sand contains clay, which helps to retain the structure and geometry of the desired part during casting. Additionally, the sand more slowly dissipates the heat from the molten metal. To produce a mold, a cylindrical shape is inserted beneath the spout of the mold frame. Once this is in place, sand is packed tightly around the cylinder. To assist with the packing, either a hammer or hydraulic press can be used with a flat rigid plate to help

distribute the load evenly. When the sand is tightly packed, the cylinder is removed from the spout slowly, ensuring that the walls of the cavity are not damaged.

Following the mold production, the crucible is prepared to melt the solder. To minimize foreign contaminants, the crucible is cleaned prior to the introduction of the bulk solder. From this point, the volume of solder used to fill the sand mold cavity is put into the crucible. Using a blow torch with propane gas, the solder is melted in the crucible, as demonstrated in Figure 6.

In order to minimize oxidation and debris during the current processing, the solder was melted in the crucible, then borax flux sprinkled over the top of the liquefied solder, then heated again to activate the flux to trap foreign particles and oxidation. The flux, once heated, creates glassy beads which encapsulate the foreign particles. The borax powdered flux was used twice in succession for each sample, before pouring.

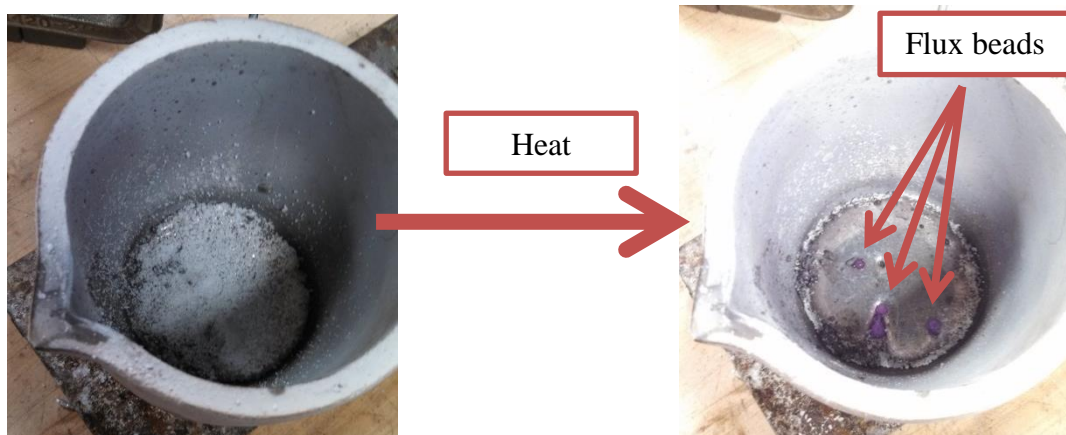


Figure 7 - Heating of borax flux during solder melt

To embed the specimen in the solder, the carbon fiber is held in place, using alligator clips and a stand, in the cavity. Therefore, the carbon fiber rod is centered in the cavity and once filled with solder the fibers will be encapsulated. These specimens were inserted into the cavity

to be embedded approximately 1 inch into the solder ingot. The carbon fibers were flayed prior to insertion to maximize the surface connection on the fibers.

In addition to the original pouring method, it was decided that using a liquid flux could help the mechanical adhesion properties between the carbon fiber and the solder. Kester 1544 activated rosin liquid flux was applied to the pyrolyzed end of the carbon fiber rod. This was done by dipping the end into the liquid flux, then removing the excess flux with a paper towel. The dipped end was flayed out, to provide more contact area between the carbon fibers and solder. After pouring, the fibers tended to be repelled to the outside of the mold (which can be easily seen with Sample 3C). Despite having less contact area, compared to previous specimens, the loads sustained by these specimens were higher than the fibers that had not been treated with the liquid flux. A diagram of the steps of this process can be observed in Figure 4, located on page 15.

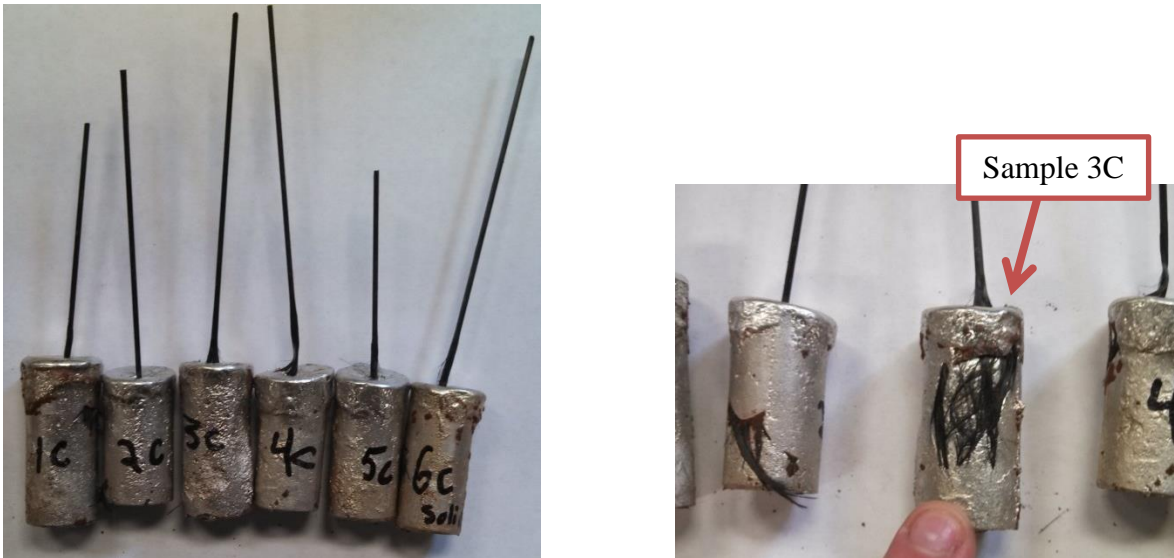


Figure 8 - Prepared pyrolyzed solder ingot specimens

3.3.2 Direct soldering

3.3.2.1 Electroplated carbon fibers

Once the plated carbon fiber specimen is dry, it is able to be soldered onto a nickel tab. First, remove the tape carefully, if it has not already been done, and place in an extra hands device (for electronics). Take a nickel tab and mark 0.25 inches down from the end to solder by scoring the metal. Wipe the tab off with a KimWipe to help remove and surface contaminants or oils before soldering. Place this tab into the other clip on the extra hands. Line up the end of the plated carbon fiber sleeve with the 0.25 inch marking on the nickel tab. The placement can be seen in Figure 9.



Figure 9 - Nickel plated carbon fiber sleeve and nickel tab placement for soldering

Apply about two drops of Kester 1544 activated rosin liquid flux to the plated end of the carbon fiber. Spread the carbon fiber around onto the nickel tab end so that it is evenly distributed and has flux on both the tab and on the fibers.

Heat a soldering iron and once hot, clean the soldering tip off to remove oxides. Using SAC305 solder, melt some solder onto the iron and in a painting like motion, coat the plated part of the end of the nickel plated fibers with the solder by moving from the middle to the end of the specimen. Then proceed to heat the carbon fiber and tab with the soldering iron and deposit the SAC305 solder. In brush-like motions, coat as much of the carbon fiber as possible with the deposited solder and spread evenly across the nickel tab, ensuring that the tab, itself, has been wetted with solder.

Once the specimen is soldered, allow the solder to solidify before moving. Take the solidified specimen and repeat the process with the other plated side and a new nickel tab. This specimen is now ready for electrical and mechanical characterization. Due to the difference of tow fiber counts between the pultruded carbon fibers and the pyrolyzed carbon fibers, direct comparisons between performance are somewhat difficult to directly compare. While both of the fiber types exhibit similar inherent resistances, the available surface area differs. Not all of the fibers are able to wet or connect via a joint, but the available surface area can be compared. Assuming an average of 5 μm fiber width, and 10,000 fibers in a 6.35 mm joint, this equates to 0.001 m^2 of surface area per joint.

3.4 Intermediate carbon fiber processing

While there is some evidence of wetting of carbon fibers when solder is applied to the bare fiber, the results are minimal and do not provide much mechanical adhesion. To remedy this situation, the carbon fibers are coated with metals that are known to adhere to the selected solders. In order to connect these fibers, various intermediate steps have been taken to enhance the wettability of the solder without sacrificing the conductivity of the interface.

3.4.1 Physical vapor deposition

A physical vapor deposition (PVD) technique was investigated as a processing step to coat the carbon fiber rods with various metals in order to increase mechanical adhesion. Typically PVD is used to deposit thin metallic films on surfaces such as semiconductors.

3.4.1.1 DC magnetron sputtering

The following PVD process was completed using a DC Magnetron Sputtering Machine. Figure 10 shows the purple glow of the plasma in the vacuum chamber, which collides with a metal target (in this case, nickel) to release the metal atoms from the target and reattach themselves to the carbon fiber rod. The pyrolyzed carbon fiber rod is rotated in the chamber in 30 degree increments with even time spacing in order to uniformly coat the fibers.

This process is a line-of-sight deposition. For this reason, only the surfaces of the exposed carbon fibers are coated with the metal. The fibers in the center of the bundle do not have a significant amount, if any metal deposits. Additionally, this process requires a high vacuum environment, which requires the chamber to be evacuated overnight. Therefore, the process is not time efficient and yields low quantities during production.

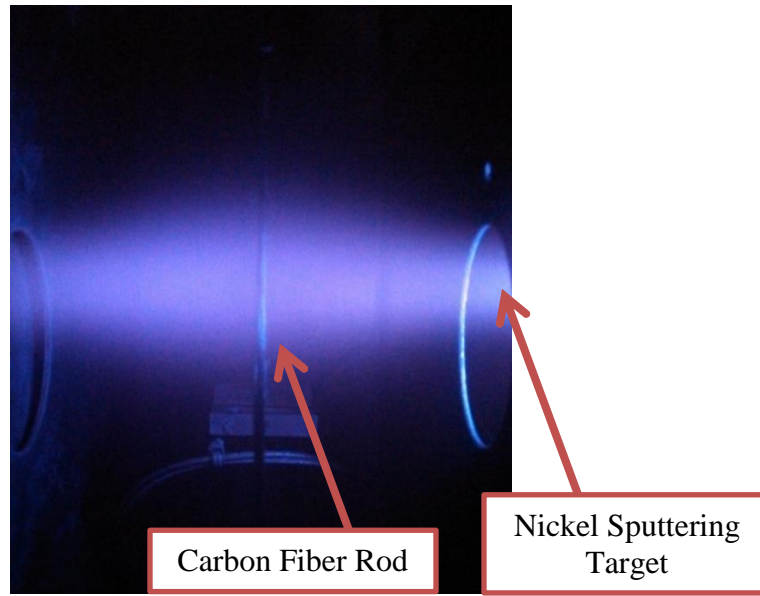


Figure 10 - DC magnetron sputtering physical vapor deposition of carbon fiber

3.4.1.2 Electron beam

Electron beam physical vapor deposition is an alternative PVD method to sputtering. This process also requires a high vacuum environment which leads to low quantity yields with a large time investment. The process is carried out by placing an ingot of the desired coating metal on an actively-cooled crucible in the base of the chamber. An electron beam is produced beneath the platform to protect it from metal contamination. This beam is directed by magnetic fields to become incident upon the coating metal. The combined energy of the beam and the high-vacuum environment cause the metal to sublime and be projected upward as a gas. These metal atoms attach to surfaces one-by-one. The target, located directly above the metal is coated by these atoms and produces a thin metallic layer on the surface.

A disadvantage to electron beam PVD is that many apparatuses do not contain setups that allow the rotation of specimens, because they are typically intended for the deposition of thin-

films on flat substrates. Additionally, there is no focus of the deposition, but rather a gaseous cloud of the target metal deposits itself on any surface available.

3.4.2 Silver epoxy

The usage of silver epoxy was investigated for a potential solder-free interconnection method to bond the carbon fibers to a metallic, particularly nickel, tab. The silver epoxy was selected due to its relatively simple application method, conductivity, and does not require any special devices to properly implement.

The silver epoxy used is manufactured by MG Chemicals as a high conductivity cold solder. The reported volume resistivity of the silver epoxy is $0.0174 \Omega\text{-cm}$, with a working time of 10 minutes. Similar to many epoxies, the silver epoxy is a 2-stage system, requiring resin and hardener components, which when combined, react chemically to form a cross-linked thermoset polymer. What allows this epoxy to be conductive is the addition of silver particles suspended in the resin and hardener. The volume of silver is sufficient enough to create a conductive connection through the epoxy, thus electrically connecting the joined components. This epoxy mixes with a 1-to-1 ratio of resin to hardener and comes in syringes.

Specimens are prepared to be adhered and then the epoxy is mixed. Once a homogeneous epoxy mix is formed, the epoxy is applied to the carbon fiber and nickel using a wooden applicator. The epoxy is worked into the carbon fiber bundle using the applicator to ensure uniform application. After ensuring that there is enough epoxy to cover the fibers and attach them to the nickel tab, another joint is produced using the same method.

3.4.3 Electroplating

To process the 0.1 inch diameter carbon fiber sleeve, segments are unrolled and straightened from the storage roll. With the end taped to prevent unraveling, a segment is straightened out so that 1.5 inches of free fiber is laid flat on the table. With the aid of guiding marks, a small piece of electrical tape is placed at each end of the 1.5 inch length, leaving 0.25 inches free on both sides. Another piece of tape is placed further down the sleeve to ensure that the carbon fiber does not unbraid and become free fibers after being cut. Once these pieces of tape are in place, the carbon fibers are cut, leaving the 0.25 inches free on both sides of the taped 1.5 inch specimen. Once the 1.5 inch sleeve is cut, it is able to be processed via electroplating. An example of the prepared braided carbon fiber sleeve is displayed in Figure 11.

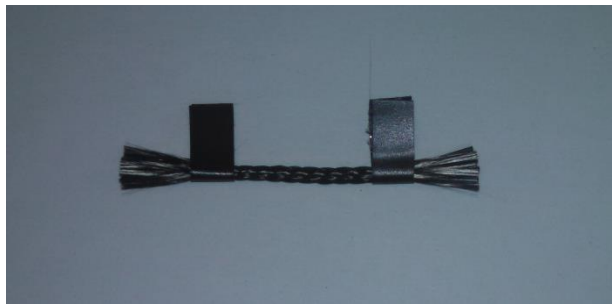


Figure 11 - Prepared 1.5 inch braided carbon fiber sleeve

To prepare the electroplating bath and setup, first fill a glass dish with approximately $\frac{1}{2}$ - $\frac{3}{4}$ inches of Watts nickel plating solution. Watts nickel plating bath is composed of nickel sulfate, nickel chloride and boric acid. The formulation used in this process is Transene Company, Inc.'s Watts Nickel Plating Solution. Place the dish on a hot plate with stirring functionality. Place a small magnetic stir bar (approximately 0.5 inches) into the solution and set the stirring to level 5 of 10. This will provide slight agitation yielding a more uniform

temperature distribution throughout the bath and increased coverage on the carbon fibers. With the agitation, turn on the hotplate to heat the mixture to approximately 130 °F.

While the mixture is being heated to the proper plating temperature, insert the two nickel electrodes into the container. Each electrode is a pure nickel bar purchased from Jemco Jeweler's Supply. Each bar measures 3 inches by 1 inch. These nickel electrodes should be partially submerged in the bath, standing perpendicular to the bottom of the container, and connected to one another electrically. Additionally, the electrodes should be on opposite sides of the dish to ensure a more complete coverage of the carbon fiber sleeve to be plated.

To connect the setup electrically, connect the positive terminal of the power supply to the nickel electrodes. The power supply's negative terminal is to be connected to the carbon fiber segment to be submerged into the plating solution. With the programmable power supply, set the program to 7 Volts for 20 seconds.

Connect the carbon fiber segment to the negative terminal of the power supply by clipping an alligator clip onto the side opposite than the one to be plated. Lower the carbon fiber segment into the nickel plating bath so that a free end is submerged just above the tape used to mark the 0.25 inch free end. The setup can be seen in Figure 12.



Figure 12 - Watts nickel plating setup for braided carbon fiber

Once the solution is at the proper plating temperature, the electrodes are submerged, the solution is mildly agitated, and the carbon fiber sleeve is submerged, the programmable power supply is turned on and the program 7V for 20s program is run.

In this 20 second time frame, the voltage is held at 7V, but the current increases on a milliamp scale. The typical current of the carbon fiber while being plated ranges from 600 mA to 900mA, depending on where the carbon fiber was connected by the alligator clip on the top by the negative terminal. During the processing, bubbles may form on the surface of the carbon fiber. This is normal, but should be avoided to ensure uniform plating. If there are a lot of bubbles, a different voltage or time may be more appropriate for the plating.

At the end of the 20 second plating, a visible semi-bright layer of nickel has been deposited onto the carbon fiber, stopping at the electrical tape marker. Raise the specimen out of the plating bath and disconnect the carbon fiber sleeve from the negative terminal. Reconnect

the sleeve with the unplated free end facing down into the bath. Lower the free end into the bath and repeat the plating procedure.

Once finished, lift the specimen out of the bath and disconnect it from the terminals. Submerge and slightly agitate the specimen in a water rinse bath to help to dilute and remove any Watts plating solution that has wicked into the carbon fiber sleeve. After diluting and slightly agitating the plated sleeve, remove it from the water and place on a dry paper towel to carefully dab dry. To accelerate the drying process, the specimen can be placed in an oven, set to 200 °F for approximately 15 minutes after dab drying to ensure a fully dry specimen. Note: if the specimen is oven dried, remove the electrical tape and use either high temperature tape or handle carefully to avoid the unraveling of fibers. Otherwise, wait until the specimen has dried in before further processing.

3.5 Mechanical characterization

3.5.1 Pull-out testing

Mechanical pull-out testing was performed to characterize the strength of embedded fibers and specimens in the solder ingots. To provide an accurate measurement of these specimens, the ingot was held in place using a metal plate with a hole for the carbon fiber rod or nickel tab to be connected to a chuck. The metal plate is secured to the base of the apparatus to restrict the movement of the ingot when an upward force is applied. The chuck, connected to the force transducer is used to clamp down on the carbon fiber rod or the nickel tab. When the ingot is flush against the metal plate and the specimen is firmly clamped down in the chuck, the specimen is ready to be measured.

The force transducer is an IMADA force measurement system and the distance traveled is measured by a Mitutoyo 272-312-10 vertical Digimatic scale unit with an 8 inch range. The scale unit is able to accurately record movement up to a resolution of 0.01 mm. Prior to recording the measurements, both the scale unit and the force transducer are zeroed by pressing the “zero” buttons on each individual device. When ready to start the measurement, the displacement velocity is set on the IMADA apparatus and the device is started. When the specimen completely detaches from the solder, the device is stopped and the data is processed. Using data acquisition software, the data is imported to Microsoft Excel, where the data is then manipulated to produce graphical displays and comparisons of the data.

3.5.2 Shear bonding testing

The strength of the solder joints was tested using the apparatus in Figure 13. The load cell is connected to a National Instruments DAQ card by which voltage measurements are filtered in Signal Express software to collect data. The load cell is calibrated by using an object of known weight to obtain a voltage reading. In the tests completed, this ratio was 290 mV/kg.



Figure 13 - Solder joint load apparatus with force transducer

Once the strength of the solder joints was enhanced, the load apparatus in Figure 13 was not strong enough to test the interfacial strengths. These specimens were then measured using the IMADA apparatus and the process mentioned in the “3.5.1 Pull-out testing” section. Instead of using the metal plate to hold the specimen down, another chuck was attached to the base, which allowed strong mechanical clamping on both sides of the specimen. When measuring the strengths for the braided carbon fiber specimens, the carbon fiber must be connected to another medium, such as a nickel tab, to be connected to the chuck. Due to the high clamping force that the chuck provides, the carbon fibers are sheared when tightened, and thus do not allow proper testing to be carried out. An image of the setup can be observed in Figure 14.



Figure 14 - IMADA force measurement setup for shear joint testing

3.5.3 Microscopy

3.5.3.1 Specimen preparation

In order to observe detailed images of specimen cross-sections, the specimen of interest has to be prepared in a special manner to be observed under high magnification microscopy. The process involved is called potting, grinding and polishing. Once a specimen to be cross-sectioned is identified and trimmed down, it is placed in a mold to be potted and prepared. Two potting methods were used to take high-magnification imagery of the specimens. The first method involves encapsulating the piece of interest in epoxy, which is degassed in a vacuum chamber and allowed to cure for the required amount of time. The second method involves using a Buehler Pneumat 1 Mounting Press. For this method, a specimen is placed in the cavity, plastic injection molding powder is poured in to encapsulate the specimen, and then the cavity is closed. Heat is then applied to the chamber which the cavity resides, and approximately 550 kPa

(80 psi) of pressure is applied to the encapsulated specimen. Over the course of 7 minutes, the plastic is melted around the specimen. The heating source is removed after these 7 minutes and a heat sink is applied to cool the specimen for another 7 minutes, while remaining under pressure. At the end of this time, the pressure is relieved, the cover removed, and the specimen is ejected from the cavity, ready for the grinding and polishing stages.

To grind and polish these encased specimens, Buehler and Allied High Tech Products devices are used with 240 grit silicon carbide abrasive disks to reduce the encasement to a level of interest in the specimen. Following this stage, 400, 600, 800, and 1200 grit abrasive disks are used in succession to reduce the abrasion on the surface of the specimen. Once the 1200 grit paper is used, the specimen is polished with 1 μ m, 0.3 μ m, and 0.05 μ m alumina polishing suspensions in succession to provide a smooth surface for investigation at high magnifications.

3.5.3.2 Optical microscopy

Polished specimens were observed using a microscope with 6 interchangeable objective lenses for varied magnifications. The magnifications included are 2.5x, 5x, 10x, 20x, 50x, and 100x. Additionally, the microscope includes light settings such as bright field, dark field, and polarization of the light. While color imagery can be beneficial, 100x optical magnification can lead to a lack of overall focus of the image, which leads to using an ESEM for specimen investigation at higher magnifications.

3.5.3.3 Environmental electron scanning microscopy

An FEI Quanta 200 environmental electron scanning microscope (ESEM) was utilized to produce images of specimens that exceeded 100x magnification. This device functions by scanning an electron beam over the surface of the specimen, which interact and diffract,

producing various signals which are interpreted by one of two sensors. These sensors include a backscattered electron detector, also known as a solid state detector (BSE or SSD), and a secondary electron detector, which is also known as a large-field detector (SED or LFD). Since the specimens observed are conductive, they must be grounded and a high-voltage acceleration of 30kV is used to produce the image. Additionally, the spot size can be changed to alter the resolution of the image, but the typical and default size is 3.0.

3.5.3.4 Energy-dispersive X-ray spectroscopy

The environmental scanning electron microscope also includes energy-dispersive spectroscopy (EDS or EDXS) capabilities. This allows the user to focus on a location on a specimen and determine the elemental composition of the point of interest. This functions by measuring the intensity and energy distribution of the X-ray signals generated by the electron beam striking the surface of the specimen.¹⁴

3.6 Electrical measurements

3.6.1 Two-point resistance measurement

Two-point resistance measurements were used during the initial electrical characterization experiments to help gain an understanding of the resistive properties of the specimens. This was accomplished by using a multimeter with resistance measurements and metallic probes. First, the probes are touched together and the resistance measurement is recorded as the inherent resistance of the contacts. Following this step, the specimens were measured by placing the probes in the desired locations and the resistances were recorded. To ensure accuracy, the inherent resistance was checked after several measurements to maintain consistency. To determine the measured resistance, the inherent resistance was subtracted from

the measurement. The multimeters used were able to report results accurately with a 0.1 Ω resolution.

3.6.2 Four-point resistance measurement

An additional technique was utilized to take measurements of the interfacial resistance of the SAC305 solder specimens which have been treated with the Kester 1544 activated rosin liquid flux. The resistance can be more accurately measured using a four-point method, rather than using the two-point multimeter measurement. While measuring the resistances in series, clear results were not observed, and no conclusions were able to be made from the data. Turning to an alternate process of measuring the interfacial resistance, more clear results were found.

Utilizing National Instruments LabVIEW SignalExpress software with a Digital Acquisition Card (DAQ), readings of voltage across the specimen and the current through the specimen were recorded. By connecting the specimen to a power supply and varying the voltage, a voltage and current profile can be created, which can be utilized to calculate the interfacial impedance using Ohm's Law:

$$V = IZ \Rightarrow Z_{DC} = \frac{V}{I} = R$$

Since the applied voltage was direct current, the impedance is simply the resistance R. Upon initial measurements, the impedance values tended toward the value of the shunt resistor, for the setup was not optimized for proper measurement. After correcting the setup, as shown in Figure 15, measurements were taken. The C+, C-, V+, and V- terminals represent the inputs into the DAQ and the 11 Ω resistor is the shunt resistor that SignalExpress uses to calculate the current. Since there was a lot of noise for both the voltage and current readings, an infinite

impulse response (IIR) low-pass filter with Butterworth topology of the second order was applied to the signals with a cutoff frequency of 5 Hz. This filter greatly improved the results and allowed further analysis to be taken.

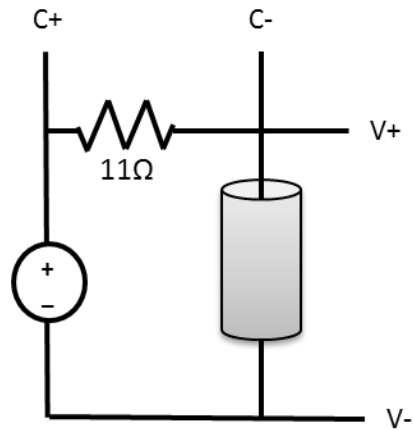


Figure 15 - Electrical schematic of DAQ 4-point resistance measurement of specimen

While manually sweeping the voltage of the power supply, the measurements of the filtered current and voltage across the specimen were taken. The current and voltage readings can be observed in the graph in Figure 16, depicting the inputs versus time.

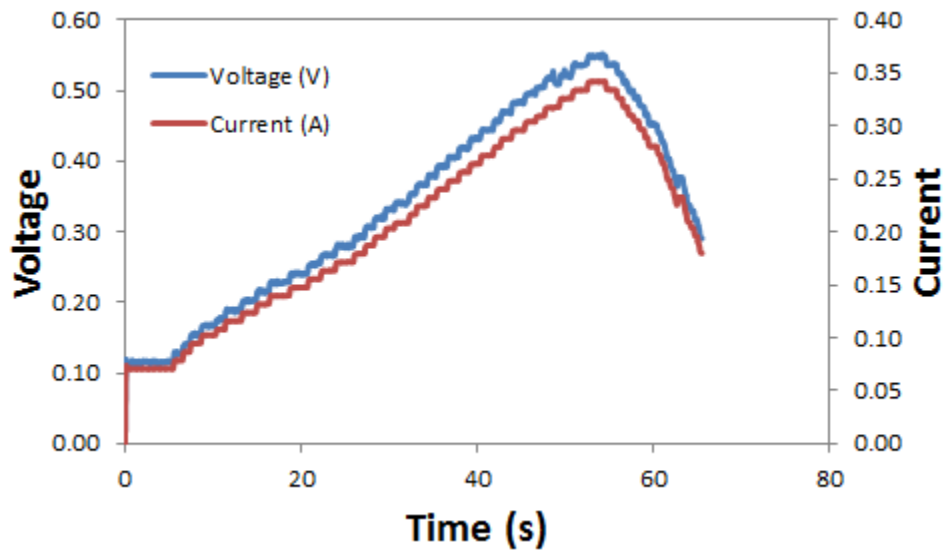


Figure 16 - Voltage and current versus time used for resistance measurement

To improve the previous setup, the shunt resistor has been changed from 11Ω to 100Ω due to a high amount of noise at lower voltages. In addition, to correct this, the cutoff frequency was lowered to 2 Hz from 4 Hz and the IIR filter was raised from a second order to a fourth order filter.

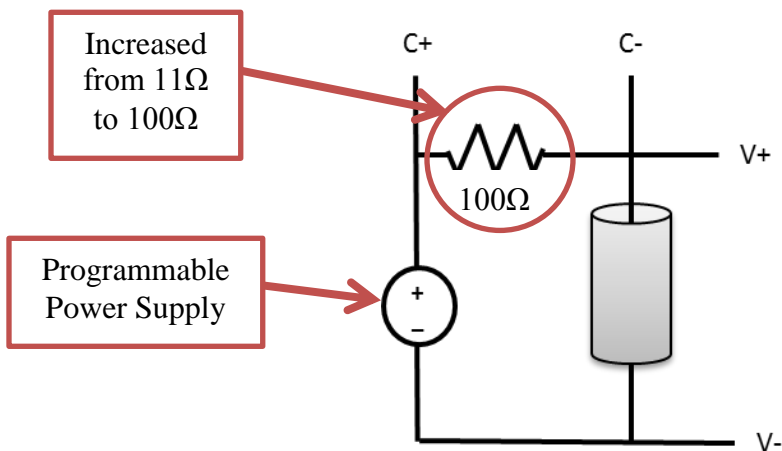


Figure 17 - Revised electrical schematic of 4-point resistance measurement setup to reduce noise and increase repeatability

The physical setup for this can be seen in Figure 19. The positive and negative terminals connect directly to the power supply. In addition, the shunt resistor bridges the “C+” and “C-” connections, as seen in the electrical schematic. The protruding wire on the specimen on the negative terminal has been added to ensure a quality electrical connection to the solder ingot.

Since the resistance is constant, we take a linear trend line and look at the slope of the equation and use the R^2 value to determine how well the trend line fits the data. As demonstrated by the graph in Figure 18, the slope or resistance of the specimen is approximately 1.42Ω . The R^2 value is very high, demonstrating the high conformity of the data to the linear regression. This example is for specimen 3e.

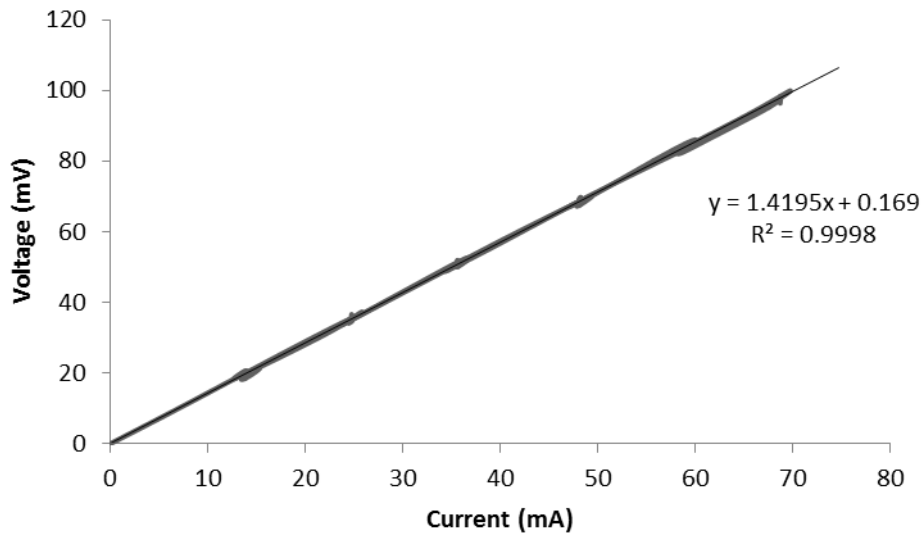


Figure 18 - Voltage versus current of specimen 3e for resistance measurement

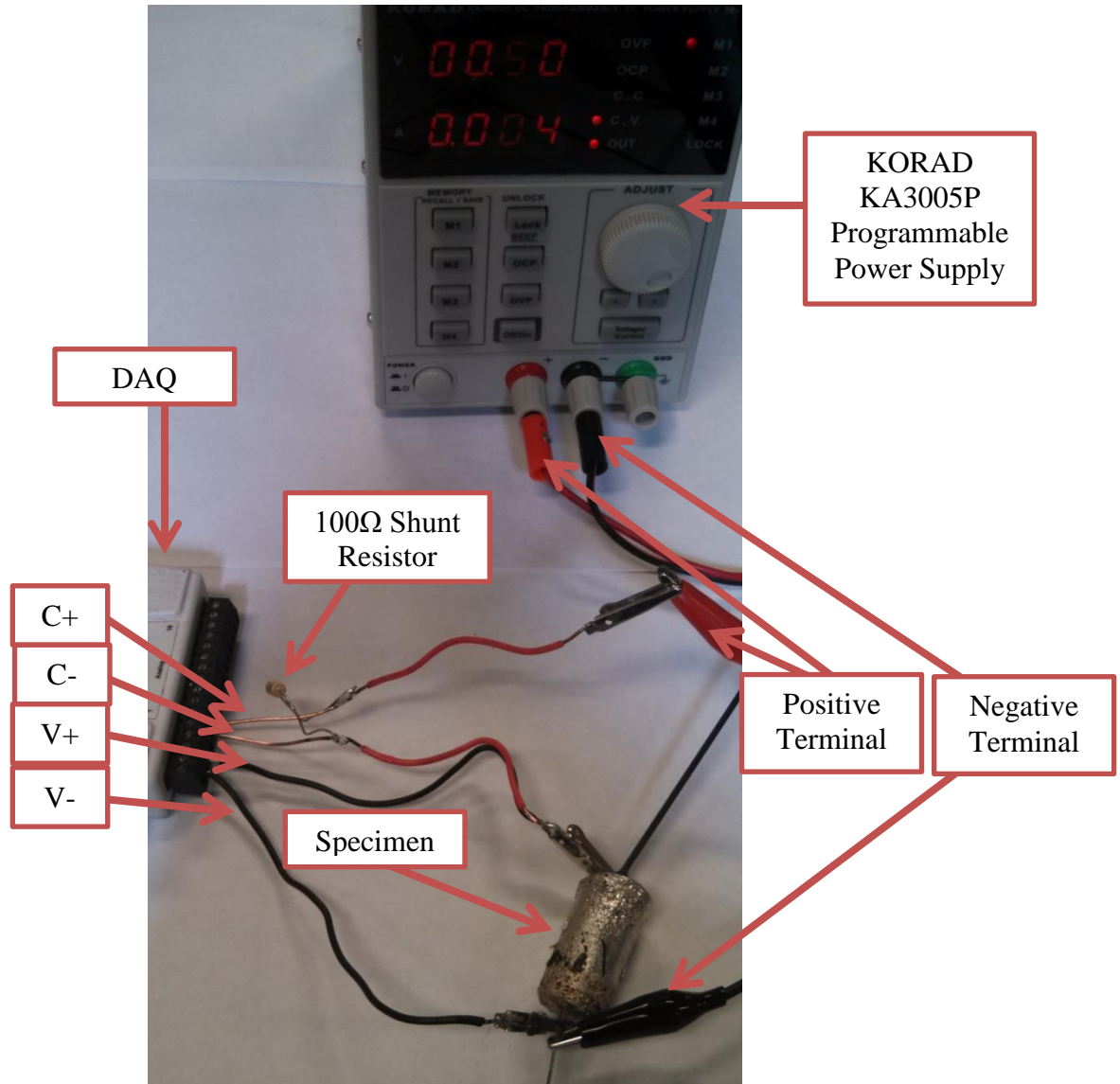


Figure 19 - Physical setup for revised 4-point resistance measurement

Measurements of the filtered voltage and current were taken while altering the voltage and current of the power supply. This was accomplished by programming a set profile that the power supply could follow. An example of current and voltage readings can be observed in Figure 20, depicting the inputs versus time. The electrical loading profile is much more structured and repeatable due to the programming capabilities of the KORAD KA3005P Programmable Power Supply.

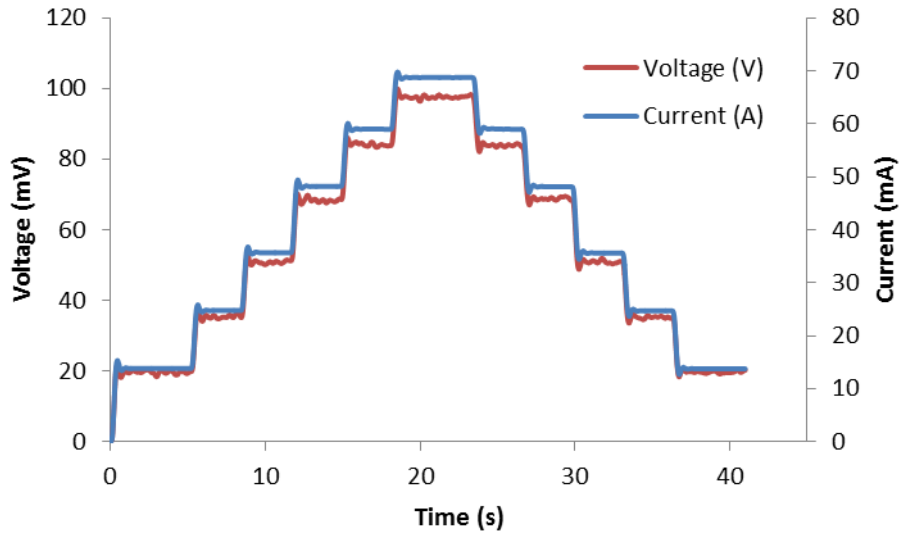


Figure 20 - Voltage and current versus time from improved resistance measurement setup

3.6.2.1 Ring Tongue crimping

A new connection method has been investigated to provide more consistent and uniform contact for measurements. Previously, alligator clips had been attached directly to the pyrolyzed carbon fiber. Figure 21 depicts the two connection methods. Now, electrical wire crimp terminals are being used to maintain consistent and uniform contact to the carbon fiber.

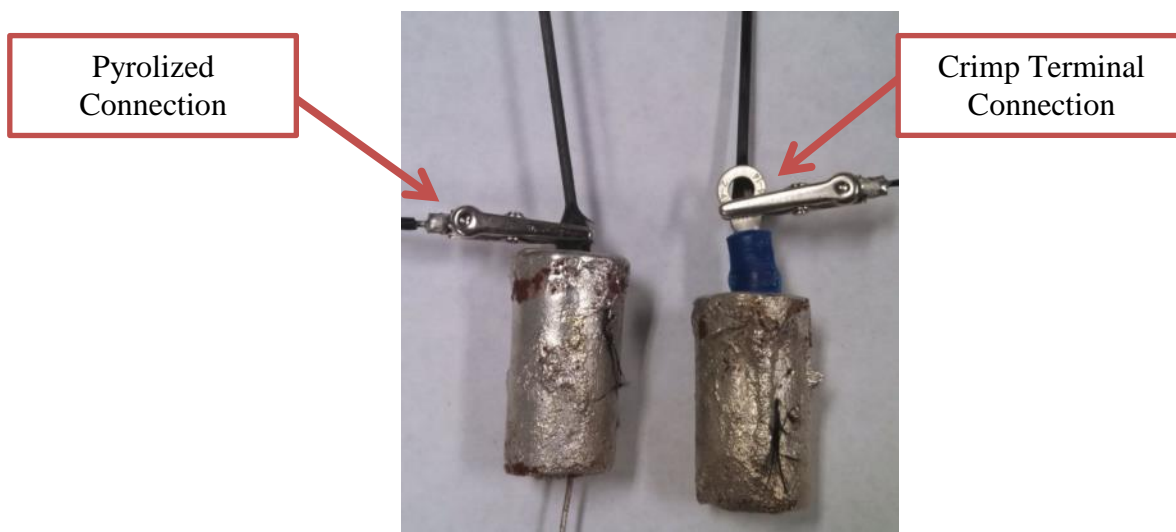


Figure 21 - Visual comparison of alligator clip versus crimp terminal electrical connections

First, the crimp terminal is slipped over then end of non-pyrolized portion of the carbon fiber rod protruding from the solder ingot. The terminal is then moved as close to the top of the solder ingot as possible. Once the crimp is in position, an electrical multi-tool or set of crimping pliers is used to crimp the terminal onto the pyrolized portion of the carbon fiber rod. To ensure proper connection, the terminal is crimped firmly in the middle, then again on the top and the bottom of the insulating sheath.

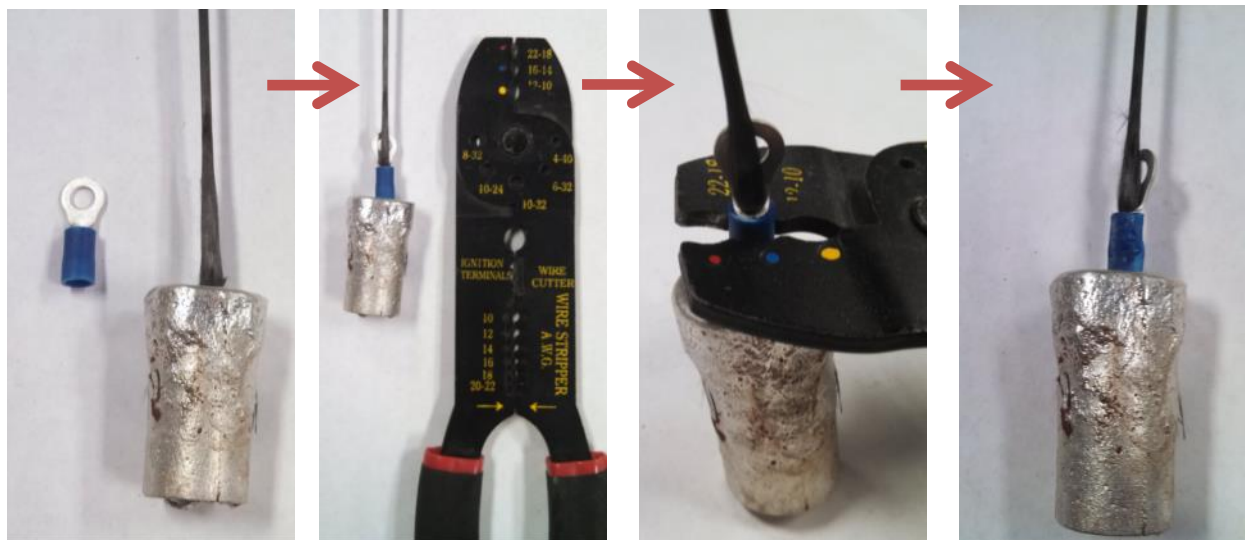


Figure 22 - Process of connecting ring-tongue crimp connection to pyrolized portion of specimen

3.6.2.2 Milliohmmeter resistance

In order to further characterize the nickel specimen resistances and to qualify the resistance measurements taken from the power supply and DAQ setup, the various nickel specimens were measured using an Agilent 4338B Milliohmmeter. The milliohmmeter uses a 4-point measurement by subjecting the specimen to a determined current load and measuring the voltage drop between the two voltage leads. Before using the measurement system, the terminals are shorted and the system is calibrated to account for internal resistances.

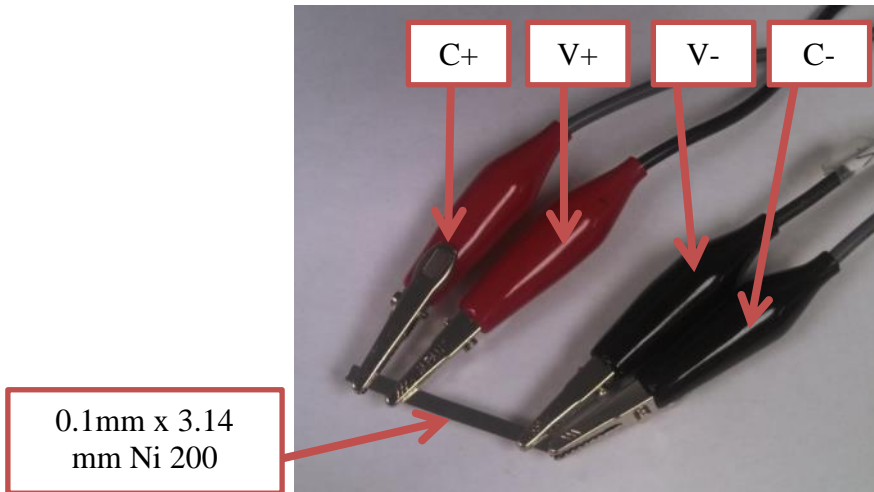


Figure 23 - 4-point resistance measurement of nickel 200 tab using Agilent Milliohmmeter

The settings used to take measurements consisted of automatic current level selection and the averaging of 16 measurements to provide the displayed resistance measurement. While taking measurements, the current terminals are left stationary at the ends of the sample, while the negative voltage lead was moved closer to the positive voltage lead. The distance measurements were taken between the closest parts of the two voltage leads.

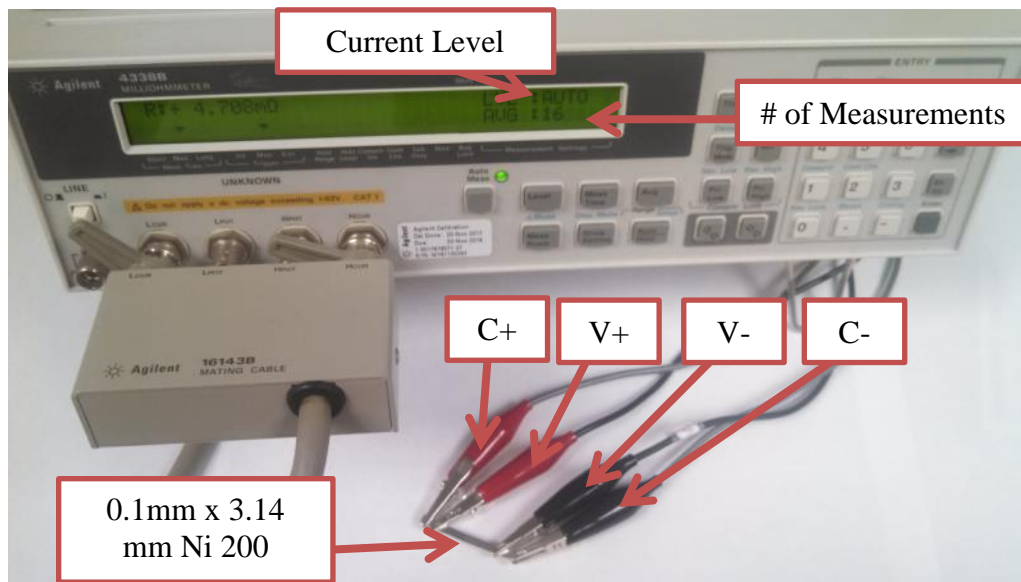


Figure 24 - 4-point resistance measurement of nickel 200 tab using Agilent Milliohmmeter

Chapter 4: INITIAL EXPERIMENTS

4.1 Uncoated pultruded carbon fiber

4.1.1 Mechanical characterization

4.1.1.1 Pull-out testing

The following specimens, displayed in Figure 25, are uncoated pultruded carbon fibers, which have been embedded approximately 1 inch into the SAC305 solder ingots using the sand casting technique.

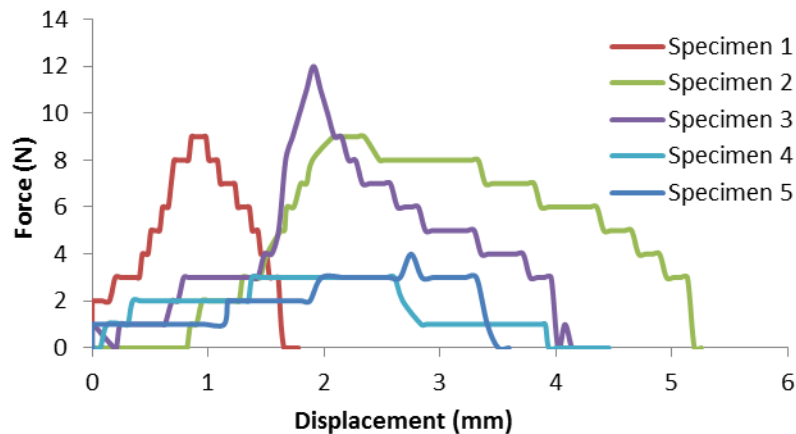


Figure 25 - Force versus distance for pull-out testing of uncoated pyrolyzed pultruded carbon fibers

The pull-out results demonstrate inconsistent failure profiles, which indicate the adhesion properties of the uncoated and pyrolyzed carbon fibers in the solder ingots. The forces incurred by these specimens have a maximum of 12 Newtons, which is not significant enough to act as a functional solder joint. In addition, after failure, it can be observed that there is mechanical resistance during the removal of the specimen. Instead of an abrupt failure and reduction of the force to zero after the maximum load, the loading profile decreases at a rate indicative of some adhesion.

4.1.1.2 Nickel tab connection

Mechanical test specimens were made by physically soldering the crimped pyrolyzed carbon fiber rods to crimped nickel tabs. The connection is very fragile and breaks with little bending in a similar manner to the joints made by soldering to the nickel tabs of lithium-polymer batteries. The weak adhesion of the carbon fiber-nickel tab connection was qualitatively evident by the difficulty in soldering the joint due to the lack of wetting. This resulted in very poor quality connections, which is evident by the lack of fiber adhesion displayed in the picture of the mechanical test specimen provided in Figure 26.



Figure 26 - PVD nickel plated carbon fiber soldered to nickel tab

4.1.1.3 Microscopy

Both the optical and ESEM microscopy results displayed in Figure 27 clearly indicated the formation of copper-tin (CuSn) intermetallic particles in the solder matrix, which was confirmed by EDXS elemental analysis. Furthermore, these particles, which have dendritic morphologies, were found to be of much finer size near the interface, ranging from approximately 10-50 microns in the matrix to below 10 microns near the interface. Given the high thermal conductivity of the carbon rod relative to the melt, it is hypothesized that there is a

“quenching” effect that the rod provides to the melt acting as a “fin” to remove heat more rapidly from the core.

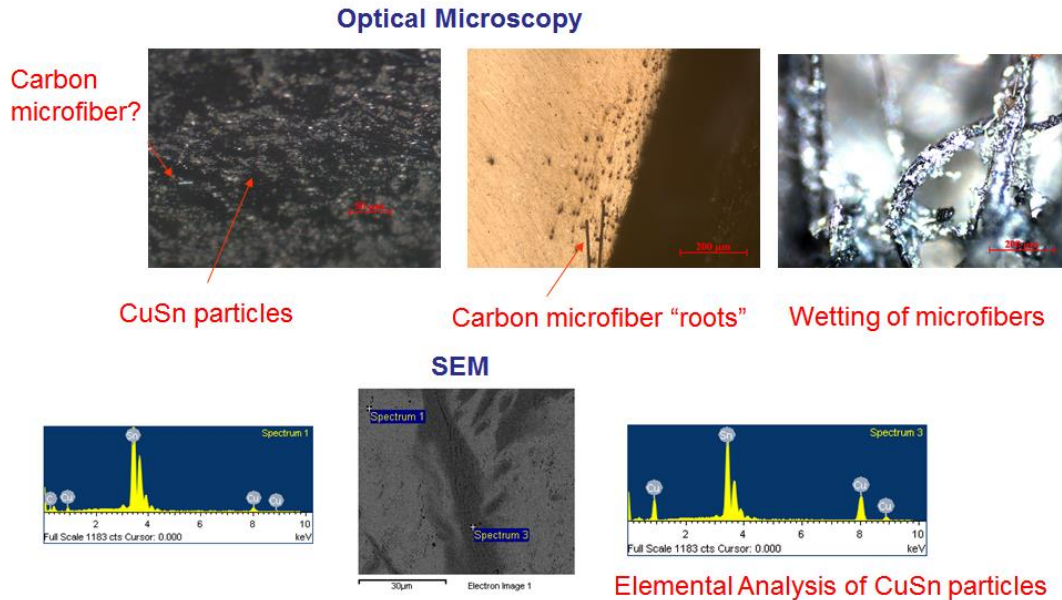


Figure 27 - Optical and ESEM microscopy images of carbon fibers with EDXS analysis

Furthermore, there was additional evidence of adhesion mechanisms consisting of “wetting” of the microfibers by the solder melt, and the “rooting” of the pyrolyzed carbon fiber into the melt by individual microfibers. It is the prevalence of these mechanisms that appear to give rise to the increase in the interfacial strength, and therefore is a candidate for further investigation to improve the mechanical properties.

The cross-section which was used to image the specimen can be seen in Figure 28. From this image the “flaying” of the pyrolyzed end of the carbon fiber is clearly evident. Furthermore, it has “mesoscopic” structure that further enhances the interfacial strength through a larger volume for the “rooting” effect attributed to enhanced mechanical interlocking. For purposes of this investigation, the geometric aspects of this flayed mesoscopic structure will be ignored and

the diameter of the unpyrolized fiber will be used for all calculations. Clearly, there could be an additional characterization component where the “effective diameter” of the flayed fiber can be determined from the extent of the flaying and used to compare the variation in strength with the diameter, however it would not be used in any calculations.

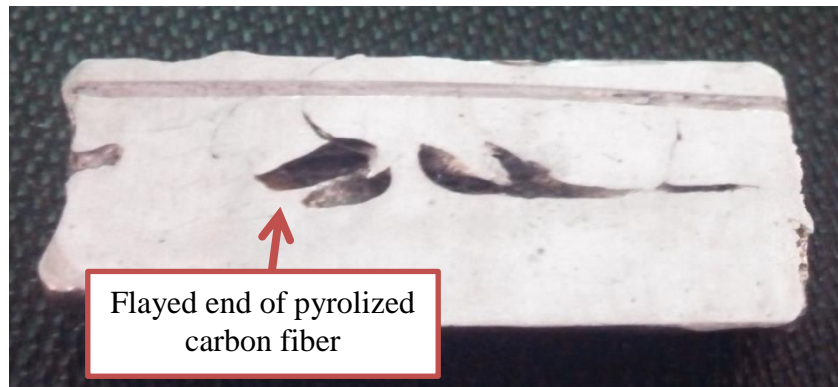


Figure 28 - Cross section of SAC305 solder ingot with non-flux-treated pyrolized carbon fibers

4.1.2 Electrical characterization

The tests and results indicated in Figure 29 demonstrate that the open mold produced a low resistance of 9.4 ohms, but that the lowest resistance of 3.1 ohms was found using the fresh solder in the sand cast mold. Furthermore, there was strong position dependence of the resistance on unpyrolized surfaces of the fibers. 6 different positions were tested where the variation in position was approximately 25 mm relative to the carbon fiber-solder base of the specimen. These indicated that the inherent resistivity of the carbon fiber was quite high. In contrast, a copper-solder specimen was prepared which showed no measurable variation in resistance with length and had an inherent interfacial resistance of 0.6 ohms.

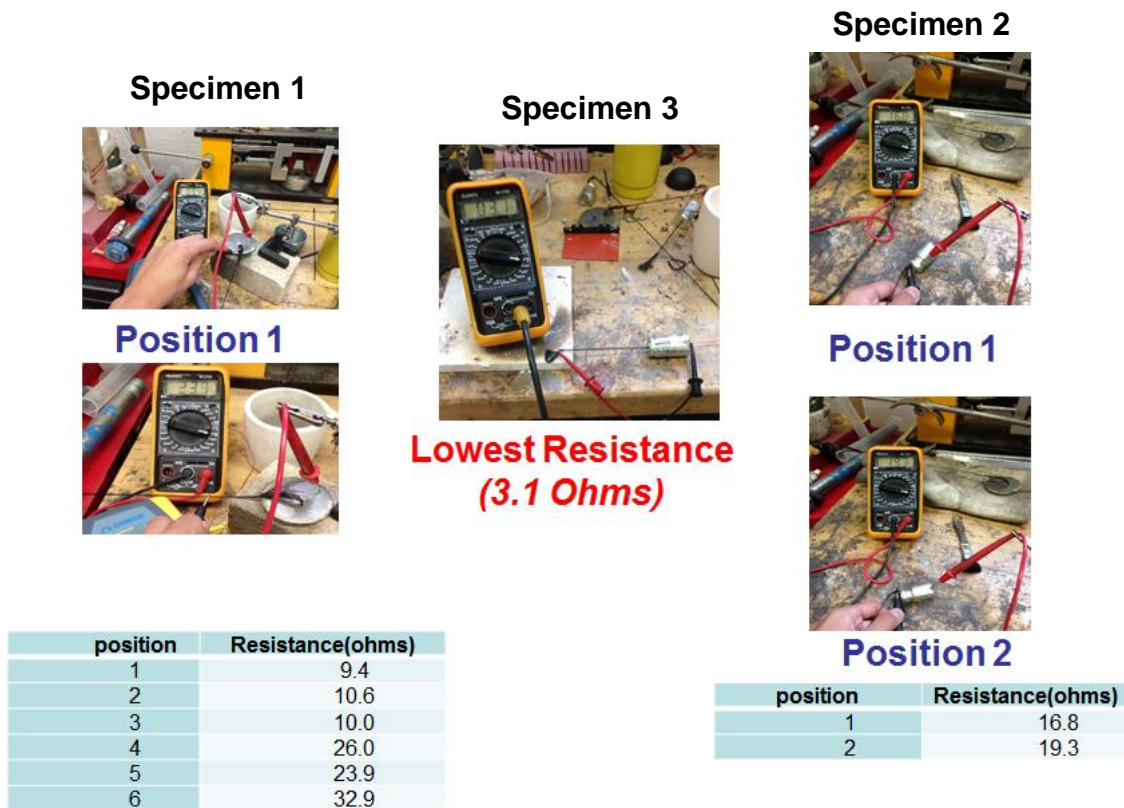


Figure 29 - Resistance measurements of pultruded carbon fibers with varying measurement positions

To characterize the pultruded carbon fiber rods used throughout the experiments, measurements were taken to understand the resistance profile for pyrolyzed and unpyrolyzed 0.075 inch pultruded carbon fiber rod, which have been recorded and displayed in Figure 30.

The unpyrolyzed rod demonstrated resistances that initially became larger with length, then started fluctuating. Each trial performed demonstrated similar results at the same lengths. While the assumption was that the resistances would increase linearly, this was not seen with the unpyrolyzed rod. In fact, the resistance appears to oscillate around 20 W. An explanation for this behavior may be due to the contact area between the various outside layers of the carbon fiber rod and the contact leads. Since the fibers are held together by epoxy, there is most likely an insulating epoxy barrier around the fibers. At lengths up to about an inch, the resistance may be coming solely from the continuous fibers on the surface of the rod (that are being contacted by

the leads). Reason for the decrease in resistance at longer lengths could be due to crossing of fibers within the rod, creating more pathways for conduction. The longer the length of rod measured, the higher probability that fibers will be crossed with others, providing more pathways of flow, thus reducing the resistance.

The fully pyrolyzed rod demonstrated the results that we were initially expecting. The two tests were very consistent and the progression of resistance vs. length was very linear. After averaging the results of the two tests, the R^2 value was 0.994, demonstrating the high conformity to the linear regression. The regression trendline indicates that the fully pyrolyzed rod increases approximately 0.240 Ω /in with a y-intercept of 0.269 Ω , which is near identical to the resistance that was measured for the solder. Therefore, it appears that the inherent resistance of the interface is negligible for the carbon-metal connection, and that the resistivity of the pultruded carbon rod is much higher than for the solder. Based on the packing fraction of 0.67 provided by the supplier and the diameter of rods used in these experiments (2 mm instead of 1 mm), the inherent resistivity of the carbon microfibers is calculated to be 2×10^{-5} Ω -m which is typical of graphite along the c-axis of the unit cell.¹⁵

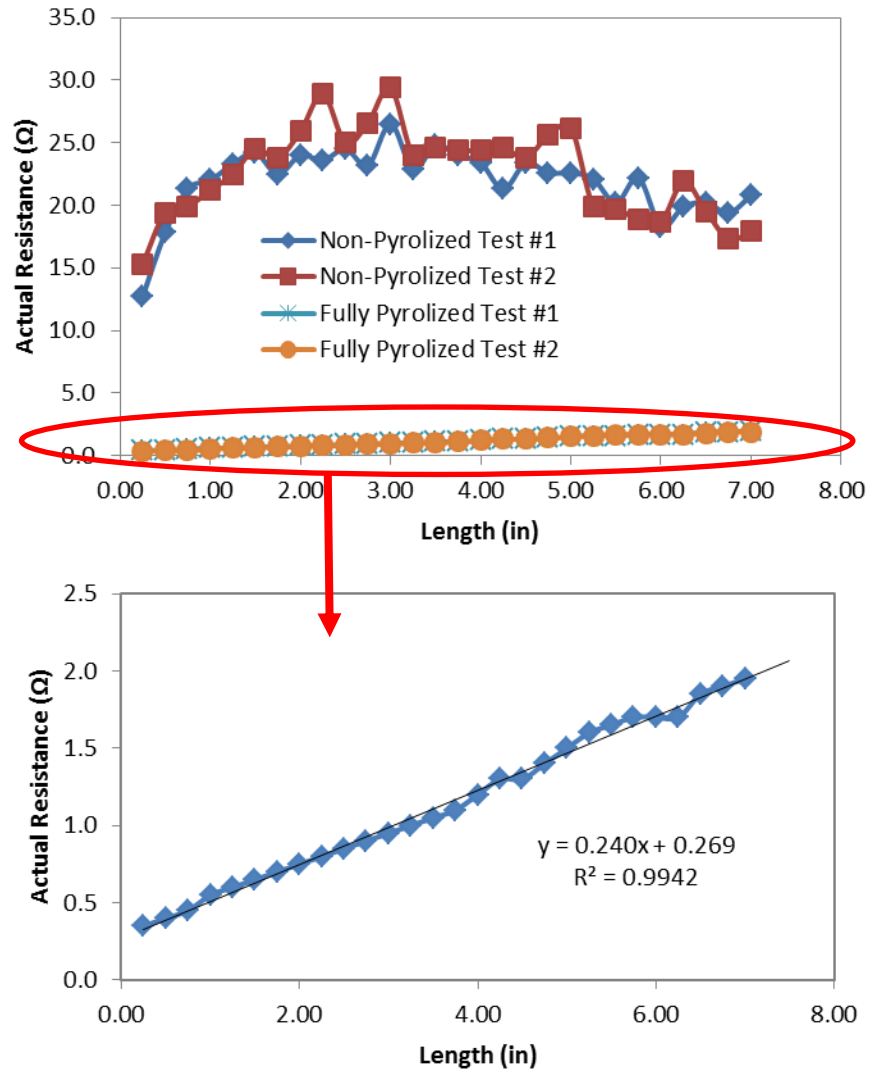
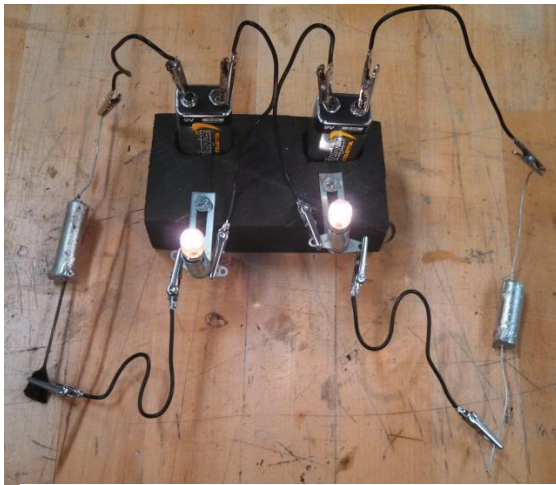


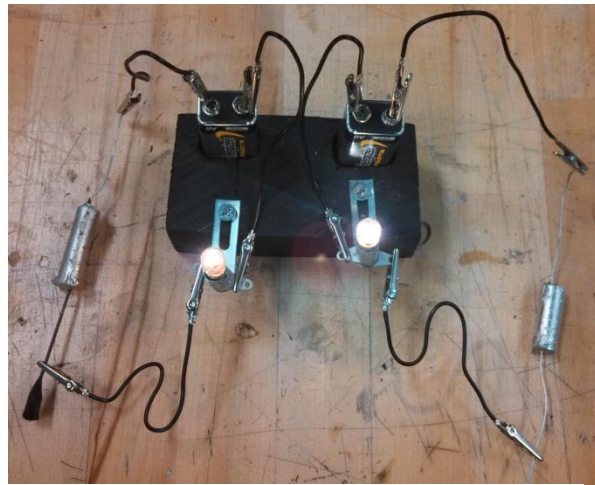
Figure 30 - Resistance versus length of pyrolyzed and non-pyrolyzed carbon fiber specimens

Additional demonstrations of the practical electrical and mechanical performance of the carbon-metal junctions can be seen in Figure 31. Both pyrolyzed and unpyrolyzed surfaces of the carbon rod demonstrated enough conductivity to be used to power a small 4 watt light bulb with a 9V battery. However, they were clearly less intense than when an Al-Cu alloy was used in place of the carbon fiber, with the pyrolyzed surface being more conductive than the unpyrolyzed. To further demonstrate the difference between the conductivity of the pyrolyzed and unpyrolyzed

carbon fiber, temperature readings were taken of the bulb after it was left on for five minutes. The unpyrolized conductor yielded a bulb temperature of 95°F, while the pyrolized conductor yielded a temperature of 106°F. For the Al-Cu alloy it was nearly identical to the pyrolized carbon fiber. Therefore, the performance of the pyrolized carbon-metal interface was found to be similar to that of a common metal wire.



Pyrolized Pultruded Carbon Fiber



Pultruded Carbon Fiber

Figure 31 - Electrical circuits using both pyrolized and non-pyrolized pultruded carbon fiber rods

4.2 Kester 1544 flux coated carbon fiber

4.2.1 Mechanical characterization

4.2.1.1 Pull-out testing

The graph in Figure 32 compares the load profiles of samples 3B and 3C. The carbon fiber rod in 3B was fully immersed in the SAC305 solder, while the 3C sample was not fully immersed. Despite having unadhered fibers, the maximum force incurred by specimen 3C was greater than that of 3B. In addition to having a greater maximum force, it is evident that the flux

adds in an additional mechanism of failure, such as the flux adhesion or friction. There is much more energy required to achieve complete failure within the specimen with the liquid flux applied. While both specimens reach the first failure mode at 2.5mm or less of displacement, 2B completely fails around 4mm, while 3C fails around 29mm. Calculating the area under the curves yields an energy of 0.0169 J for 3B and 0.2658 for 3C, a 15.7 times increase in work done until failure.

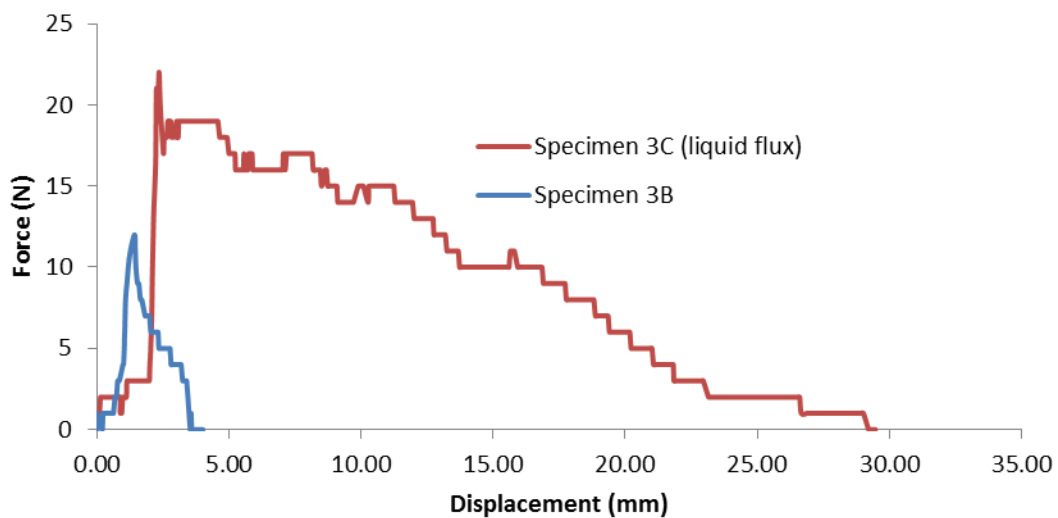


Figure 32 - Force versus displacement of flux treated and non-flux treated carbon fiber specimens

The following graph, displayed in Figure 33, compares the force vs. displacement curves for the set of hollow-core carbon fiber rods, dipped in the Kester 1544 flux. Each specimen demonstrates the additional failure mechanism, which requires more energy to induce a total failure in the specimen. Compared to previous testing, these results demonstrate overall higher resistance to failure at higher loads. Other failure mechanisms may also be present in these samples. It can be observed in the curves that the specimens display abrupt decreases in force at several points during loading, especially close to the maximum load. At these times during loading, loud cracking can be heard, which may suggest the failure of the carbon fiber roots

(which would mean the limiting interfacial force was being reached) or abrupt changes in the flux adhesion.

Since specimen 5C was completely immersed in the solder, it would support the idea that the limiting interfacial force was being reached because the individual carbon microfibers were reaching their ultimate tensile strength. However, based on the mechanical properties and structure of the pultruded carbon fiber rods, it is estimated that the rods should have a limiting load of approximately 1962 N. Therefore, it is highly unlikely that the upper limit of the interfacial force is being reached.

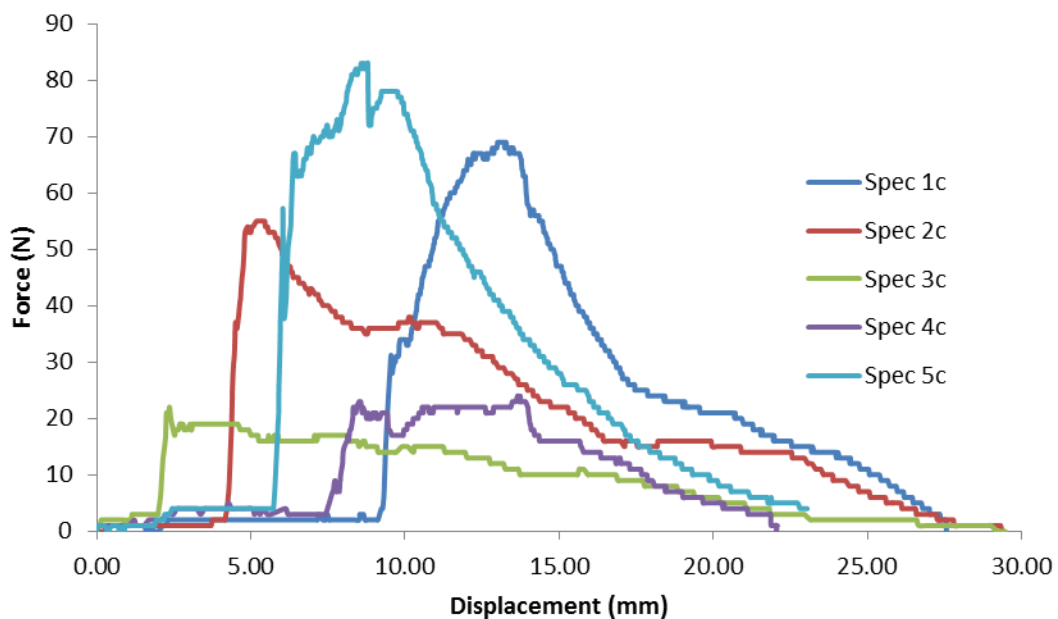


Figure 33 - Force versus displacement of flux treated hollow-core carbon fiber specimens

A final comparison can be made between the hollow-cored specimen with the highest load (5C) and a solid-cored specimen (6C). The force versus displacement curve can be seen in Figure 34. Calculating the energy of each of the specimens, 5C required 0.632 J until ultimate failure, while 6C required 1.892 J until ultimate failure. This was an increase of 3X the energy

required for ultimate failure between these two specimens and about 3.6X the maximum load. The increase in load and energy is also consistent with the increase in the amount of individual carbon microfiber surface area for the solid rods, which would be approximately 33% more than the hollow rods, but not completely. This would tend to indicate another mechanism that is enhancing the pullout strength of the solid carbon fiber rods. Thus, the Kester 1544 activated rosin liquid flux combined with solid carbon fiber rod seems to be a promising avenue to investigate.

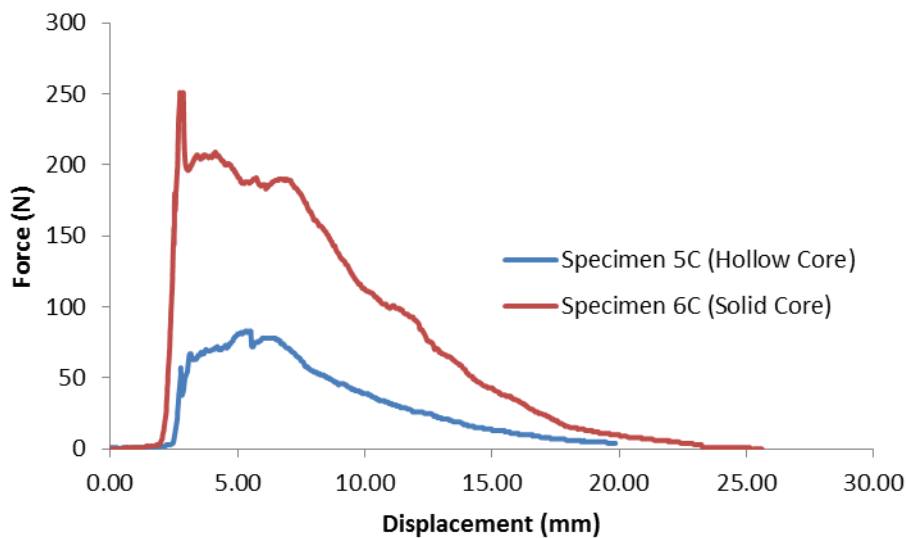


Figure 34 - Force versus displacement of flux treated hollow and solid-core carbon fiber specimens

4.2.1.2 Microscopy

While utilizing the Environmental Scanning Electron Microscope on a specimen of extracted carbon fibers after pull-out testing, fracturing of the carbon fiber can be seen in Figure 35. This provided clear evidence that the loads achieved with the enhanced adhesion reported previously were reaching the tensile limits of some of the fibers. Also, Figure 36 is an ESEM image of the wetted solder on the surface of the carbon fibers. EDS analysis was performed on

the point of interest identified as “Spectrum 2,” confirming the presence of tin and copper which, in addition to the previous optical micrographs, provides confirmation the presence of the copper and tin in the solder wetted on the carbon fibers. Although there is presence of wetting, it is not very prevalent, and does not provide much mechanical advantage without the presence of intermediate additives.

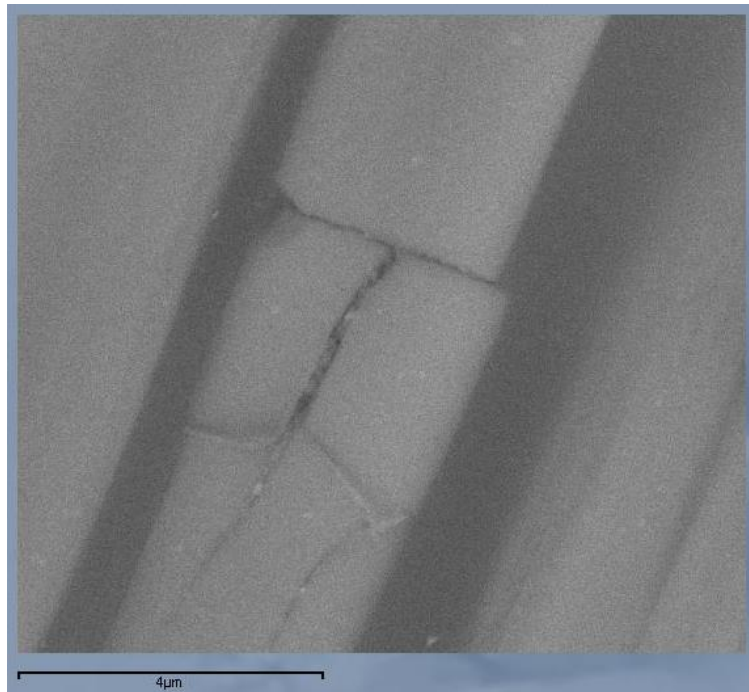


Figure 35 – ESEM image of fracture of carbon fiber after loading

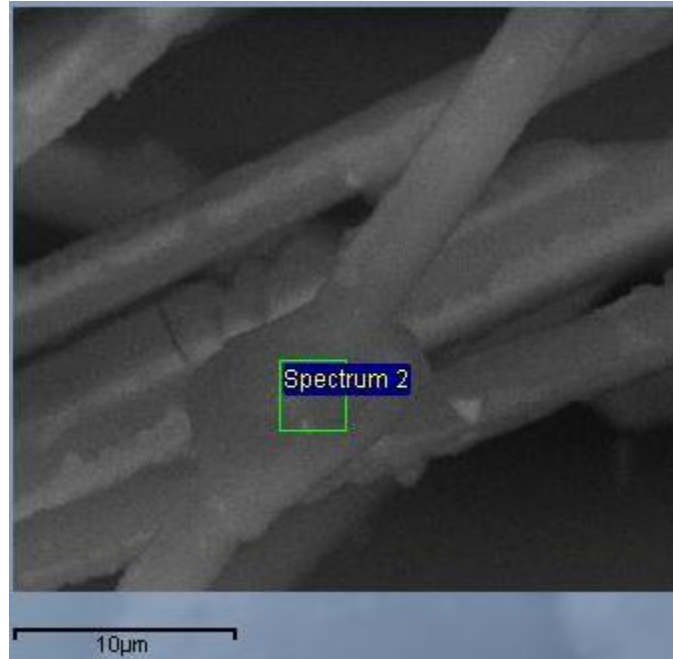


Figure 36 – ESEM image of evidence of solder wetting on carbon fiber

4.2.1.3 Battery connection

Attempts were made to solder the ends of the pyrolyzed carbon fiber to the tabs of the lithium-ion batteries. The inherent issue with the carbon fiber to metal connection is apparent. It is difficult to get the carbon fiber to wet with the solder. The soldered connections are shown in Figure 37.



Figure 37 - Carbon fiber soldered onto a lithium-ion battery for electrical testing

The use of Kester 1544 activated rosin flux facilitates the soldering process and appears to improve the mechanical strength by improving the adhesion of the carbon fiber strands to the nickel tab. However, due to the poor wetting properties between the carbon fiber and nickel surface, a large amount of solder is required to form a joint. The joint formed is very fragile and will break off with little force, such as prodding the joint with a fingertip.

Additionally, the large volume of solder required to create functional joints provides another inhibition to practical usage. By flowing large amounts of melted metal, the heat must dissipate. The nickel tabs on the battery can act as heat sinks if the surface is heated too long. This can damage the battery components and internal chemistry if too much heat is provided.

4.2.2 Electrical characterization

As demonstrated by the graph in Figure 38, the slope (resistance) of the specimen is approximately 1.61Ω . The y-intercept is nearly zero, and the R^2 value is very high, demonstrating the high conformity of the data to the linear regression. The measured resistance is a 2x improvement over previous specimens manufactured using the only the borax flux.

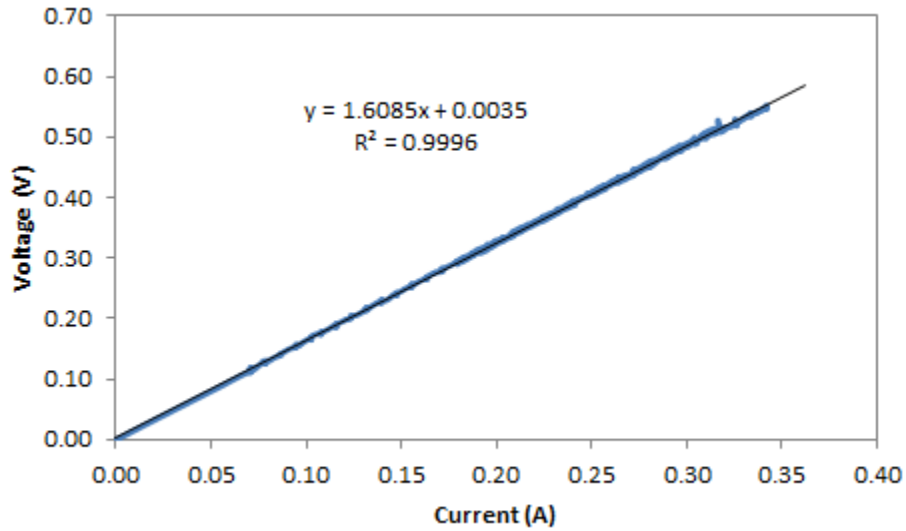


Figure 38 - Voltage versus current of specimen from 4-point resistance measurement

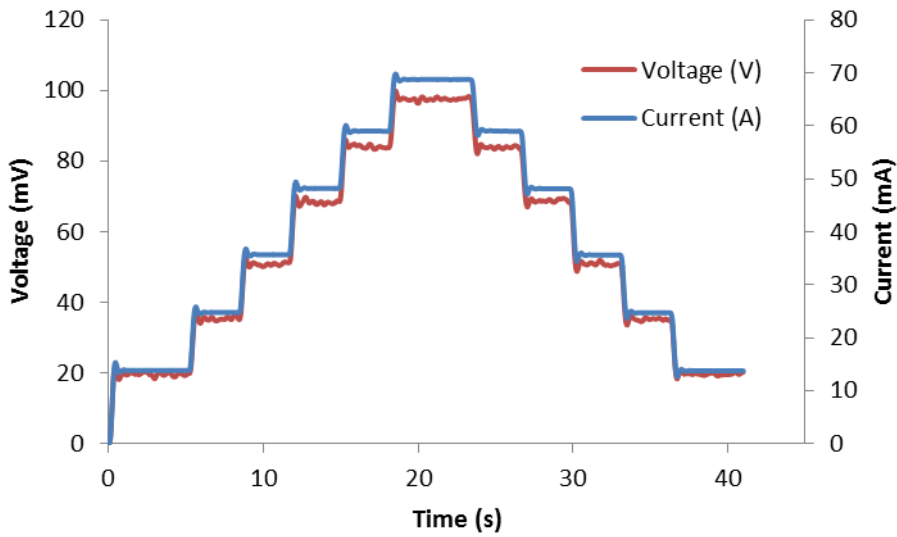


Figure 39 - Voltage and current versus time plot of specimen from 4-point resistance measurement

Since the resistance is constant, taking the linear trendline and observing the slope of the equation indicates the resistance. Additionally, the R^2 value is used to determine how well the trendline fits the data. As demonstrated by the graph in Figure 40, the slope or resistance of the

specimen is approximately 1.42Ω . The R^2 value is very high, demonstrating the high conformity of the data to the linear regression. The specimen used in these tests is specimen 3e.

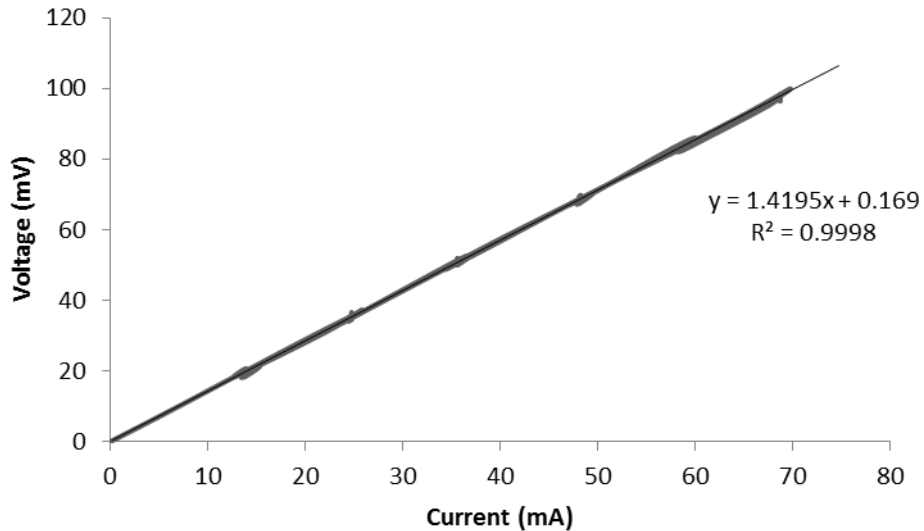


Figure 40 - Voltage versus current of specimen 3e during 4-point resistance measurement

Specimen set E utilized the same processing techniques of using borax flux with the SAC305 solder melt and the Kester 1544 activated rosin liquid flux dipped pyrolyzed carbon fiber rods. A sample of this data has been displayed to identify a verification of the material interfacial resistance.

For additional electrical characterization, the resistance was measured along with time, current, and voltage for each specimen. The profiles of specimen 3e can be viewed in Figure 41 through Figure 43. These plots demonstrate that the resistance remains constant along the tested current and voltage ranges. Although abnormal behavior is noticed incrementally as the voltage and current increases (as marked on the Resistance vs. Current/Voltage graphs in Figure 41 and Figure 42), the phenomena can be attributed to the step increases of the power supply interacting with the data collection filters. The behavior is accentuated at the lower voltages and currents

and this can be seen on the left and right sides of the Resistance vs. Time graph in Figure 43, where lower power is incurred by the specimen.

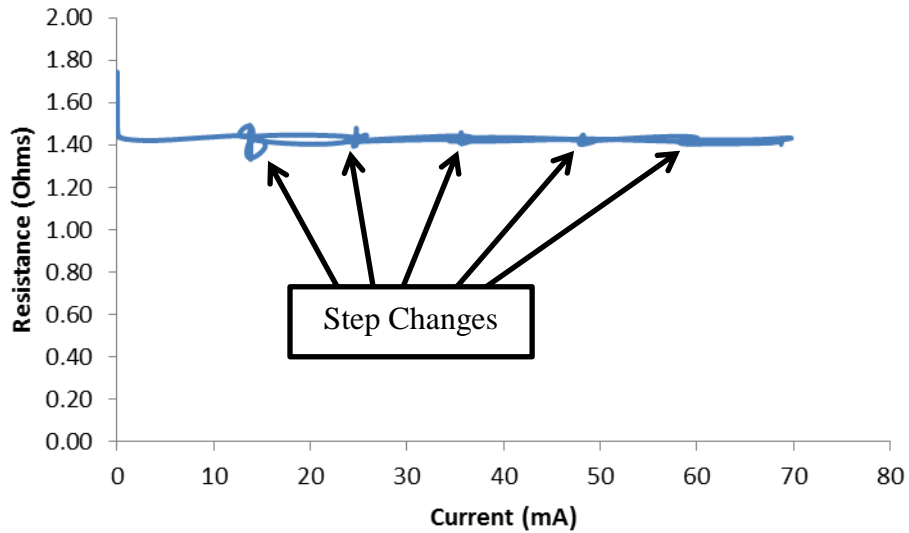


Figure 41 - Resistance versus current of specimen 3e with step change locations indicated

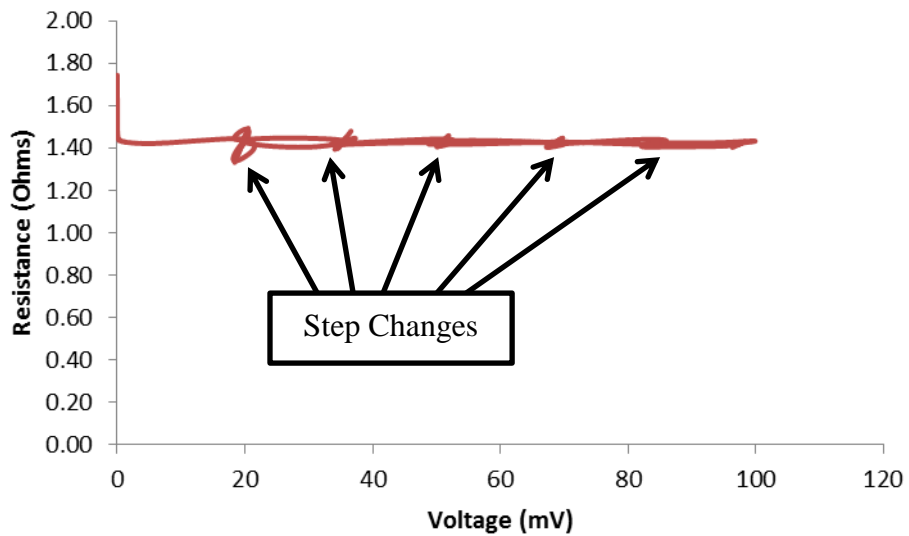


Figure 42 - Resistance versus voltage of specimen 3e with step change locations indicated

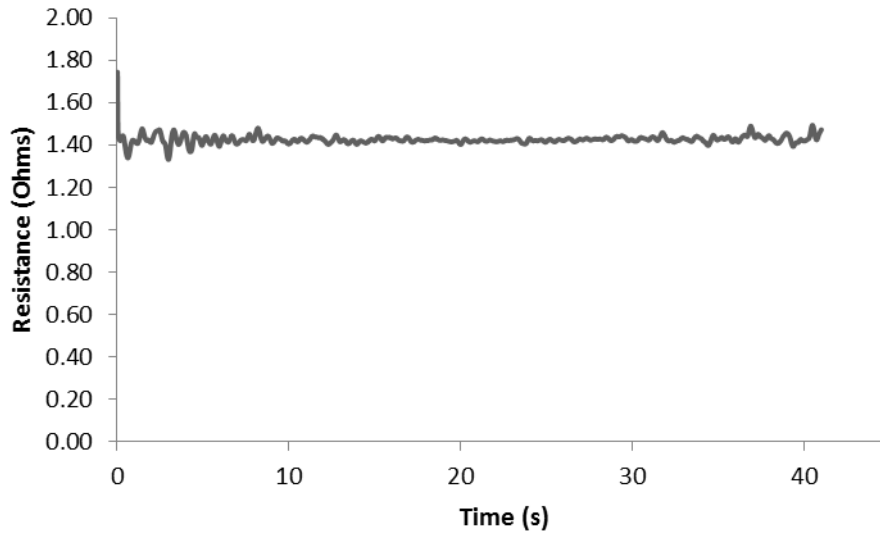


Figure 43 - Resistance versus time of specimen 3e during 4-point resistance measurement

While previously, analyzing the data exported from SignalExpress proved to be very time consuming, a macro was developed with additional Visual Basic programming to greatly improve the processing time of the exported data. It is no longer as time prohibitive to run multiple trials on the same specimen to compare the data and confirm consistency. With the programmable linear power supply, an additional element of consistency has been added by taking measurements with the same current/voltage loading profile for each test.

To measure the consistency of the data, Specimen 3e's voltage and current profile was altered and the same readings were taken again. With the current configuration, the profiles at lower currents/voltages yield a noisier response, which gives the impression of inconsistent data. The following graph in Figure 44 depicts the voltage and current profile of the lower power readings. It can be seen that the voltage provides a noisier response than the current. This mismatch accounts for the abnormal graphic response of the Voltage vs. Current graph in Figure 45.

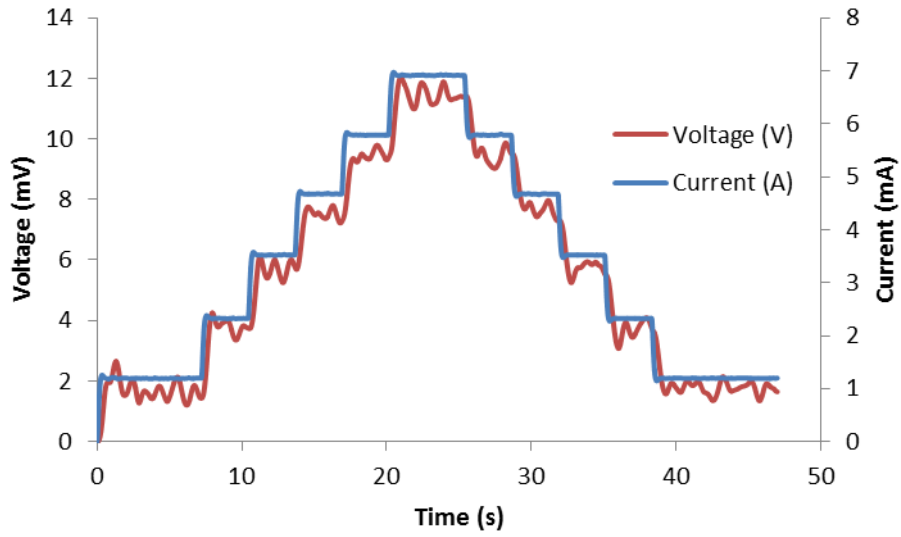


Figure 44 - Voltage and current versus time plot of specimen 3e from revised 4-point resistance measurement

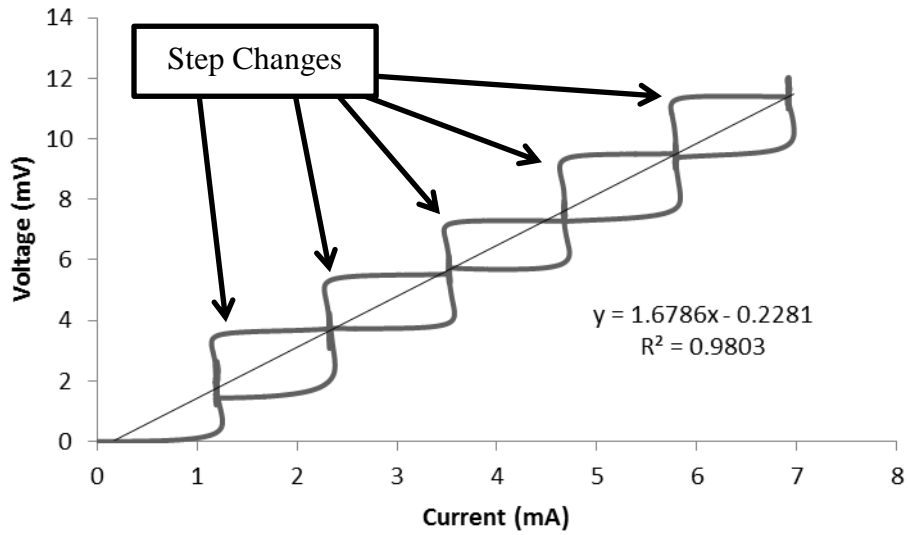


Figure 45 - Voltage versus current of specimen 3e with step change locations indicated

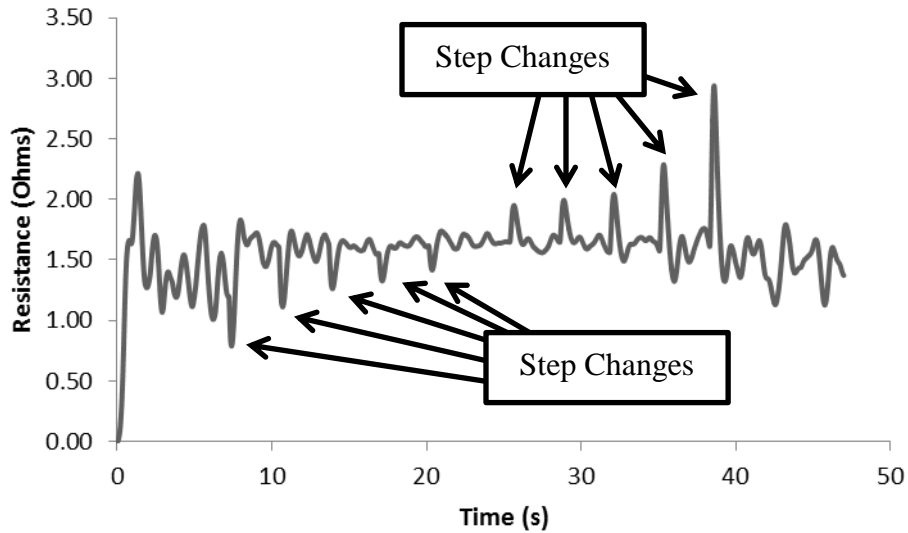


Figure 46 - Resistance versus time of specimen 3e with step change locations indicated

The step changes have been indicated on the graphs. These show that the graphic abnormalities are due to the noisiness of the voltage and primarily the step changes. While all of the points are connected on the Voltage vs. Current graph, the majority of them are during periods of constant voltage and current. Since they are connected, this is more difficult to see. Running a linear regression to take the step changes into account, we see that the voltage is within the same range as done at the higher power profile. The conformity of the linear regression provides an R^2 value of 0.98, which demonstrates high conformity despite the visual abnormality.

4.2.2.1 Mechanical crimping of carbon fiber

The electrical performance data was plotted before and after the application of the crimps. This was accomplished by taking three separate measurements of the specimen, using the current profile demonstrated in Figure 47.

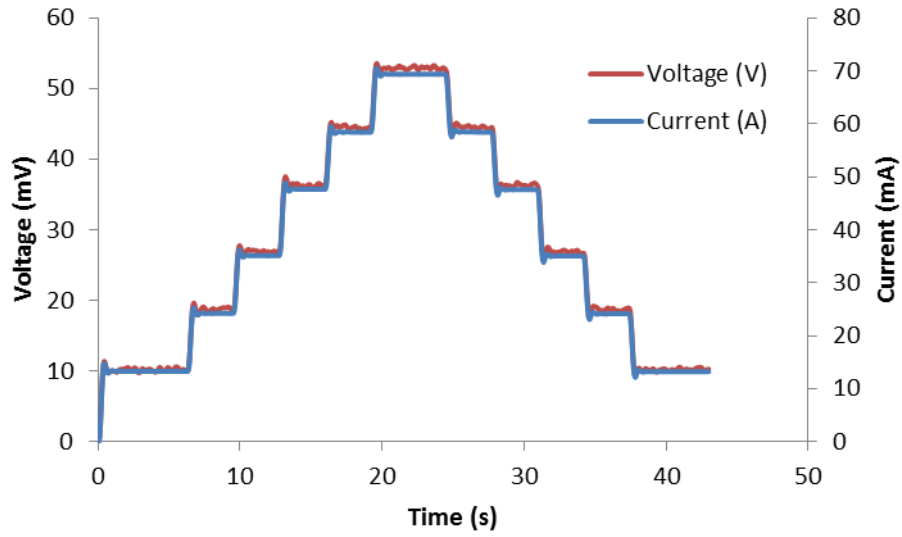


Figure 47 - Voltage and current versus time profile used for evaluating crimped carbon fiber resistances

After each measurement, the specimen was disconnected and reattached to the 4-point measurement setup, as provided in Figure 48.



Figure 48 - Visual display of crimp tab connection on pyrolyzed section of carbon fiber specimen for electrical characterization

Once all three measurements with the bare carbon fiber were taken, the metal terminals were crimped onto the base of the CF, as demonstrated in Section 3. It should be noted that the crimps were not in contact with any part of the solder ingot and were only in contact with the pyrolyzed carbon fibers.

The resistance trials of one specimen that was measured can be seen in Figure 49. The first chart is before crimping and the following chart (Figure 50) is after crimping. Not only do we see more variation in the slopes of the data, representing the resistance in ohms, but we also see that the values of the resistances are much higher without the use of mechanical crimping to measure the resistances.

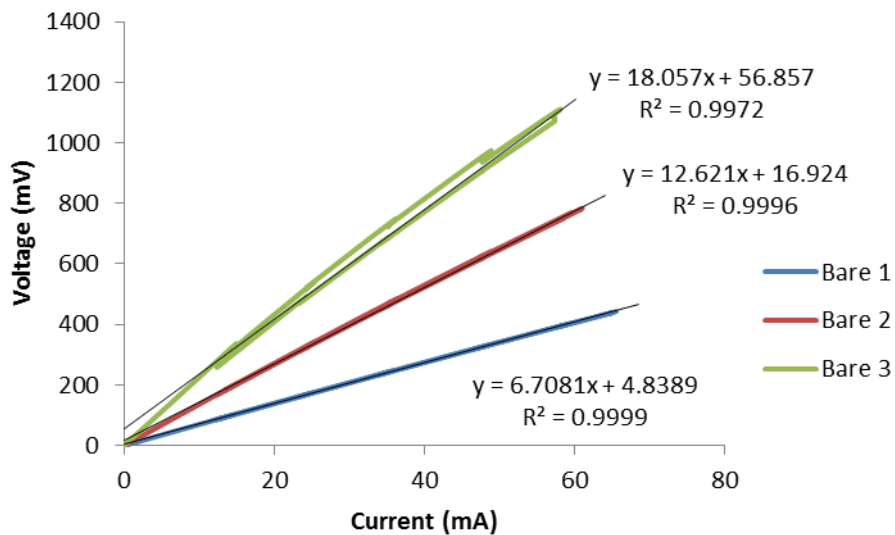


Figure 49 – Three trials of voltage versus current plot of electrical characteristics for non-crimped specimen 1

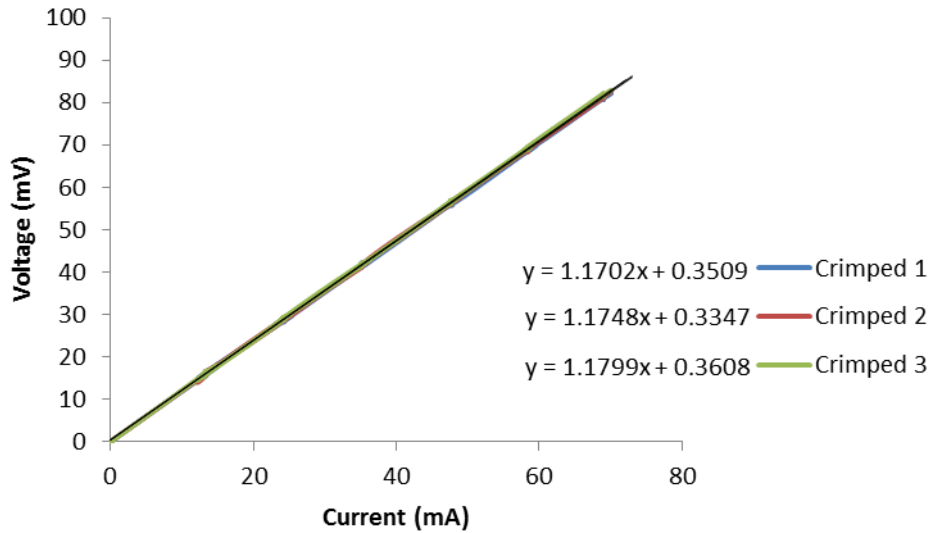


Figure 50 - Three trials of voltage versus current plot of electrical characteristics of crimped specimen 1

The chart displaying the crimped specimen data is much more consistent, compared to that of the bare carbon fiber connection. The R^2 values for each of the crimped trendlines were 0.9999, demonstrating an extremely high correlation to the data.

Data from a second specimen can be observed in Figure 51 to help verify the previous findings. In both of the following charts, the trendlines had over 0.9990 for their respective R^2 values.

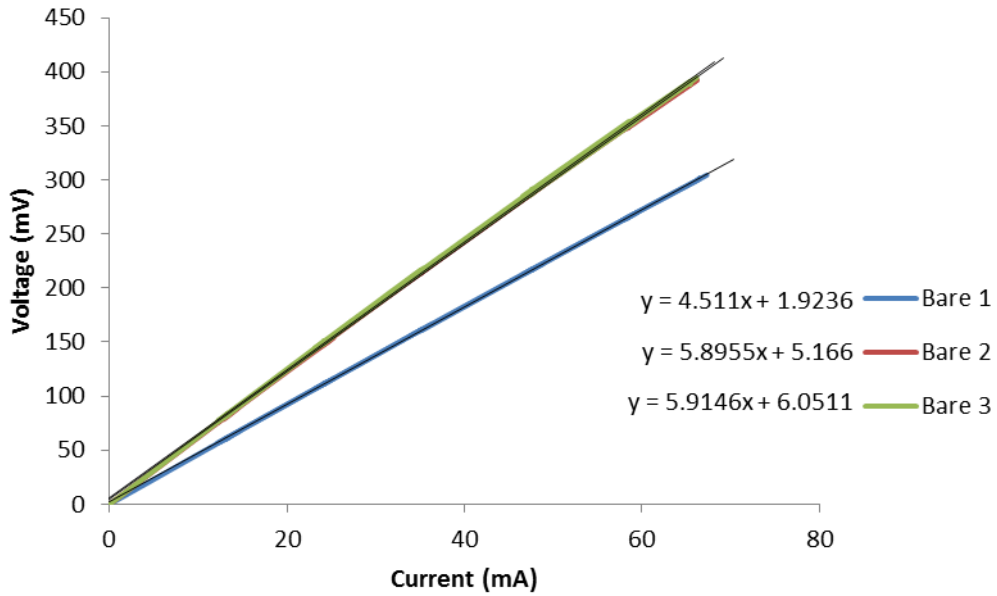


Figure 51 - Three trials of voltage versus current plot of electrical characteristics for non-crimped specimen 2

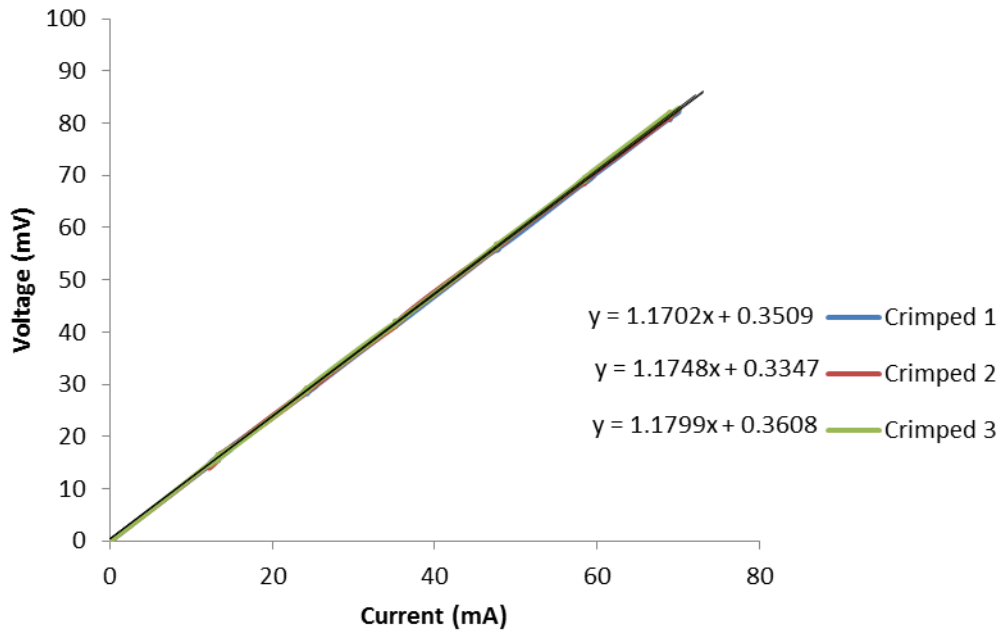


Figure 52 - Three trials of voltage versus current plot of electrical characteristics of crimped specimen 2

It can be seen again that there are definite reductions in measured resistance by using mechanical means to create a better connection to the carbon fiber, in addition to reduced

variance between the measurements. Table 2 demonstrates that the simple addition of a mechanical clamp while performing measurements decreases the measured resistance of the specimen by at least 85%. In addition to improving the measured resistances, the measurement trials were much more consistent, improving the standard deviation by at least 250 times.

Table 2 - Statistical comparison of resistance measurements between non-crimped (bare) and crimped specimens

	Specimen 1		Specimen 2	
	<u>Bare</u>	<u>Crimped</u>	<u>Bare</u>	<u>Crimped</u>
μ (Ω)	5.4404	0.7621	12.4620	1.1750
% Improvement		86.0%		90.6%
σ	0.8049	0.0032	5.6761	0.0049
× Improvement		254.4		1169.8

As an additional validation and demonstration of the performance of the crimped method, a nickel specimen was used in a light bulb circuit with a voltage of 7.4V to replicate a 2S Li-Ion cell configuration (assuming a nominal cell voltage of 3.7V). The setup can be seen in Figure 53. (Note: Neither the alligator clip nor the crimp are touching the solder ingot, and the only connection to the ingot is through the carbon fiber)



Figure 53 - Carbon fiber in SAC305 ingot connected in series with light bulb and power supply

Once the nickel specimen was measured, the bulb was allowed to cool to room temperature and the crimped carbon fiber specimen was placed in the circuit to replace the nickel specimen. This process was then repeated for a second trial. The temperature of the bulb was recorded every minute for 5 minutes, in addition to the circuit current. The data collected is plotted below, in Figure 54.

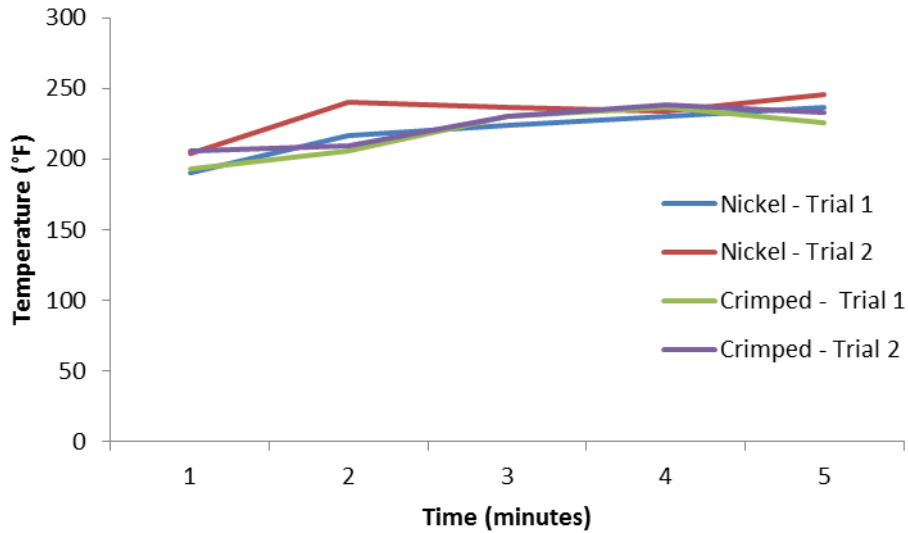


Figure 54 - Bulb temperature versus time comparison of nickel wire and crimped carbon fiber used in electrical circuit

While previously, there was a noticeable difference between the carbon fiber sample and the wire sample, this demonstrates and reflects that the crimped carbon fiber specimens do have a substantial increase in desirable electrical properties. In addition, the bulb brightness was significantly dimmer without the crimping, and after the specimens were crimped the brightness was nearly indistinguishable from brightness produced with the nickel tab specimen.

4.2.2.2 Battery connection

The crimped pultruded carbon fiber connection was found to be sufficiently conductive that it was possible to conduct demonstration of the power delivery through these connections with the lithium-ion cell. The connection between the light bulb and carbon electrodes were made at the terminals of the crimps. This minimized the inherent resistance of the carbon fibers, and maximized electrical power delivery to the light bulb, as seen in Figure 55.



Figure 55 - Crimped carbon fiber terminal connections to lithium-ion battery, lighting a bulb

The following pictures in Figure 56 compare the brightness of the light bulb when one circuit is made at the crimped terminal on the carbon fiber (left) and the connection made directly on the tab of the battery (right). Qualitatively, the connection at the nickel tab lights the bulb slightly brighter than the connection at the crimped terminal.



Figure 56 – Bulb brightness comparison between carbon fiber and nickel tab connections

Qualitatively, these demonstrations indicate the viability of using the carbon electrodes with lithium-ion cells for power delivery to electrical systems. However, due to the fragile nature of these connections, more quantitative data was unable to be provided.

4.3 Physical vapor deposition

4.3.1 Mechanical characterization

Due to the fragile nature of the carbon fiber-nickel tab specimens, a technique for improving the adhesion was investigated. Pyrolyzed carbon fiber tubes were coated with nickel using electron beam vaporization. 10 sample carbon fiber tubes were prepared in the manner described in the previous section by burning off the epoxy on one end. These samples were sent to the FabLab at the University of Maryland. On this test run, 3000 angstroms of nickel were

deposited on the test samples in one direction. The base pressure of the chamber prior to deposition was 8×10^{-7} torr. The deposition rate was $10 \text{ \AA}/\text{sec}$. The rate and thickness of the nickel coating was monitored using an Inficon film thickness monitor. A picture of the coated samples is provided in Figure 57.



Figure 57 - Picture of PVD nickel coated carbon fibers

Qualitatively, while the presence of a nickel coating is apparent by the silver dusting, this coating is not very thorough or robust. Much of the nickel coating is spread over the side of a brush and not heavily concentrated in the tips where they may have the most influence on adhesion to solder.

This small amount of nickel slightly improves adhesion of carbon fiber to nickel in certain samples produced by soldering when the solder sticks to carbon fiber strands with significant nickel. As many of the strands don't retain enough of a nickel coating to show improvement, possible areas of improvement would be to either increase the amount of nickel coating or improve the adhesion of the nickel to the carbon fiber strands.

The images provided in Figure 58 include an example of a nickel coated specimen that exhibits enhanced wetting characteristics. While only a few strands appear to adhere to the solder, this level of adhesion is superior to what was experienced prior to coating the carbon fiber strands with nickel. Taking a close look, the small amount of solder appears to wet on the joint instead of just forming clumps as experienced with uncoated fibers. Using a multimeter with the leads touching the two crimps, the resistance reads approximately 13 ohms.

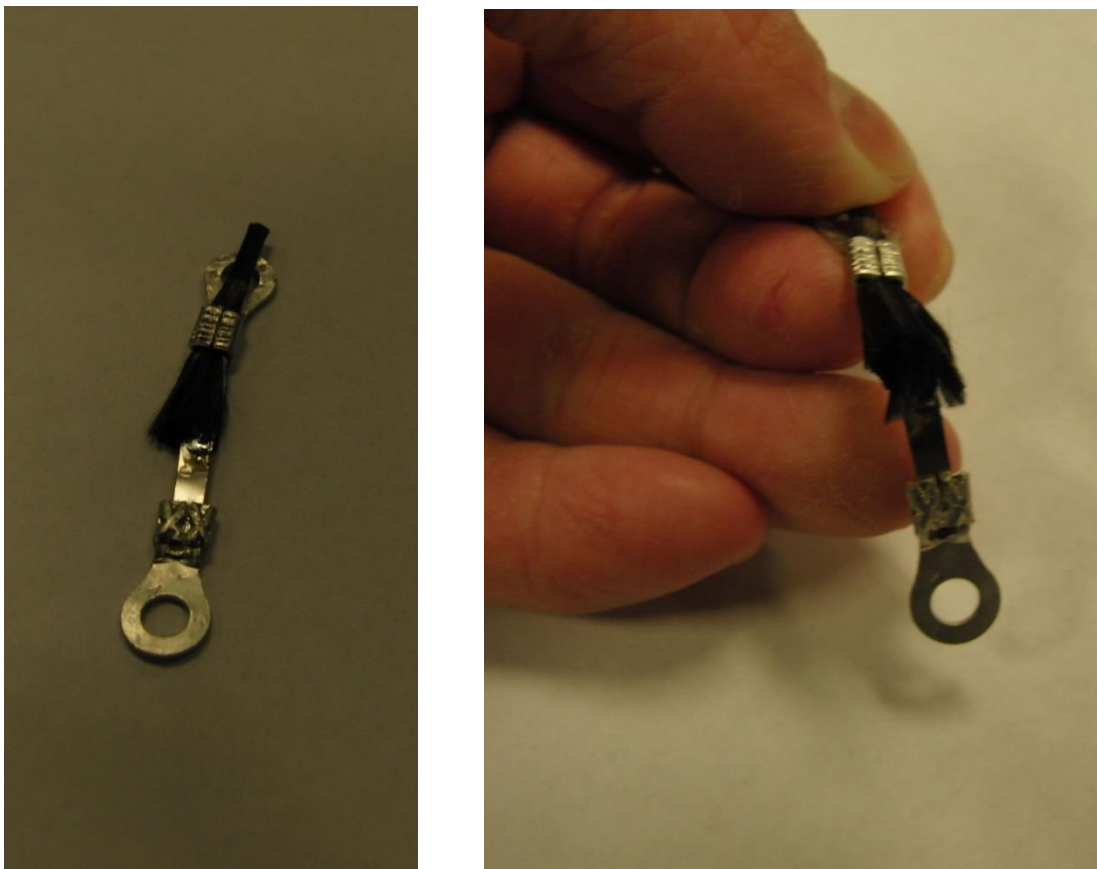


Figure 58 - Pictures indicating the quality of the PVD nickel coated CF solder joints to nickel tabs

4.3.1.1 Adhesion testing

As the solder joints are very fragile, these joints were soldered on the test apparatus to facilitate testing. Crimped coated carbon fiber tubes and crimped nickel tabs are screwed into the test apparatus separately through the ring tongue terminal. Align the coated carbon fiber tubes

and nickel tabs so that they are along the same plane. Bring the side of the nickel tab in contact with the ends of the coated carbon fiber strands. Make sure they are touching as shown in Figure 59. Solder the joint on the test apparatus.

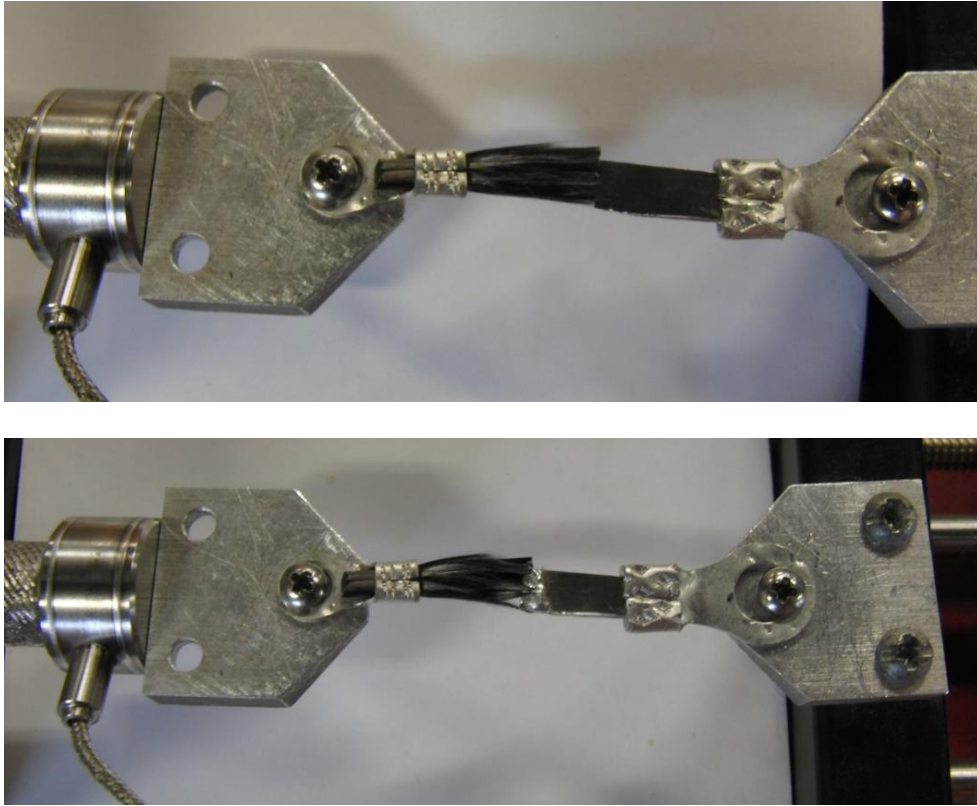


Figure 59 - Pictures indicating the steps of soldering the carbon fibers to a nickel tab for adhesion testing

One recurring issue with this testing is the adhesion of the carbon fiber to solder. Many times, the soldered joint would not adhere well to the coated carbon fiber strands. Many of these joints would break with minimal stress. It is difficult to determine whether there is significant adhesion prior to running the test as the specimen is already loaded in contact on the test apparatus.

Another complication is the integrity of the carbon fiber strands. If a successful attempt to solder is not made early, the carbon fiber strands become damaged by the heat and stiffen. Consecutive attempts to solder are typically less successful than the initial attempts.

With the test joint soldered on the apparatus, zero the voltage reading on the load cell. This can be done by moving the side with the nickel tab until the voltage reading is approximately zero. Begin logging data on the computer and hit the start button on the test apparatus. Watch the joint break and stop logging. If the carbon fiber adheres well to the solder, there will be an audible snap during breakage. This will leave strands of carbon fiber on the solder joint as pictured in Figure 60.



Figure 60 - Individual carbon fibers remaining attached to nickel tab after adhesion failure

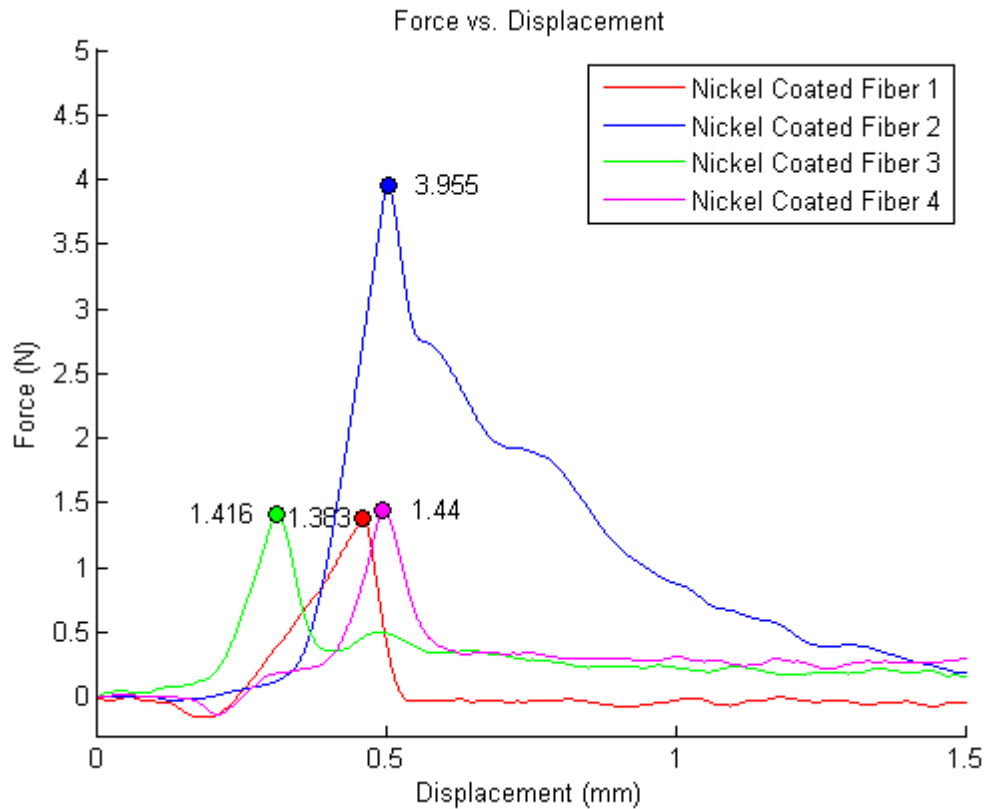


Figure 61 - Force versus displacement of PVD nickel coated carbon fibers

The above graph in depicts the loads of four samples. Of the nickel coated fiber samples, specimen 2 broke with an audible snap of the carbon fiber strands. This is the type of joint that is ideal for testing. The decreasing in the load, rather than an abrupt change indicates that there may be pullout mechanisms present in either the solder connection or the ring tongue crimp used to hold the carbon fiber to the apparatus. Both of these scenarios demonstrate additional adhesion to the solder joint on the nickel tab. The others that break at smaller loads may not achieve sufficient adhesion. Ideally, joints with better adhesion will be produced with a more uniform coating and increased adhesion of nickel to the carbon fiber. The highest strength joint using the solder was only able to hold about 4 N (0.9 lbf), but was successfully able to demonstrate an increase over the 1.4 N (0.3 lbf) specimens by having an improved solder connection. Therefore,

it can be seen that peak load-bearing capacity of 4 N was achieved, with an associated work-to-failure of 0.01 J. It is important to note that these are “sub-optimal” designs, where increasing the coverage and thickness of the nickel coating can substantially improve the mechanical properties.

4.4 Nickel tab

4.4.1 Mechanical characterization

Mechanical characterization of the nickel tab material has also been investigated. The nickel-SAC305 specimen was created using the proscribed method used with the carbon fibers, including the utilization of the Kester 1544 activated rosin liquid flux. The nickel tab material was a segment of the 0.08m Nickel 200. Previous to the loading, the tab segment of the specimen was measured with digital calipers. The dimensions were, 0.1 mm x 3.14 mm, equating to a cross sectional area of $3.14 \times 10^{-7} \text{ m}^2$.

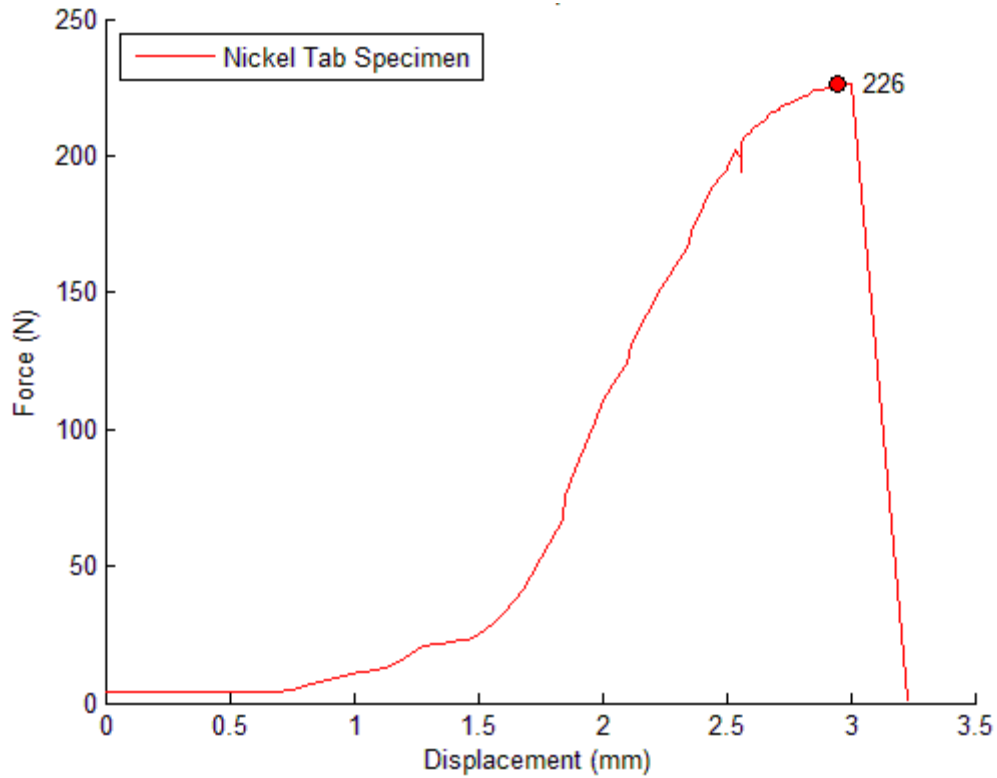


Figure 62 - Force versus displacement of nickel tab in SAC305 solder ingot

As displayed by the graph in Figure 62, the maximum loading was 226 N, in which the specimen failed completely. By using $\sigma = \frac{F}{A}$, we can determine that the maximum engineering stress of the nickel tab was 719.7 MPa. The failed specimen can be seen in Figure 63.



Figure 63 - Failed nickel tab specimen embedded in SAC305 solder ingot

With this specimen, the nickel tab failed before any evident pullout had occurred. All of the plastic deformation and failure had been localized to the protruding tab portion of the specimen. The testing determined that the interfacial strength of nickel-SAC305 interface at 1 inch of depth is stronger than the inherent strength of the nickel tab material. Thus, it was not possible to determine the interfacial strength using this method.

4.4.2 Electrical characterization

In addition to the carbon fiber testing, the nickel tab/solder resistance was characterized. Since the resistance was extremely low for the nickel tab to solder interface, the equipment could not read an accurate resistance using the tab only. To account for this the resistance measurements were taken of the nickel tab specimen in series with a nominally 11Ω resistor, and then again with only the 11Ω resistor. The values of the 11Ω resistor alone would be subtracted from the series configuration to identify the resistance of the nickel tab.

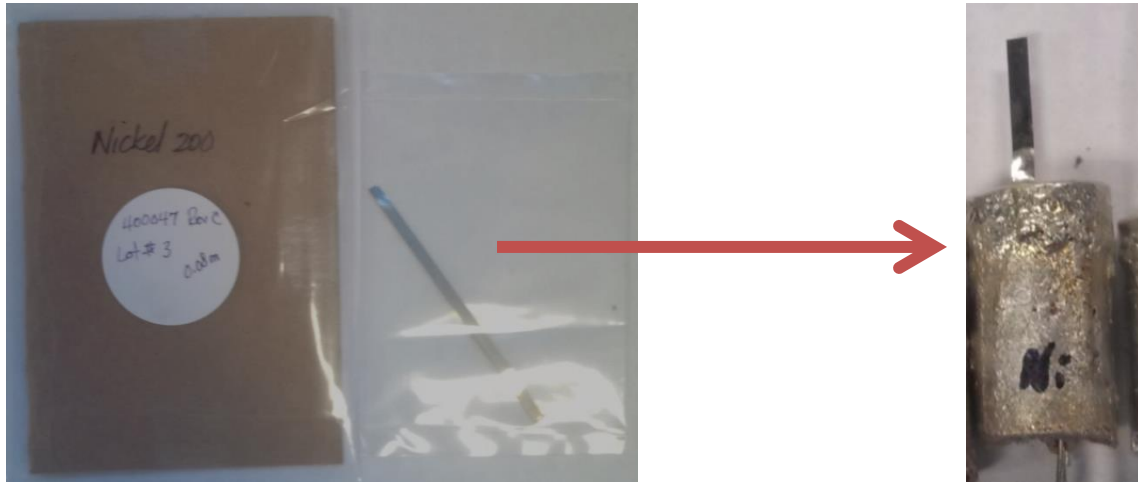


Figure 64 - Nickel tab before and after embedding in SAC305 solder ingot

The graph in Figure 65 is the voltage vs. current profile of the nickel tab in series with the nominally 11 Ω resistor. We can see that the actual resistance is less than 11 Ω , but this does not matter, as long as the profiles remain similar for both readings.

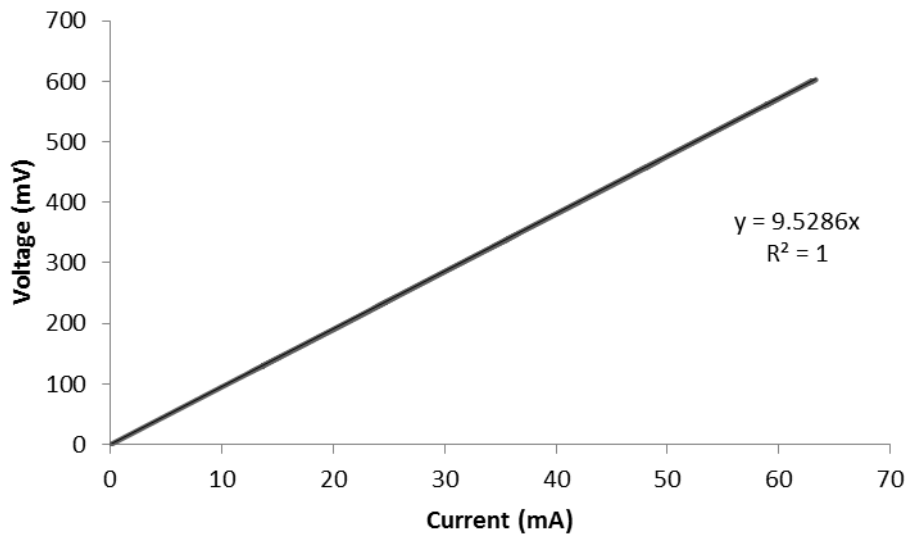


Figure 65 – Voltage versus current profile of the nickel tab in series with 11 Ω resistor

The following graph in Figure 66 is the voltage vs. current profile of the 11 Ω resistor alone in the circuit.

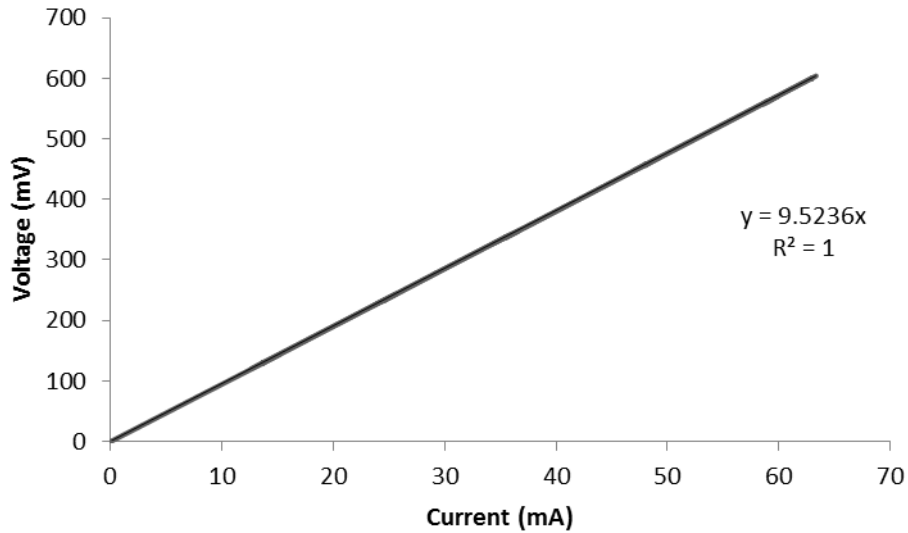


Figure 66 - Voltage versus current profile of 11 Ω resistor

Subtracting the slope of the 11 Ω circuit from the slope of the combined resistor-nickel tab circuit gives us the resistance of the nickel tab/solder specimen. Thus, we have the nickel tab specimen resistance as 5.0m Ω . The R^2 value for both of these plots is 1.0, meaning that the linear regression trend line is a nearly perfect fit for both, providing higher confidence of the specimen resistance. The specimen resistance can be evaluated with finer measurement tools to extract the interfacial resistance.

Three specimens were measured with the Agilent Milliohmeter and the resistance versus length profiles were plotted, along with linear regression curves and the regression results. The following plot in Figure 67 is the 400047 Nickel 200 (0.1 mm x 3.14 mm) tab specimen.

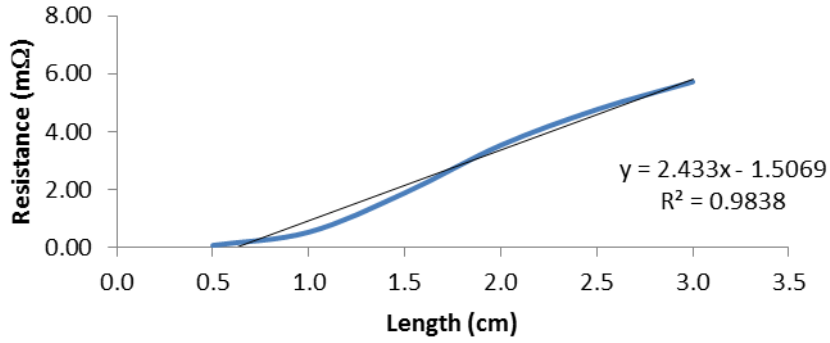


Figure 67 - 400047 Nickel 200 (0.1 mm x 3.14 mm) tab specimen resistance versus length

This plot demonstrates a resistance per unit length of 243.3 mΩ/m. Using Pouillet’s law,

$R = \rho \frac{l}{A}$, the equation can be rearranged to find the resistivity:

$$\rho = \frac{R}{l} A = 0.2433 \frac{\Omega}{m} \times (0.0001 \times 0.00314) m^2 = 7.64 \times 10^{-8} \Omega - m$$

This resistance remains consistent with the estimated resistivity of nickel at 20°C of $7.0 \times 10^{-8} \Omega - m$.

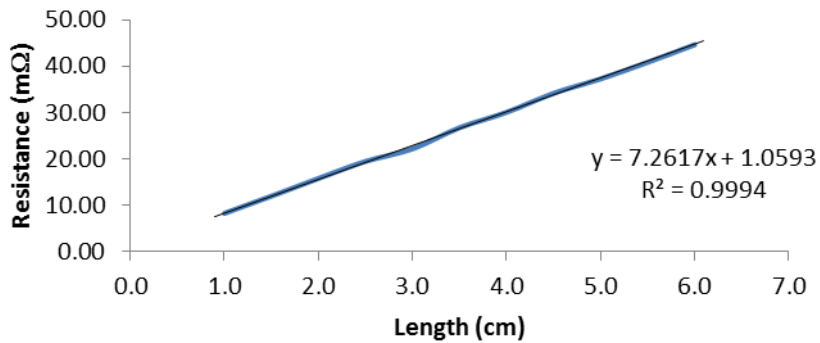


Figure 68 - 400353 Nickel 200 (0.05 mm x 1.53 mm) tab specimen resistance versus length

The plot in Figure 68 is for the 400353 Nickel 200 (0.05 mm x 1.53 mm) tab specimen.

The regression analysis demonstrates a resistance per unit length of 726.2 mΩ/m. In addition,

the R^2 value for the regression is 0.999, indicating near perfect conformity to the data. The resistivity is then calculated.

$$\rho = \frac{R}{l} A = 0.7262 \frac{\Omega}{m} \times (0.00005 \times 0.00153)m^2 = 5.55 \times 10^{-8} \Omega - m$$

The setup for the specimen resistance testing can be seen in Figure 69.

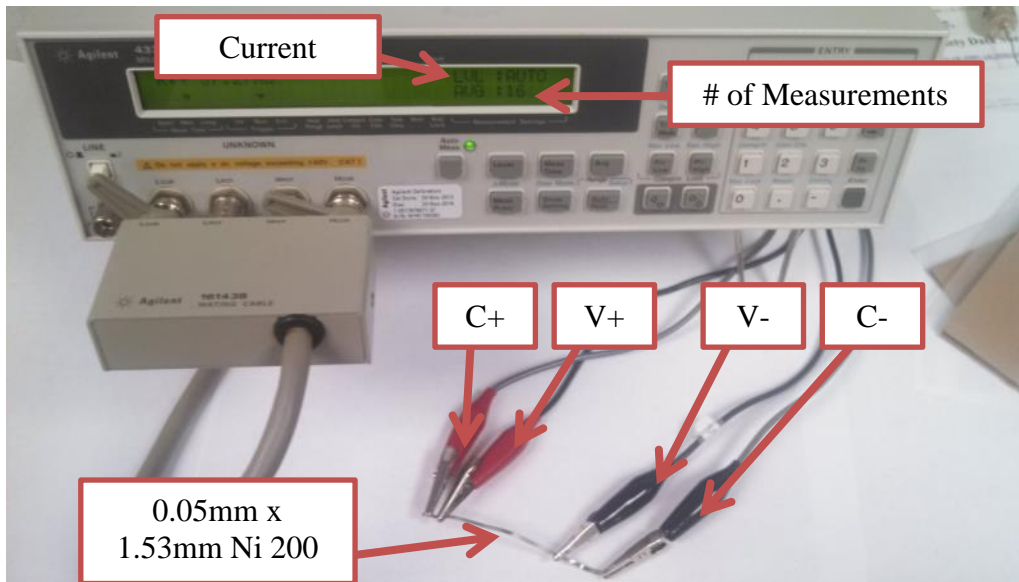


Figure 69 - Agilent Milliohmmeter setup for nickel tab resistivity measurements

The following plot in Figure 70 is for the 400047 Nickel 200 (0.1 mm x 3.14 mm) tab and SAC305 solder specimen. The origin of the length scale indicates the location of the nickel tab at the nickel-solder interface. Since the tab material is the same 400047 material tested previously, it makes sense that the resistivity is similar. This time, the resistivity also includes the interface between the nickel and solder.

$$\rho = \frac{R}{l} A = 0.2596 \frac{\Omega}{m} \times (0.0001 \times 0.00314)m^2 = 8.15 \times 10^{-8} \Omega - m$$

It is important to note that the inherent resistivity of SAC305 is reported to be $1.3 \times 10^{-7} \Omega - m$. Thus, as expected the resistivity is between the measured resistivity of the Nickel tab and SAC305.

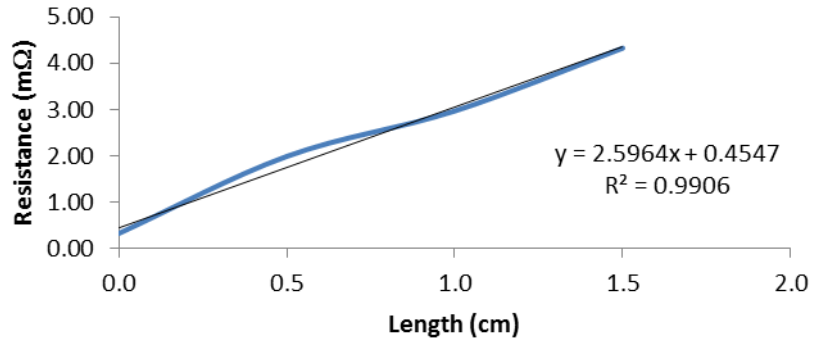


Figure 70 - 400047 Nickel 200 (0.1 mm x 3.14 mm) tab specimen resistance versus length

Chapter 5: EXPERIMENTS USING SILVER EPOXY

5.1 Mechanical characterization

Another approach to create a carbon fiber-nickel connection was investigated where specimens were produced by bonding the carbon fiber strands to nickel tabs using silver epoxy instead of solder. These specimens took a much larger load over those made only joining with solder. The example in Figure 71 is characteristic of the manner in which the specimens produced with silver epoxy break.

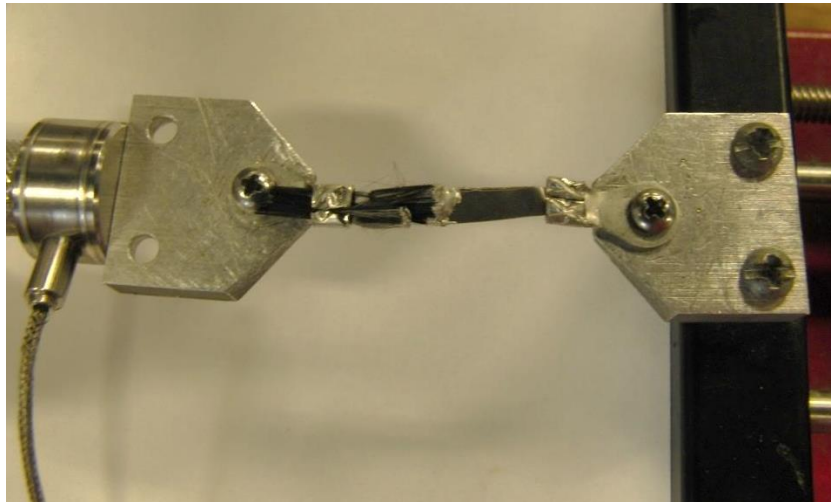


Figure 71 - Demonstration of silver epoxy shear loading failure

With a 1000 Hz sample rate and a load apparatus setting of 3.000 ml/hr, it was calculated that the travel of the apparatus is 15.64 mm/min. Additionally, the load cell was calibrated to 0.290 V/kg, which is equivalent to 0.2957 V/N. Using the sample interval in conjunction with the travel rate, the distance traveled was calculated from the sampled data. The distance was plotted against the corresponding calculated voltage from the Omegadyne Inc. LCFD-10 load transducer. Five of the samples have been compared in the graph in Figure 72.

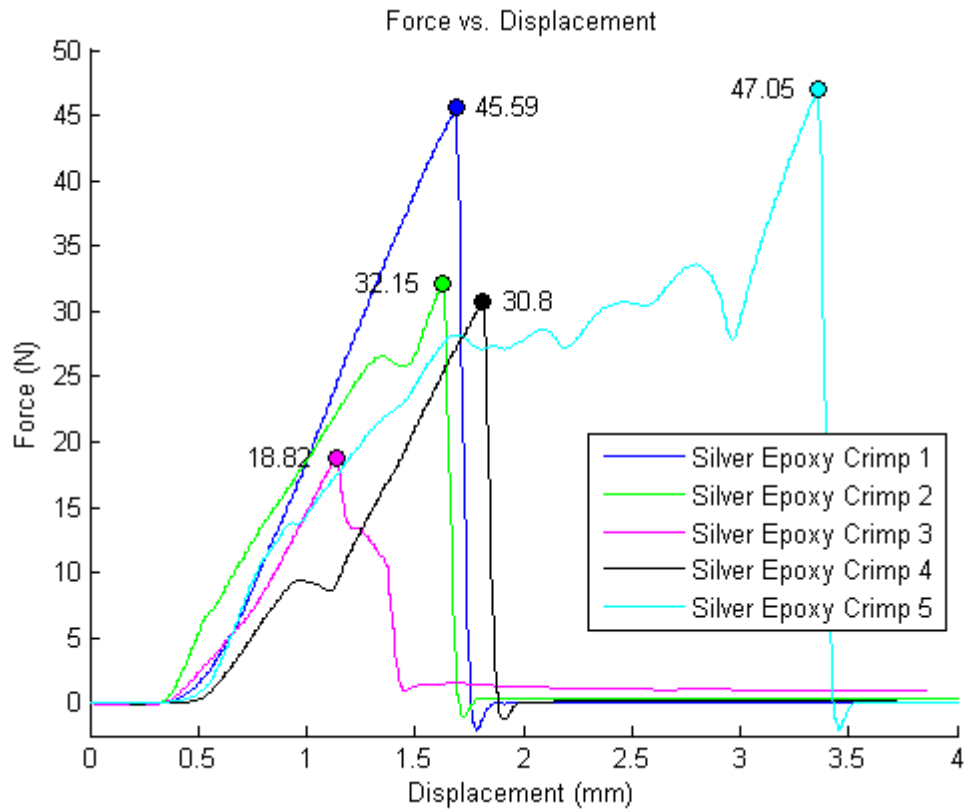


Figure 72 - Force versus displacement of pyrolized pultruded carbon fiber attached to nickel tabs with silver epoxy

It can be seen that there is an order of magnitude greater load bearing capacity of 47 N and work-to-failure of 0.08 J relative to the PVD nickel-coated fibers. This compares favorably to the carbon fiber specimens that were embedded in solder, where solid core carbon fiber specimens with no flux achieved 40 N of load-bearing capacity with a work-to-failure of 0.2 J. The silver epoxy clearly exhibits improved adhesion over the PVD nickel-coated fibers, which is attributed to the improved coverage of fibers with the silver epoxy. However, it is believed that the nickel-coated fibers can be designed to achieve greater adhesion than the silver epoxy, and approach or exceed the strengths achieved using flux with the solid core carbon fiber specimens embedded in solder. It is also important to note that approximately 5 mm of the carbon fiber

were bonded with the nickel tabs, as opposed to 25 to 50 mm of the carbon fiber being embedded in solder.

5.1.1 Braided carbon fiber specimens

To more accurately compare the results between the silver epoxy and the electroplated carbon fibers described in “Chapter 6,” the specimens were prepared in a similar manner. As displayed in Figure 73, the braided carbon fiber was attached to 0.25 inches of a nickel tab using silver epoxy. These three specimens were compared using the shear testing configuration on the IMADA force measurement apparatus.



Figure 73 – Prepared specimens for braided carbon fiber connected to nickel tabs via silver epoxy

The results from the shear testing indicated consistency between specimens. Displayed in the graph in Figure 74, the results of the shear testing have failure loads at 72, 49, 74 Newtons respectively. As seen in Figure 73, specimen 2 has less silver epoxy than specimens 1 and 3. This could be a contribution to the lower force incurred by the specimen. Additionally, it can be observed that the specimens fail abruptly. Without an additional failure mechanism, the

specimens fail with brittle detachment from the nickel tabs. The force incurred at failure corresponds to the strength of the bond with the least adhesion. Since the testing must be performed with two bonds per specimen, unless they are both equivalent and fail simultaneously, the test only indicates the weaker of the two joints.

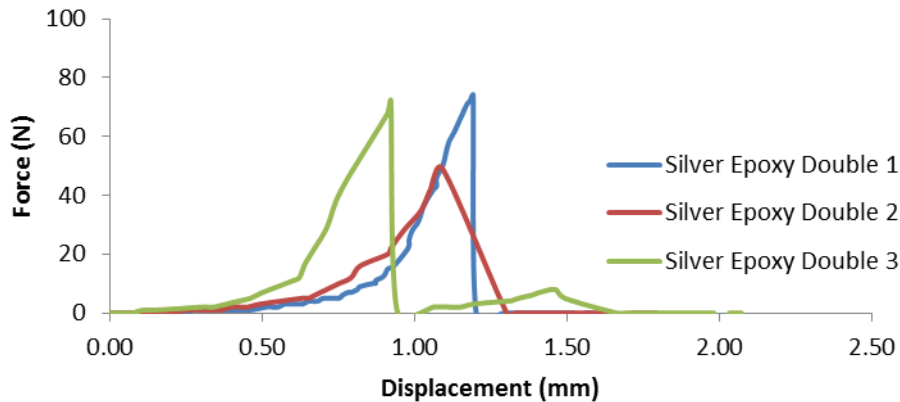


Figure 74 - Force versus displacement of braided carbon fiber specimens with silver epoxy bonding

5.2 Electrical characterization

5.2.1 Pultruded carbon fiber

Resistance measurements were taken initially with the pultruded carbon fiber attached to a nickel tab using silver epoxy. These resistances, the slopes of the plots displayed in Figure 75. The tested specimens were measured very close to the interfaces, which may provide difficulty for direct comparison to other carbon fiber measurements. Despite the shift in measurement, the interfacial resistances have been calculated and demonstrated to be low in comparison to the embedded carbon fibers in the solder ingots.

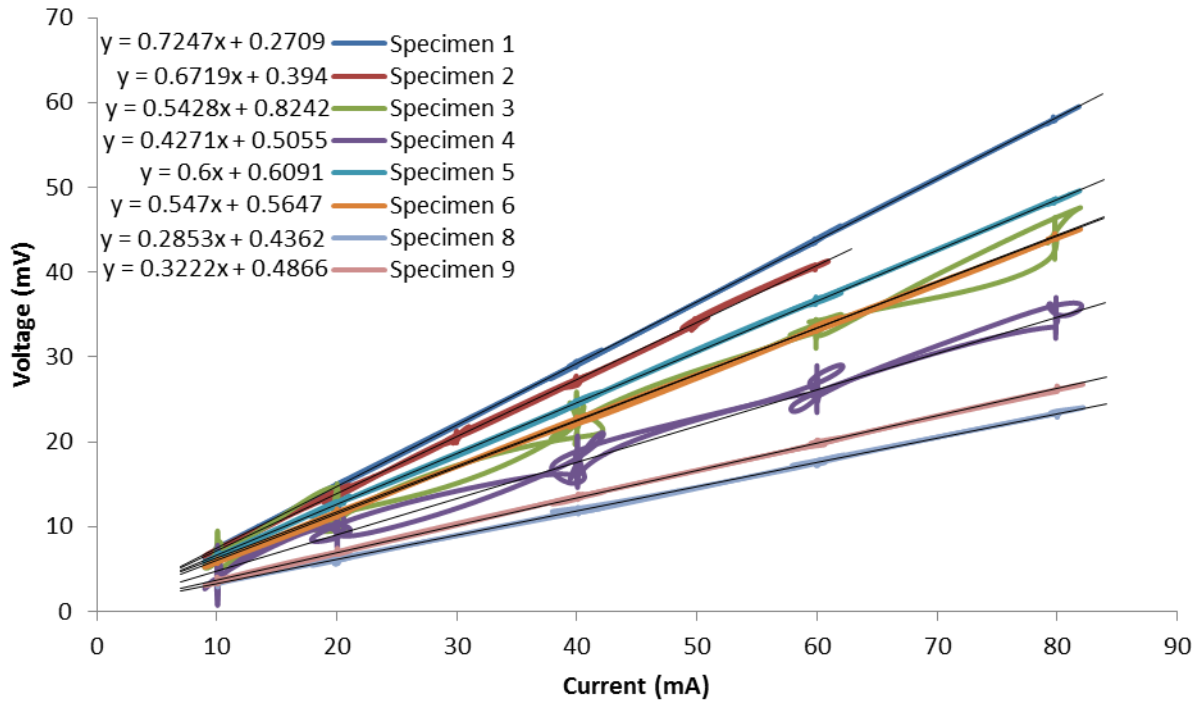


Figure 75 - Voltage versus current of silver epoxy bonded specimens

The slopes of these plots indicate the resistance in ohms incurred by the specimens. Since the probes were used closely to the joints, the resistances primarily represent the interfacial resistances between the carbon fiber and silver epoxy. Even with similar application of the silver epoxy, the resistances fluctuate from 0.28Ω to 0.72Ω . The inherent resistance of the carbon fiber and the surface area covered by the silver epoxy play a large role in the determination of the resistances.

Regardless of the variation in resistances, the results indicate higher conductivity with silver epoxy bonding, rather than the usage of carbon fiber embedded in the SAC305 solder ingot using the Kester 1544 activated rosin liquid flux. Providing up to an 80% reduction in the resistances is a crucial step in producing a product that can be used in electrical circuits. Furthermore, the silver epoxy specimens were scaled to be measured on a nickel tab as a part of

an electrical circuit. The SAC305 solder ingot was not scalable and was only able to be used for characterization testing.

5.2.2 Braided carbon fiber

As displayed in Figure 73, braided carbon fiber specimens were created by bonding the carbon fiber to the nickel tabs using silver epoxy. To provide a better comparison to the electroplated nickel carbon fibers for electrical performance, the resistances were acquired using the same method.

Figure 76 demonstrates the resistances acquired from the silver epoxy test specimens. These specimens exhibit higher repeatability than the pultruded carbon fibers, due to the standardization of the processing procedures. Furthermore, the resistances are only about 0.1 - 0.2 Ω higher than the electroplated specimens that were soldered to the nickel tabs, as discussed in “Chapter 6.”

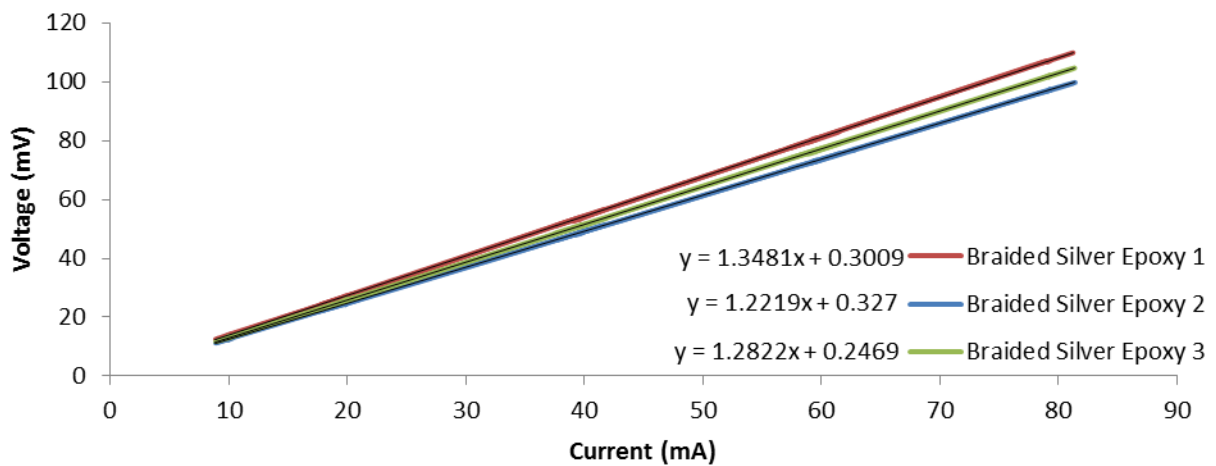


Figure 76 - Voltage versus current of braided carbon fiber specimens with silver epoxy bonding

Chapter 6: EXPERIMENTS USING ELECTROPLATING

6.1 Mechanical characterization

6.1.1 Shear load testing

The mechanical test specimens are the same as those used for the electrical testing. In order to understand the relative strength of the carbon fiber to metal bond, the specimens are first tested to identify relative shear strength. Since each specimen differs by the solder joints, this method is only able to identify force and displacement, and not stress and strain.

The specimens are loaded onto a setup which axially tensions the specimen and is connected to a force transducer. In addition to a force measurement, the distance is measured and recorded as well. In order to accommodate the level of force that the samples are able to withstand, a double chuck system is used. As seen on the left hand side of Figure 77, there is a chuck anchored to the bottom of the device, and another at the top. The specimens are fixed into these two and are tightened using the chuck key.



Figure 77 - Force measurement setup before (left) and after (right) failure

After taking measurements of five different specimens, the range of ultimate forces was from 253 Newtons to 423 Newtons. This equates to approximately 57 lbf to 95 lbf. The results of the pull tests can be viewed in Figure 78. Additionally, since these tests were performed using specimens with two solder joints, they each identify the weaker of the two joints, meaning there is one joint in each test which has a greater bond strength.

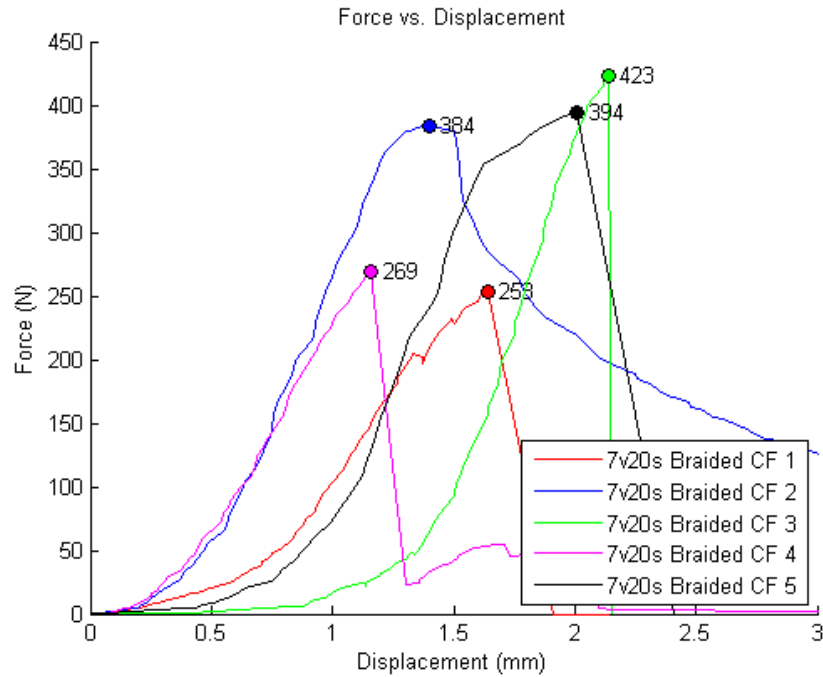


Figure 78 - Force vs. displacement of braided carbon fiber sleeve soldered to nickel tabs

As an additional note, specimen 2 (blue in Figure 78) did not fail. The specimen would slip out of the apparatus before either of the soldered joints would break. While the profiles of the other specimens indicate a steep drop in force after the maximum point as the force at failure, specimen 2 trails off showing the slipping of the joint. It should also be noted that every specimen had to be loaded several times before failure because of slipping during setup. While this reduces the accuracy of the actual maximum forces because of possible high stress fatigue damage, the compiled results indicate that there is a high stress incursion by these joints and that they are relatively strong compared to the average stressed experienced by electrical joints.

It was also possible to compare the slope and maximum load from the mechanical test data in Figure 78. These results are shown in Figure 79. There is a clear correlation between the slope and maximum load with a slope of 0.807 mm, which is a strong indication that these values depend upon the amount of surface area that is wetted on the braided carbon fiber. Since the

electroplating process has not been optimized for coverage of the braided carbon fibers, it is highly likely that the mechanical properties can be improved even further resulting in carbon-metal connections with even greater mechanical integrity.

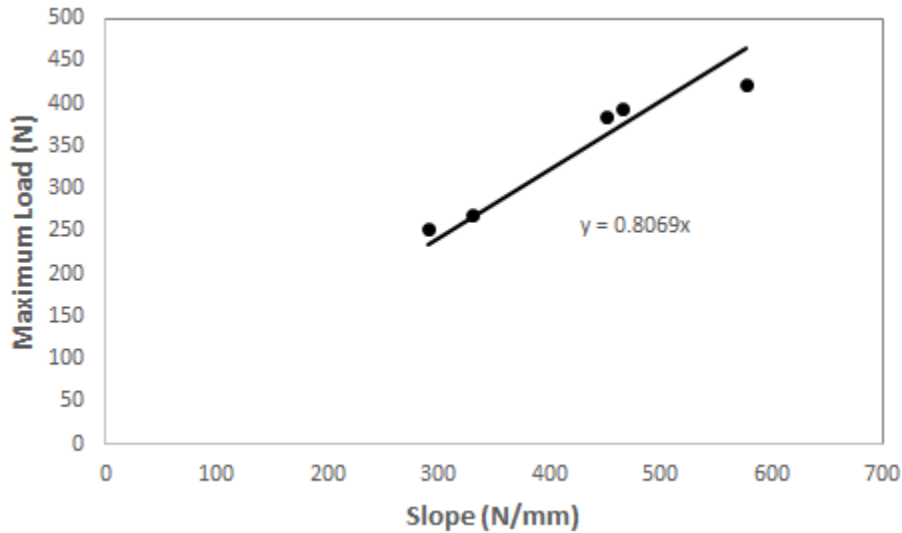


Figure 79 - Comparison of slope and maximum load from mechanical tests of braided CF with electroplated Ni soldered to Ni tabs using SAC305 with flux.

6.1.2 Microscopy

To further understand the mechanisms of adhesion of the carbon fiber ESEM microscopy was used to identify unique characteristics of the plated carbon fibers. In addition to the ESEM, the EDS chemical analysis was used to identify the elemental makeup of the components observed in the ESEM images.

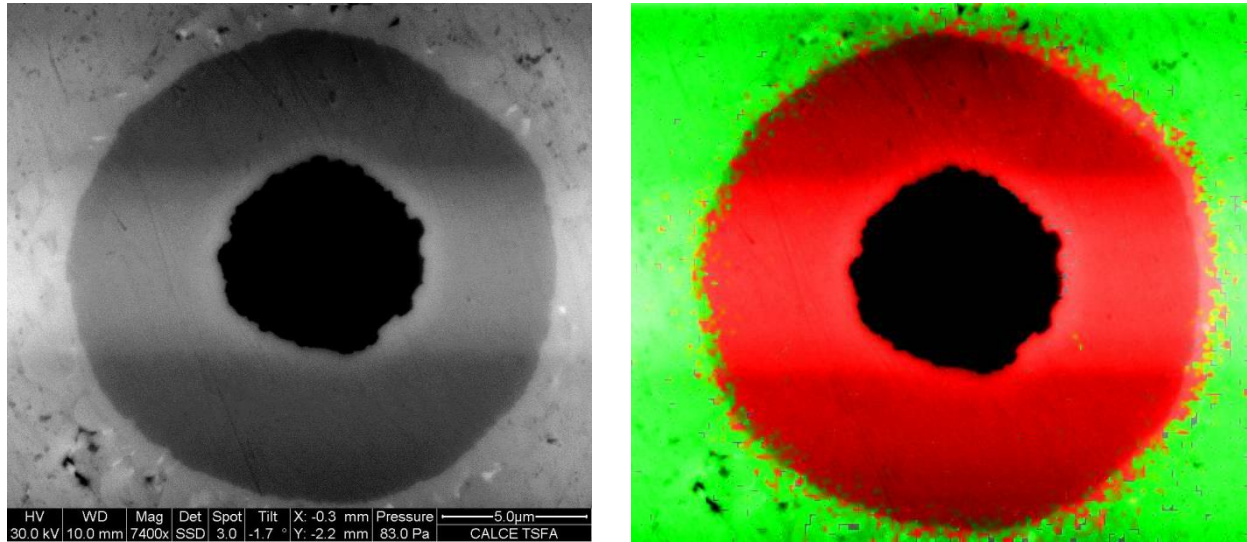


Figure 80 - ESEM images of plated carbon fiber with EDS elemental composition composite image

The images displayed in Figure 80 help to identify some of the mechanisms that lead to the mechanical adhesion of the nickel to the SAC305 solder. The left image displays a 7400x magnification of a carbon fiber cross-section embedded in a SAC305 matrix. The image on the right identifies the nickel as red and tin as green. It is clearly evident that the nickel plating is fully surrounded by the tin metal matrix at this cross-section. What provides interest in these images is the ring of tin around the nickel plating. Here, a different structure is present than the bulk of the solder, as displayed in Figure 81. This annulus of tin also contains a higher concentration of lighter particles. Using EDS to confirm the elemental composition, the structures surrounding the nickel plating were identified as tin-nickel-copper intermetallic structures. Primarily presumed to be Ni_3Sn_4 from the EDS data and common nickel-tin intermetallic formations, the intermetallic structure can provide a mechanical bonding mechanism, which increases the adhesion.

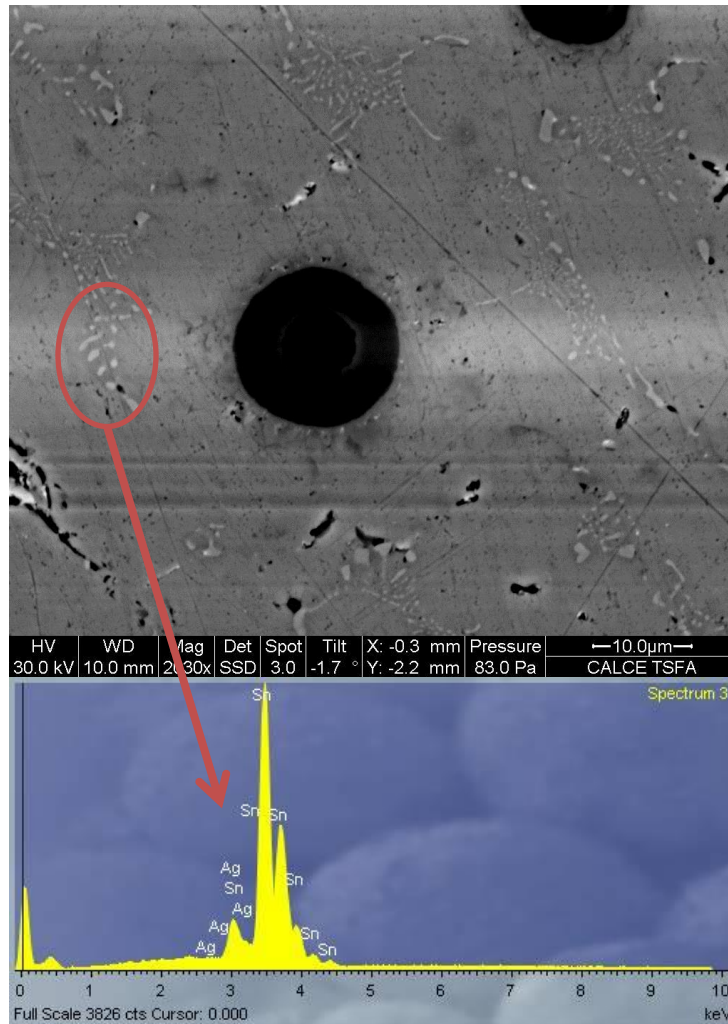


Figure 81 - Plated carbon fiber encased in SAC305 matrix with spectral analysis of the bulk solder

Further characterization of the interface was done by comparing images of the nickel tab and SAC305 interface. Compared in Figure 82, this interface once again highlights a presence of formations present at the interface, but not in the bulk of the solder. Higher concentrations of these structures may serve as an adhesion mechanism which is present along the length of the interface. Since the observed portions are simply cross-sections, the structures extend along the interface to provide locking mechanisms with the material. With semi-dendritic properties, these lighter structures act as anchors, which hold the nickel in place in the SAC305 matrix. The right image in Figure 82 once again compares the nickel (red) and tin (green) interface, which

demonstrates a “locking” structure, further substantiating the evidence of the interconnection at the interface.

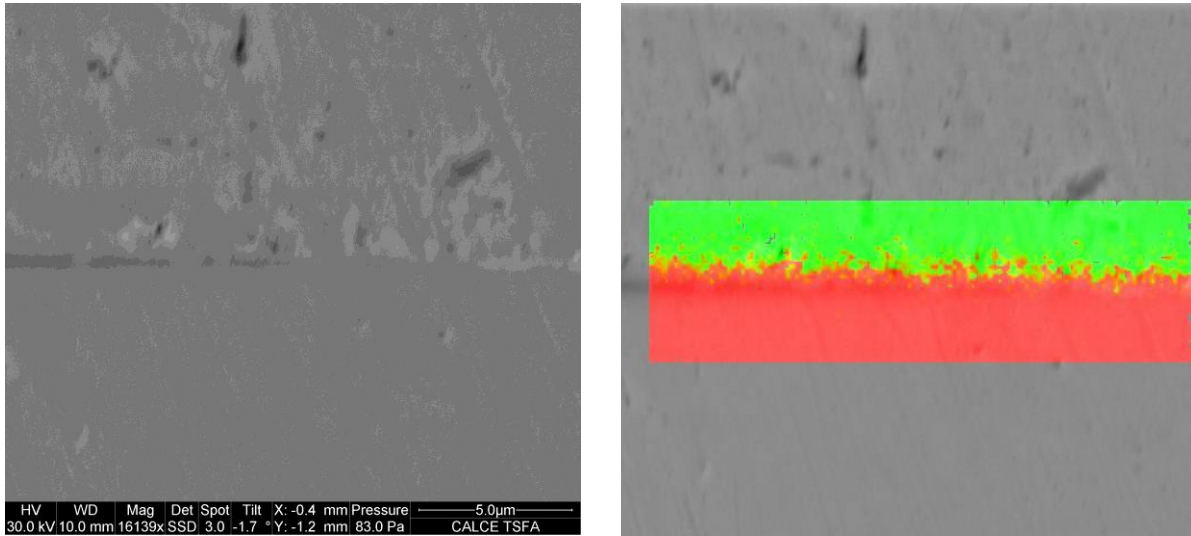


Figure 82 - ESEM images of nickel tab – SAC305 interface with EDS elemental composition composite image

The carbon fibers alone were imaged to identify any unique features present. Beside for the obvious presence of nickel, a unique aspect of the fibers is that the nickel has globule-like formations at the ends of approximately 30% of the carbon fibers. These formations do not occur along the majority of the plating, but rather only the first 100 - 200µm. A selected location with a high presence of these formations can be observed in Figure 83. It is hypothesized that these formations assist in the structural aspect of adhesion by acting as anchors in the solder matrix. Furthermore, while it has been demonstrated that the formations of dendritic and structural growths around the nickel may increase the adhesion, the three-dimensional morphologies of the nickel globules may add additional strength in combination with the nickel-solder interfacial interactions.

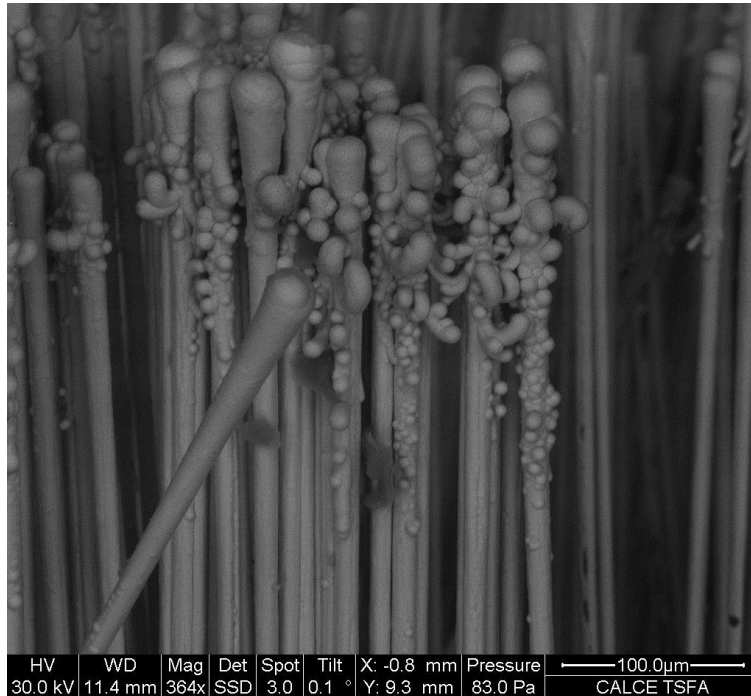


Figure 83 - ESEM image of globule formations on the end of nickel plated carbon fiber specimens

6.2 Electrical characterization

The specimens produced for the mechanical tests are the same ones produced for the electrical tests. Three specimens of nickel plated carbon fiber segments were tested electrically to determine the resistances over the 1.5 inch length, with 0.5 inches of total plating. By using the 4-point resistance measurement, the specimens were connected at the ends of the carbon fiber sleeves using the alligator clips. Running a voltage sweep profile of 1-2-4-6-8-6-4-2-1 volts over approximately 20 seconds, the voltage across the specimen was recorded, in addition to the current through the circuit. Since the shunt resistor to measure current is approximately 100 Ω , the actual voltage through the specimen is on the millivolt scale.

The results of the unsoldered but plated carbon fiber sleeve segments can be seen in Figure 84. The figure displays the consistency between specimens. Through short circuit testing of the resistance testing setup, there is approximately 0.02 Ω of resistance inherently in the setup.

The slope of the plot indicates the average resistance over the voltage and current profile. Since this was calculated using a linear regression scheme, the R^2 value was taken to identify the conformity to the actual data. With R^2 values of approximately 1 (rounded due to $R^2 > 0.9999$), the regression developed slope is accurate. This indicates that the 1.5 inch segments of plated carbon fiber yield approximately 1.1Ω of resistance.

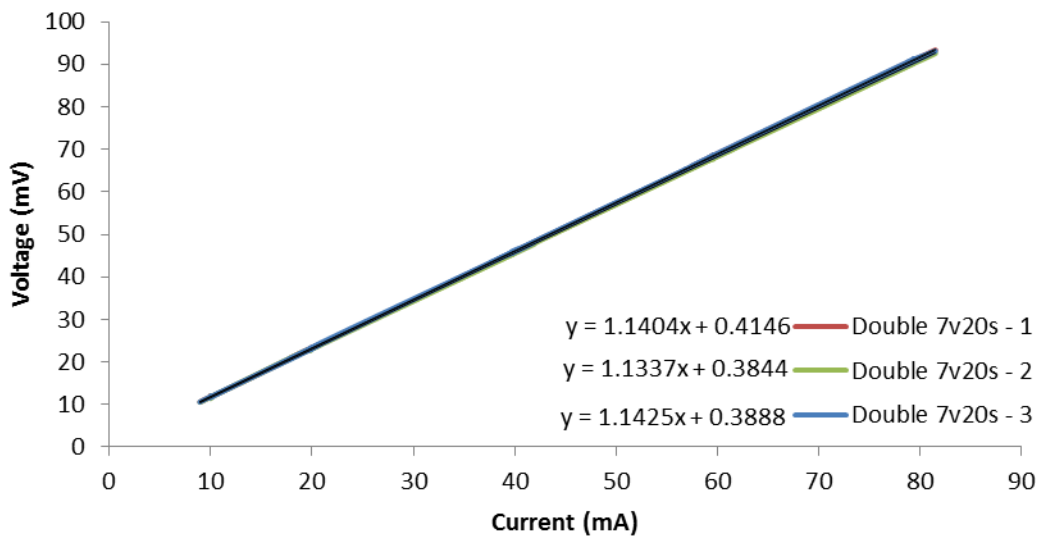


Figure 84 - Voltage vs. current of unsoldered plated braided carbon fiber sleeves

Additional testing was done to identify a difference between the plated and unplated carbon fiber. This test, observed in Figure 85, should only be used qualitatively and not compared to the other electrical testing because it was performed using 10 less seconds of electroplating at 7 volts, in addition to only having one side soldered (except for the last specimen in light blue: “7v 10s Ends Soldered”, which is like the other specimens minus 10 seconds of plating). Qualitatively, the test demonstrates that the electroplating of the nickel onto the carbon fiber significantly reduces the resistance incurred by when connecting to an electrical circuit. This could be due to the increased surface area of conductive material, which allows a

better electrical connection when using alligator clips. Additionally, the plating may effectively reduce the length of the carbon fiber of which the electricity flows due to the nickel coating having a lower resistivity, and thus being the path of least resistance.

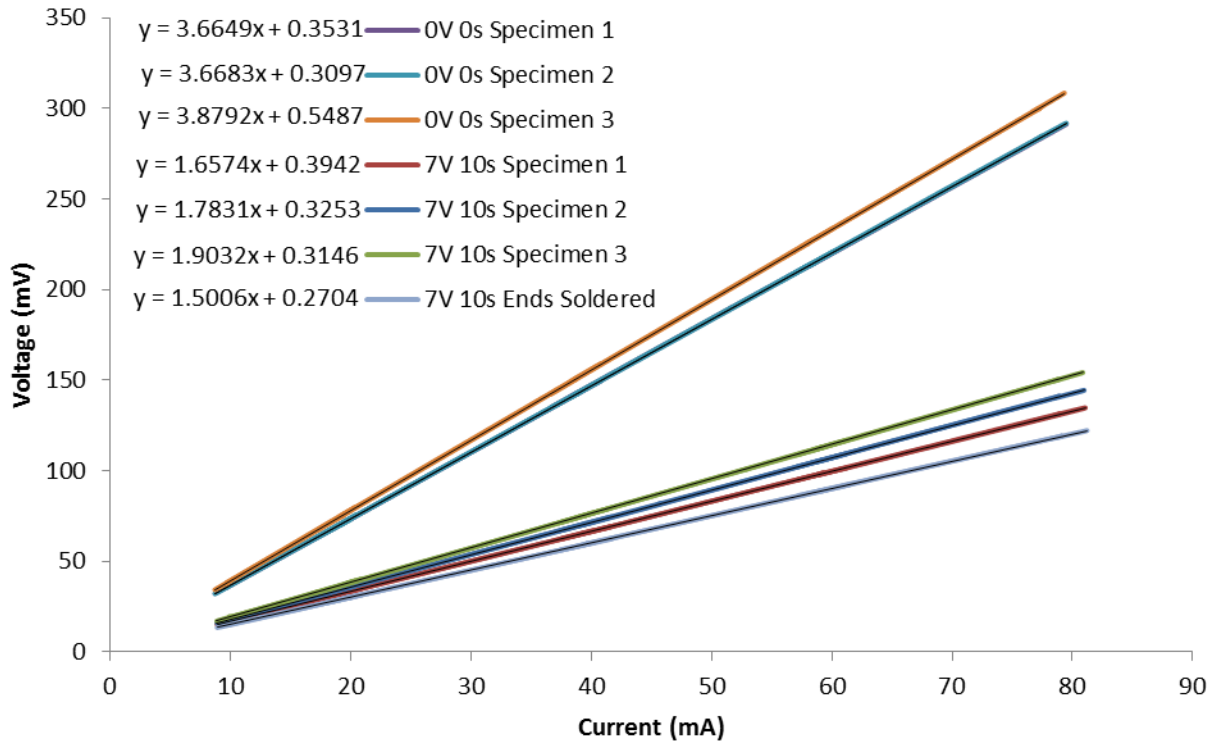


Figure 85 - Voltage vs. current comparison of plated and unplated braided carbon fiber sleeves

As a point of comparison, one of the specimens in Figure 85 (7v 10s Ends Soldered) was plated and soldered on both ends of the carbon fiber sleeve to demonstrate the difference before and after soldering. As displayed in the chart, the resistance is further reduced from the unsoldered and plated specimens. The decrease in measured resistance is most likely due to a more complete electrical connection being formed between the solder and the nickel tab than is being made between the alligator clips and the plated nickel. The braided carbon fiber alone, with the 10,000 carbon fiber filaments has an inherent resistivity of $1.1 \times 10^{-6} \Omega\text{-m}$.

For a more quantitative test, 5 different 1.5 inch specimens which have been plated and soldered to nickel tabs on both sides. These specimens were plated for 20 seconds at 7 volts and plated 0.25 inch segments on both sides. The results, displayed in Figure 86, demonstrate fairly consistent resistance measurements from these specimens. The variation of these results most likely stems from the non-uniformity of the solder joints due to a lack of manufacturability consistency for the joint connections.

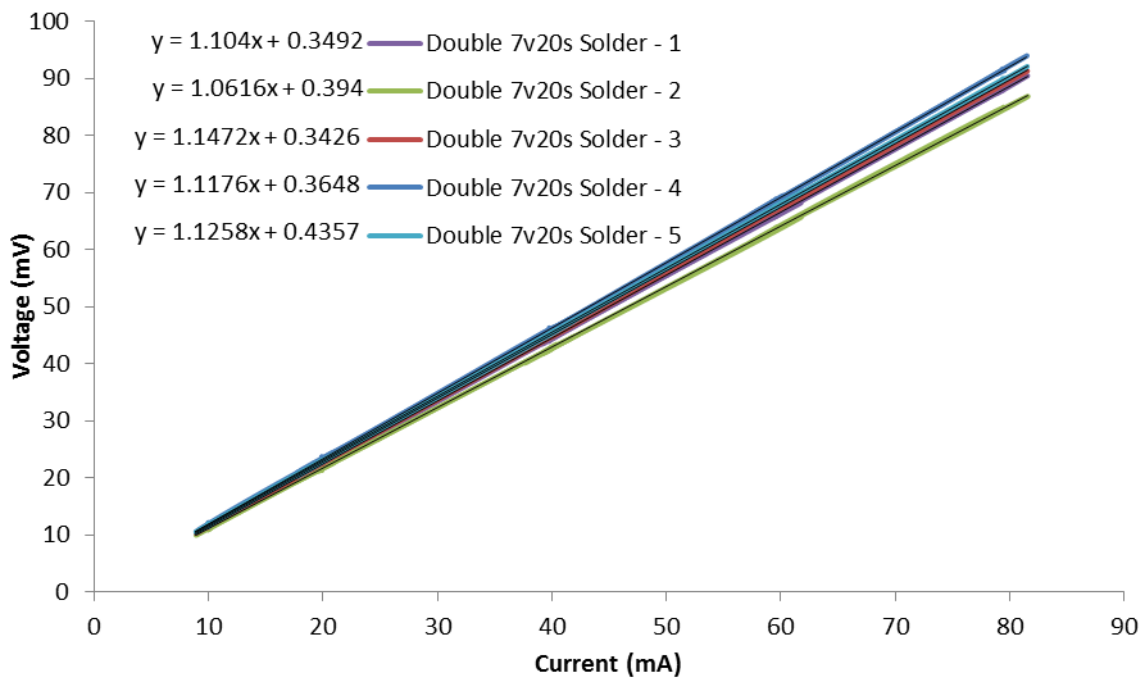


Figure 86 - Voltage vs. current of soldered plated braided carbon fiber sleeves to nickel tabs

6.2.1 Battery performance

To evaluate the electrical specimens with battery applications, the soldered carbon fiber specimen was integrated in various circuits. These circuits help to characterize the performance of the specimens in practical use applications. Both discharge circuits and charging circuits were monitored using the National Instruments SignalExpress program and acquired using a National Instruments data acquisition module.

The discharge circuits incorporated a lithium-ion single cell battery connected to a 3.8 Ω light bulb. In the connections 22 gauge wire was used and the specimen was introduced in series between the bulb and the battery. A control specimen was created to indicate the performance of the circuit using wire only. This specimen was made using a 1.5 inch length of 22 gauge wire, with 0.25 inches soldered on either side to nickel tabs. Therefore, the difference between the two circuits was a 1.5 inch length of wire and a 1.5 inch length of carbon fiber.

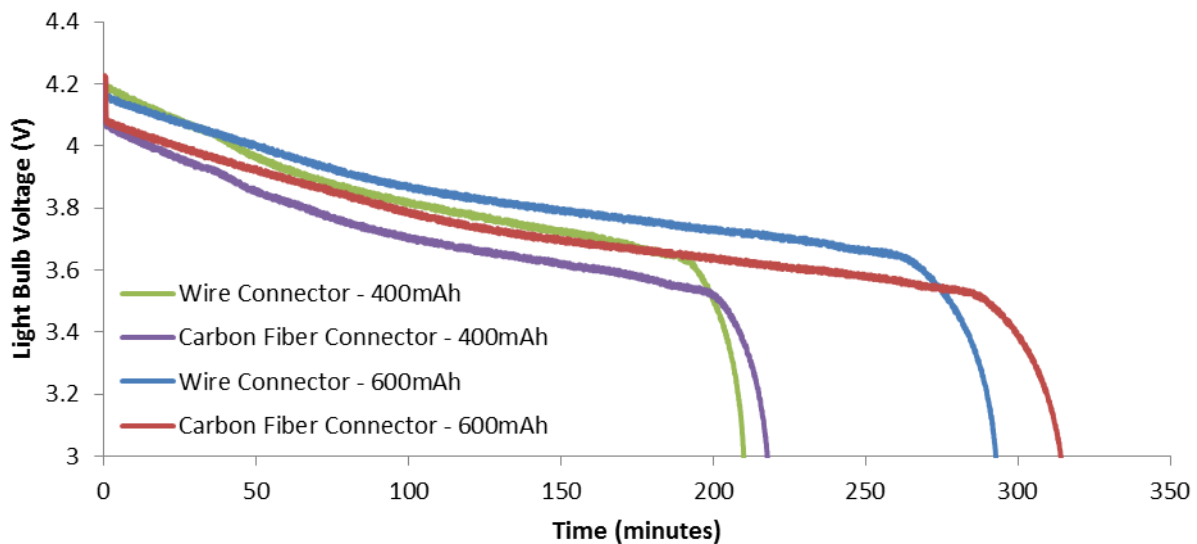


Figure 87 – Light bulb voltage versus time of discharge circuits comparing connector types

The discharge profiles of the various configurations are displayed and compared in the graph in Figure 87. It can be observed that the wire connectors perform better than the carbon fiber connectors, which add additional resistance to the circuit. Also, as expected, the 600 mAh cells perform for a longer time than the 400 mAh cells because of the increased capacity. The discharge times for the 400 mAh cells were 210 minutes for the wire connector and 218 for the carbon fiber connector circuits. Additionally, the discharge times for the 600 mAh cells were 297 minutes for the wire connector and 319 minutes for the carbon fiber connector circuits. An

interesting observation shows that the carbon fiber connector with the 400 mAh cell lagged behind the wire connector by 8 minutes, but the carbon fiber connector with the 600mAh cell lagged behind 22 minutes. A more expectable result would be 12 minutes because the capacity was increased by 50%. This could be due to differences in charging conditions, which can lead to the variation of the cell's capacity.

Thermal images were taken during the discharge of the cells in order to further characterize the properties of the carbon fiber in electrical circuits. The displayed image in Figure 88 identifies the locations of the hot spots on the wire and carbon fiber conductor specimens. HS1 corresponds to the maximum temperature on the carbon fiber, which reads 21.3 °C, and HS2 corresponds to the maximum temperature on the wire specimen, reading 20.9 °C. The heat difference during this discharge is only 0.4 °C. While this is not a large difference, it demonstrates that the additional energy displaced by the higher resistance carbon fiber is converted to heat energy. Furthermore, for the 400 mAh cells, only an 8 minute difference was observed in discharge time. This corresponds to approximately 3.5% difference in time. These temperature and time comparisons are on the same magnitude and add a potential for more accurate prediction and comparison of resistances if refined.

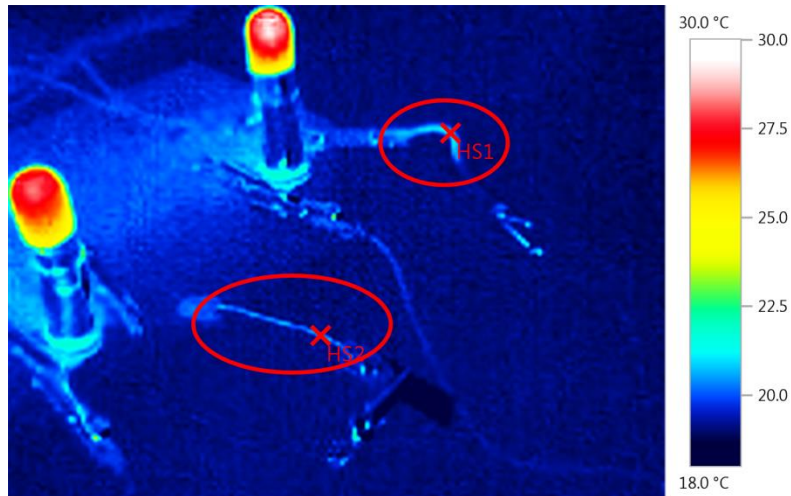


Figure 88 - Thermal image of the discharge circuits indicating the locations of the hot spots on the connectors

The charging profiles were performed using the 400 mAh cell to identify the differences between the carbon fiber and wire while charging. In order for the carbon fiber to not burn out with high current, a charging current of 0.3 A was chosen. The battery voltage was recorded directly from the battery's terminals, and the specimens were inserted between the positive terminal of the battery and the positive terminal of the charging lead. The charger used was a Hobby King Eco Six Balance Charger. To ensure that the battery conditions were the same for each specimen, the cell was rapidly discharged at 1 A to 3 V, then wait 2 minutes, and discharge the cell to 3 V using a 0.1 A discharge rate. Once the cells were discharged, the specimens were attached in series and the charge program was started. The comparison between the two charging circuits can be seen in Figure 89.

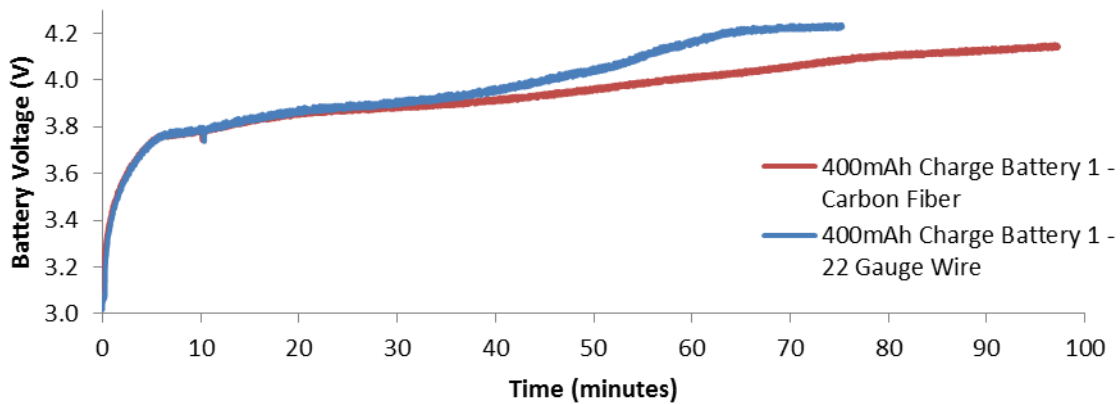


Figure 89 - Battery voltage versus current of charging circuits comparing connector types

The charging times of the 400 mAh cell for the circuits were 97.3 minutes for the carbon fiber and 75.3 minutes for the 22 gauge wire. This difference of 22 minutes equates to approximately 29% longer charging time with respect to the control 22 gauge wire specimen. Furthermore, the two charging circuits had very similar profiles for the first 20 minutes, or until approximately 3.8 volts. In addition to the added resistance in the circuit, a possible explanation for this shift is that the reference voltage on the battery charger included the carbon fiber resistance. Therefore, the charger expected a higher voltage being delivered to the battery than what was actually being provided to the battery's terminals. Instead, the voltage drop across the carbon fiber prevented the battery to be charged at the voltage intended, increasing the charge time. When the circuit reached a charge voltage of 4.2 V, the current is reduced, and thus the voltage drop across the carbon fiber was reduced. After this stage, the battery would receive closer and closer to the nominal voltage, but was still impeded by the carbon fiber specimen resistance. In Figure 89, the profile of the carbon fiber after 30 minutes matches that of the 22 gauge wire specimen but is elongated due to the aforementioned reasons.

Thermal images of the charging circuit very evidently display the differences between the temperatures reached in the two compared specimens. As displayed in Figure 90, the left circuit indicates the hot spot on the 22 gauge wire specimen as 21.6 °C, only 0.7 °C higher than the temperature during discharge. The nickel tab and alligator clip appear to be hotter than the wire itself, but this is due to the thermal reflectivity of the polished metal.

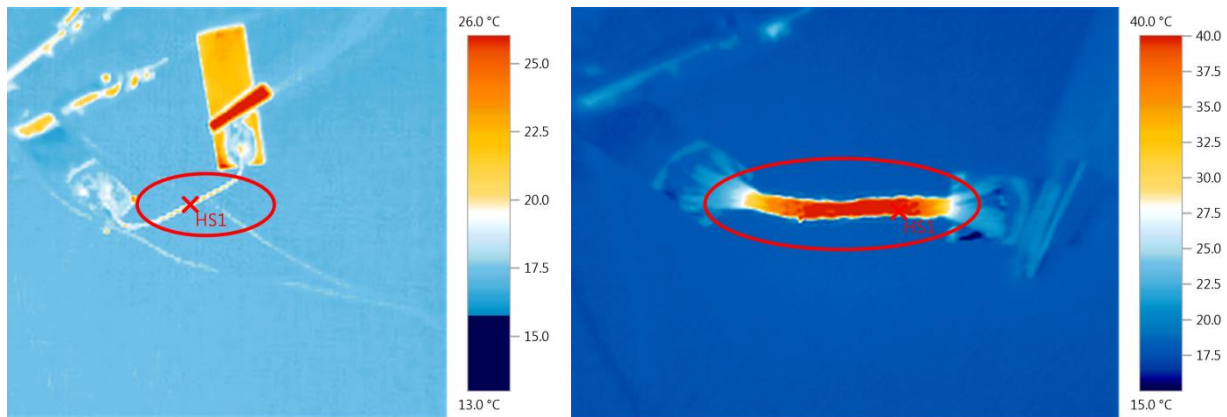


Figure 90 - Thermal images comparing the temperatures of the connectors in cell discharge circuits

For the carbon fiber circuit, a definite heating mechanism is observed using the thermal imager. The specimen on the right side of Figure 90 indicates the hot spot on the braided carbon fiber. This spot has a temperature of 44.1 °C, which is a large 22.8 °C higher than the discharge circuit. This temperature was confirmed using a thermocouple, placed on the carbon fiber interconnect to verify the heat produced as correct. The temperature difference indicates that much more of the energy is being converted to heat and would soon cause issues in electrical circuits with greater currents than 0.3 A.

Chapter 7: CONTRIBUTIONS AND SUGGESTIONS FOR FUTURE WORK

7.1 Contributions

This thesis demonstrates and investigates processing techniques which have demonstrated that carbon fiber can be connected to a nickel tab while maintaining a low interfacial resistance and high mechanical adhesion. If an electrical circuit could utilize a very flexible electrical connection, with the ability to sacrificing the inherent resistance of the carbon fiber, at low currents the device can use a carbon fiber interconnect in lieu of a metal wire. The flexibility of the braided carbon fiber maintains high mobility and electrical conduction, which can be beneficial over individual metal wires due to fatigue effects.

Implementing the electroplating technique to is fairly simple and does not require much equipment. It is relatively inexpensive compared to physical vapor deposition and silver epoxy, yet performs much better than both in mechanical and electrical testing.

The greatest achievements of this new approach are the facts that it is scalable to a battery lead sized level and the results are highly repeatable. While early testing used solder ingots to characterize the electrical and mechanical performance of the carbon fiber to metal interfaces, they could not be scaled to a nickel tab sized level due to the lack of wetting the SAC305 to the carbon fibers even when using flux. Therefore, the new electroplating process has made the connection viable by allowing for scaling of the carbon-metal connection to the battery tab level.

Mechanically, the specimens performed at levels that were only producible using 0.5-0.75 inch full immersion into a solder ingot using a rosin flux that increased adhesive strength.

The current specimens are achieving 18% higher mechanical loads with fewer carbon fibers and 1/3 to 1/2 of the attachment length. Also, the maximum load and slope of the load-displacement response correlated, which is a strong indication that the mechanical properties are dependent upon the area of the braided carbon fibers that is wetted. Therefore, additional improvements in mechanical properties are anticipated if the electroplating coverage can be optimized.

Electrically, the results of the tests are highly repeatable with the prescribed processing steps. While the electrical resistivity of the braided carbon fiber sleeve must be measured, it is presumed to be similar to the pyrolyzed pultruded carbon fibers. This indicates very little interfacial resistance due to intermetallic formations at the bonding site.

Implementing the Kester 1544 solder flux demonstrated increased wetting ability for the carbon fibers in the presence of molten SAC305 solder. This yielded higher conductivities and enhanced bonding, creating stronger bonds.

The investigation of the carbon fiber structures indicate that the structural and microstructural adhesion mechanisms vary between the use of the solder ingot with flux coated carbon fibers and the electroplated nickel coated carbon fibers. While a direct comparison cannot be made due to differences in fiber quantity, the specimens in the ingot are held in place using “clamping” mechanisms of the carbon fibers. The solder engulfs the fibers, holding them in place in a matrix. The addition of rosin flux acts as an adhesive coating which reduces slippage of the fibers and collectively increases the pull-out strength. On the other hand, the nickel plated specimens exhibit metallic bonding and the intermetallic formations at the nickel plating-solder interface. These structures, achieved through enhanced wetting serve as microstructural anchoring for the fibers, which greatly improve the adhesion strength.

Additionally, the silver epoxy was demonstrated to be a melt-free and low temperature approach to connect carbon fiber to nickel tabs. Due to the low temperature application, material viscosity, and 10 minute working time, the silver epoxy is able to be placed precisely and uniformly cover a bundle of carbon fibers.

The following tables identify summaries of the information and characteristics gathered throughout the research investigations.

Table 3 - Summary of mechanical and electrical properties

Investigated Approach	Mechanical Effects	Electrical Effects
Pultruded Carbon Fiber	Young's Modulus: 134 GPa Tensile Strength: 3.1 Gpa	Inherent resistivity of $2 \times 10^{-5} \Omega\text{-m}$
Braided Carbon Fiber (1K Tow)	Young's Modulus: 230 GPa Tensile Strength: 3.5 Gpa	Inherent resistivity of $2 \times 10^{-5} \Omega\text{-m}$
Open Mold	Controllable depth of Carbon Fiber submersion	--
Sand Cast Mold	Reduction of solder usage and a controlled specimen size	--
Carbon Fiber Pyrolyzation	Roots and flaying provide more surface area and wetting characteristics for enhanced adhesion	<ul style="list-style-type: none"> • 100x reduction of resistance compared to unpyrolyzed rod • Roots and flaying provide more surface area for conduction
Borax Flux	Reduction of surface oxidation that could impede the wetting capability	Reduction of surface oxidation that could impede the wetting capability
Solid CF Rods	<ul style="list-style-type: none"> • Increased pullout load by 3x • Increased pullout energy by 3.6x 	Increased surface area provides more paths of conduction
Physical Vapor Deposition (PVD)	Nickel adhesion to CF rod allows compatible solders to increase bond strengths	Provides avenue for bonding metals directly to the CF while minimizing interfacial compounds
Kester 1544 Activated Rosin Flux	<ul style="list-style-type: none"> • 15.7x increase in work done until failure • >3x increase in pullout load 	2x reduction of interfacial resistance
4 - Point Resistance Measurement	--	More accurate method of characterizing interfacial resistance
Programmable Power Supply	--	Consistent method of electrically loading specimens with improved voltage and current accuracy
Inherent Resistivity	--	<ul style="list-style-type: none"> • Carbon Fiber: $2 \times 10^{-5} \Omega\text{-m}$ • Nickel: $7 \times 10^{-8} \Omega\text{-m}$

Connection Method	--	Wire crimp terminal improvement: <ul style="list-style-type: none"> • Resistance: > 85% • Consistency: >250σ
Prototype Performance	--	Wire crimped carbon fibers similar to nickel tab
Nickel-coated using E-beam Deposition	Load-bearing capacity up to 4 N	--
Silver Epoxy	Load-bearing capacity up to 74 N	Up to 75% reduction over embedded crimped pultruded carbon fiber
Braided Carbon Fiber with Electroplated Nickel (CF)	<ul style="list-style-type: none"> • Load-bearing capacity up to 423 N • >4.7x increase in failure load over silver epoxy • 5x increase in failure load over hollow core submerged fully in ingot • 1.2x increase of maximum failure load of solid core submerged fully in ingot • Increased flexibility over pultruded • All increased using specimens with only ¼” length soldered to Nickel tabs 	<ul style="list-style-type: none"> • Repeatability greater than silver epoxy • Approx. 1.1Ω at 1.5” (Resistivity needed for comparison)

Table 4 - Multiphysical performance data

	Hollow Core CF-SAC305 No Flux/Flux		Solid Core CF-SAC305 No Flux/Flux		Nickel 200 Tabs	PVD Nickel-coated Solid Core CF with SAC 305 & Flux on Nickel Tab	Solid Core CF- Silver Epoxy on Nickel Tab	Braided CF Electroplated with Nickel-SAC 305 & Flux on Nickel Tab
Load Bearing (N)	12	80	40	360	220	4	47	423
Work to Failure (J)	0.02	0.6	0.2	1.9	0.24	0.01	0.08	0.4
Inherent Resistivity (Ω-m)	2x10 ⁻⁵		2x10 ⁻⁵		7x10 ⁻⁸	n/a	n/a	1.1x10 ⁻⁶

7.2 Suggestions for future work

Further research is still necessary to fully characterize the mechanical and electrical properties of the carbon to metal bonding. Investigation into different solders must be performed to identify widespread usage of the carbon fiber electrical connection.

For the electroplating processes, if the process and outcome is to be optimized, various aspects must be investigated. For instance, determining the optimal plating thickness could be necessary to avoid residual stress concentrations from forming in the plating. Furthermore, the optimal length of plating should be investigated to provide a gauge to optimize the length of the plating to the required current density of the fiber in a circuit. Minimizing the size of the bond will allow newer and more space constrained applications to be investigated.

Additionally, the optimal current and voltage densities of the plating should be investigated. While these can directly correlate to plating thickness, they also lead to formations on the surface of the carbon fiber. Producing dull, semi-bright, or bright metallic plating can directly affect the electrical and mechanical characteristics of the bond.

The plating processes described in the thesis utilized electroplating. A potential for a more controlled electroless plating process should be investigated. While these processes tend to be more costly, they provide a highly controlled deposition rate. These processes also allow for additional metal depositions to be investigated.

Further mechanical investigation should be performed to characterize the fatigue properties of the carbon fiber to nickel joints. Having a solid understanding of the fatigue properties allows implementation into various devices with expected lifetimes. These tests can be performed in a variety of temperature, humidity, and current induced environments. A more

comprehensive characterization allows models to be produced which help the user to understand, with confidence, when the device will fail.

A more comprehensive study should be focused into the normalized characterization of both the mechanical and electrical properties of the carbon fiber materials after adhesion. While many of the results are directly compared against each other, a normalized characterization of stresses should be investigated to expand the understanding of the behavior of the carbon fiber embedded in the solder. A potential means of investigating the interfacial strength is to have a single carbon fiber embedded in an effective infinite half-plane of solder and characterize the stress fields and pull-out strengths at various carbon fiber depths. Additionally, the resistivity of the coated carbon fibers should be characterized with various metallic plating diameters and lengths.

Appendix

MATLAB: Resistance processing and plotting

```
clc; clear
close all
%% Inputs
% input the file name/location with NO Extension

Folder = 'C:\Users\FOLDER LOCATION\'; % Folder location with file
FileName = 'FILE NAME'; % File name, NO extension
FileNoExt = strcat(Folder,FileName); % Combine full string without ext
delRows = 500; % delete first x-amt of time steps
endDelete = 1000; % delete last x-amt of time steps

CurrentRange = [0 90]; % in milliamps
VoltageRange = [0 0.09]; % in Volts

%% Reformatting
FullFile = strcat(FileNoExt, '.xls');

Excel_Current = xlsread(FullFile,2); % Make sure this is the Current data (2)
Excel_Voltage = xlsread(FullFile,1); % Make sure this is the Voltage data (1)
Excel = [Excel_Current, Excel_Voltage];

Excel(1:6, :) = []; % delete headers
Excel(:, 3) = []; % delete second time column

Excel(1:delRows, :) = []; % delete first x-amt of time step rows
numRows = size(Excel, 1);
Excel((numRows-endDelete):numRows, :) = []; % delete last x-amt of time step
rows

startTime(1) = Excel(1,1);
Excel(:,1) = Excel(:,1) - startTime;

numRows = size(Excel, 1);
for i = 1: numRows
    Excel(i,4) = Excel(i,3)/Excel(i,2); % Create Resistance Column
    Excel(i,2) = Excel(i,2)*1000; % Convert from A to mA
end

Time = Excel(:,1);
Current = Excel(:,2);
Voltage = Excel(:,3);
Resistance = Excel(:,4);

%% Plotting

figure(1) % Voltage vs Current Plot (slope is resistance)
hold on
```

```

plot(Current,Voltage);
p = polyfit(Current/1000, Voltage,1)
f = polyval(p, Current/1000);
plot(Current, f, '--r')
ylabel('Voltage (V)')
xlabel('Current (mA)')
legend('Resistance Data', 'Linear Fit', 'Location', 'SouthEast')
hold off

figure(2) % Current and Voltage vs. Time overlapping plot
[haxes,hline1,hline2] = plotyy(Time, Current, Time, Voltage);

ylabel(haxes(1), 'Current (mA)') % label left y-axis
ylabel(haxes(2), 'Voltage (V)') % label right y-axis
xlabel(haxes(2), 'Time (s)') % label x-axis

set(haxes(1), 'YLim', CurrentRange, 'YTickMode', 'auto')
set(haxes(2), 'YLim', VoltageRange, 'YTickMode', 'auto')
box(haxes(1), 'off')

figure(3) % Resistance vs. Voltage Plot
hold on
plot(Voltage, Resistance);
pp = polyfit(Voltage, Resistance,2)
ff = polyval(pp, Voltage);
plot(Voltage, ff, '--r')
ylabel('Resistance (\Omega)')
xlabel('Voltage (V)')
hold off

figure(4) % Resistance vs. Current Plot
plot(Current, Resistance);
ylabel('Resistance (\Omega)')
xlabel('Current (mA)')
box('off')

%% Write to file

data_cells = num2cell(Excel); %Convert data to cell array
col_header={'Time', 'Current', 'Voltage', 'Resistance'}; %Row cell array (for
column labels)
output_matrix=[ col_header; data_cells]; %Join cell arrays
xlswrite(strcat(Folder, 'Processed\ ', FileName, '_Org', '.xls'), output_matrix);
%Write data and headers

```

MATLAB: Load processing and plotting comparison

```
% For use with raw output of Force-Displacement apparatus (Excel & LabView)

clc; clear
close all

%% Formatting

% excelLoadFormat(force offset at start, file location)
% LabVLoadFormatRate(Rate[mL/h], Distance offset at start, Measure Length,
Sheet, file location)
Load_1 = LabVLoadFormatRate(1,0.5,10,1, 'FILE LOCATION SPECIMEN 1');
Load_2 = LabVLoadFormatRate(1,0.5,10,1, 'FILE LOCATION SPECIMEN 2');
Load_3 = LabVLoadFormatRate(1,0.5,10,1, 'FILE LOCATION SPECIMEN 3');
Load_4 = LabVLoadFormatRate(1,0.5,10,1, 'FILE LOCATION SPECIMEN 4');
Load_5 = excelLoadFormat(0, 'FILE LOCATION SPECIMEN 5');
Load_6 = excelLoadFormat(0, 'FILE LOCATION SPECIMEN 6');

%% Plot

hold on
% calls plotLoad function (data, color, point offset)
plotLoad(Load_1, 'red', 0.04)
plotLoad(Load_2, 'blue', 0.04)
plotLoad(Load_3, 'green', 0.04)
plotLoad(Load_4, 'm', 0.04)
plotLoad(Load_5, 'k', 0.04)
plotLoad(Load_6, 'c', 0.04)

%% Plot Formatting

axis( [0 1.8 -2.5 90]) % change the axis range
legend('Specimen 1', 'Specimen 2',...
'Specimen 3', 'Specimen 4', 'Specimen 5', ...
'Specimen 6')
title('Force vs. Displacement')
xlabel('Displacement (mm)')
ylabel('Force (N)')
legend('Location', 'SouthEast')
```

MATLAB: LabView load formatting

```
function Load = LabVLoadFormatRate(Speed,DistOffset, MeasLength, Sheet,
FileName)
% DistOffset = Starting point in mm
% MeasLength = How long the measurement should be plotted
% Sheet      = Which Excel sheet the data is on
% FileName   = Location of the file to be read

Load_a = xlsread(FileName,Sheet);
% Clear formatting for Load_1
for i= 10:-1:1
    Load_a(i, :) = [];
end

LCconv = -0.290/9.8066; % this is in V/N for the load cell
% The 10 lb load cell has an LCconv of -0.290/9.8066 V/N
% The 25 lb load cell has an LCconv of -0.1833/9.8066 V/N

Rate = 15.64/3; % This is the travel rate in mm/min (3 mL/hr = 15.64 mm/min)

Load_a(:, 1) = Speed*Rate/60 * Load_a(:, 1); % 15.64mm/min (->mm/s) @1K rate
Load_a(:, 2) = inv(LCconv) * Load_a(:, 2); % now in Newtons, not Volts
% Now the array has been formatted into displacement (mm) and force (N)
% I think this would be a decent spot for an Easter egg. ☺

indicesOffset = find( Load_a(:,1) <= DistOffset);
Load_a( indicesOffset, :) = []; % Shifts the chart to the left

startLoad(1) = Load_a(1,1);
Load_a(:,1) = Load_a(:,1) - startLoad; % correct displacement down to zero

startForce(1) = Load_a(1,2);
Load_a(:,2) = Load_a(:,2) - startForce; % correct Force down to zero

indicesCO = find( Load_a(:,1) >= MeasLength);
Load_a( indicesCO, :) = []; % Length of the measurement (cuts off end)

Load = Load_a;

end
```

MATLAB: Excel load formatting

```
function Load = excelLoadFormat(ForceOffset, FileName)
% ForceOffset = maximum force at travel
Load_a = xlsread(FileName);
% Clear formatting for Load_1
for i= 7:-1:4
    Load_a(:, i) = [];
end

Load_a(:, 2) = [];
% Now the array has been formatted into displacement (mm) and force (N)

% Offset Correction
% Corrects offset for distance traveled before loading

% Forcel for lower bound during travel period
% Forcel for upper bound of travel period

for offset = -500 : 1 : ForceOffset

Load_a( any(Load_a == offset, 2), :) = [];

startLoad(1) = Load_a(1,1);
Load_a(:,1) = Load_a(:,1) - startLoad;% correct displacement down to zero

Load = Load_a;
end
```

MATLAB: Load plotting

```
function plotLoad(LoadArray, color, offset)
% Input the formatted LoadArray and the 'color' to plot on a graph. Use
% hold on before this function to ensure that all plots will show up.

    [MaxLoad(1), Xid(1)] = max(LoadArray(:, 2)); % Finds the position of load
1

    hold on
    linePlot = ...
        plot(LoadArray(:,1), LoadArray(:,2), color);

    %Display datapoints
    MaxPoints = ...
        plot(LoadArray(Xid(1),1), MaxLoad(1), 'o',...
            'MarkerEdgeColor','k','MarkerFaceColor',color,...
            'MarkerSize',7,'HandleVisibility','off');

    text(LoadArray(Xid(1),1) + offset, MaxLoad(1), num2str(MaxLoad(1),4));

    hold off
end
```

Bibliography

- ¹ Anders, A., et al. "Joining of Metal Films to Carbon--Carbon Composite Material by Metal Plasma Immersion Ion Implantation". Apr 12, *ProQuest SciTech Collection*. Web. 28 Dec. 2012.
- ² S-Bond Technologies. "Graphite - Carbon - Carbide." *Graphite Bonding*. S-Bond Technologies, n.d. Web. 28 Dec. 2012.
- ³ Shorshorov, M. H., T. A. Chernyshova, and L. I. Kobeleva. "Interface Interaction in Aluminum--Carbon System." *Progress in Science and Engineering of Composites; Tokyo; Japan; 25-28 Oct.1982* (1982): 1273-9. *ProQuest SciTech Collection*. Web. 28 Dec. 2012.
- ⁴ Tang, Yiping, et al. "Interface Characteristics and Mechanical Properties of Short Carbon fibers/Al Composites with Different Coatings." *Applied Surface Science* 255.8 (2009): 4393-400. *ProQuest SciTech Collection*. Web. 28 Dec. 2012.
- ⁵ Shorshorov, M. H., T. A. Chernyshova, and L. I. Kobeleva.
- ⁶ Chang, Kuang-chih, Kazuhiro Matsugi, Gen Sasaki, and Osamu Yanagisawa. "Influence of Fiber Surface Structure on Interface Reaction Between Carbon Fiber and Aluminum." *Journal of the Japan Institute of Metals* 69.11 (2005): 983-88. Print.
- ⁷ Silvain, J. F., J. M. Heintz, and M. Lahaye. "Interface Analysis in Al and Al Alloys/Ni/carbon Composites." *Journal of Materials Science* 35.4 (2000): 961-65. Print.

-
- ⁸ Hua, Zhongsheng, Yihan Liu, Guangchun Yao, Lei Wang, Jia Ma, and Lisi Liang. "Preparation and Characterization of Nickel-Coated Carbon Fibers by Electroplating." *Journal of Materials Engineering and Performance* 21.3 (2012): 324-30. Web.
- ⁹ Siegbahn, Per E. M. "Trends of Metal-Carbon Bond Strengths in Transition Metal Complexes." *The Journal of Physical Chemistry* 99.34 (1995): 12723-2729. Print.
- ¹⁰ Lakomskii, V. I. "Resistivity of Carbon Material-Metal Alloy Welded Joint Interface." *Avtomaticheskaya Svarka* 3 (1996): 28-33. *ProQuest SciTech Collection*. Web. 28 Dec. 2012.
- ¹¹ "Graphlite Data." *The Composites Store*. The Composites Store. Web.
- ¹² "Carbon Fiber Braided Sleeves." *Carbon Braided Sleeves*. The Composites Store. Web.
- ¹³ *Alloy Temperature Chart*. Publication. Kester, 21 Apr. 2010. Web.
- ¹⁴ "Non-Destructive Evaluation - Energy Dispersive Spectroscopy." *The Center for Advanced Life Cycle Engineering*. University of Maryland: College Park, 2008.
- ¹⁵ Jaszczak, John A. "Graphite 2H Properties." *Graphite Properties Page*. Michigan Technological University.